Kroenke, L. W., Berger, W. H., Janecek, T. R., et al., 1991
Proceedings of the Ocean Drilling Program, Initial Reports, Vol. 130

6. SITE 804[1]

Shipboard Scientific Party[2]

HOLE 804A

Date occupied: 7 February 1990

Date departed: 7 February 1990

Time on hole: 15 hr, 15 min

Position: 1°00.28′N, 161°35.62′E

Bottom felt (rig floor; m, drill-pipe measurement): 3872.8

Distance between rig floor and sea level (m): 11.08

Water depth (drill-pipe measurement from sea level, m): 3861.7

Total depth (rig floor; m): 3921.50

Penetration (m): 48.70

Number of cores (including cores with no recovery): 6

Total length of cored section (m): 48.70

Total core recovered (m): 50.52

Core recovery (%): 104

Oldest sediment cored:
Depth (mbsf): 48.70
Nature: nannofossil ooze
Youngest age: Quaternary
Oldest age: late Miocene
Measured velocity (km/s): 1.53

HOLE 804B

Date occupied: 7 February 1990

Date departed: 8 February 1990

Time on hole: 16 hr, 30 min

Position: 1°00.28′N, 161°35.62′E

Bottom felt (rig floor; m, drill-pipe measurement): 3871.8

Distance between rig floor and sea level (m): 11.08

Water depth (drill-pipe measurement from sea level, m): 3860.7

Total depth (rig floor; m): 4009.50

Penetration (m): 137.70

Number of cores (including cores with no recovery): 15

Total length of cored section (m): 137.70

Total core recovered (m): 141.61

Core recovery (%): 103

Oldest sediment cored:
Depth (mbsf): 128.20
Nature: nannofossil ooze
Youngest age: Quaternary
Oldest age: middle Miocene
Measured velocity (km/s): 1.58

HOLE 804C

Date occupied: 8 February 1990

Date departed: 10 February 1990

Time on hole: 1 day, 19 hr

Position: 1°00.28′N, 161°35.62′E

Bottom felt (rig floor; m, drill-pipe measurement): 3872.2

Distance between rig floor and sea level (m): 11.08

Water depth (drill-pipe measurement from sea level, m): 3861.1

Total depth (rig floor; m): 4184.70

Penetration (m): 312.50

Number of cores (including cores with no recovery): 33

Total length of cored section (m): 312.50 (APC, 120.3; XCB, 192.2)

Total core recovered (m): 273.78 (APC, 120.27; XCB, 153.51)

Core recovery (%): 87 (APC, 100; XCB, 79.9)

Oldest sediment cored:
Depth (mbsf): 312.50
Nature: nannofossil chalk
Youngest age: Quaternary
Oldest age: early Oligocene
Measured velocity (km/s): 1.65/1.7

Principal results: Ocean Drilling Program (ODP) Site 804 (proposed Site OJP-6) is located near the equator on the northeastern margin of the Ontong Java Plateau (1°00.3′N, 161°35.6′E) in 3861 m of water, approximately 375 km east-northeast of Deep Sea Drilling Project (DSDP) Sites 289/586. The site serves as the deep-water end member on a Neogene depth transect designed to detect depth-related paleoceanographic signals. It was occupied with the objective of obtaining a high-resolution carbonate record in a sublysoclinal setting for studies of dissolution and biostratigraphy.

Site 804 is located near the center of a slight depression about 4.5 km wide, along a single-channel seismic (SCS) line acquired by the *Thomas Washington* during ROUNDABOUT Cruise 11. It was positioned upslope of proposed Site OJP-6, on the *JOIDES Resolution* SCS crossing line, about 1′N of the intersection with the ROUNDABOUT line (1145 UTC, 23 December 1989) (see Hagen et al., and Mayer et al., this volume, for details of the surveys). Our SCS crossing profile showed that the section would not be ideal, that is, it would include disturbed zones and possibly hiatuses. Unfortunately, this situation is normal for this region at this water depth, even under the best of circumstances.

Three holes were drilled at Site 804. Hole 804A, a dedicated hole, was cored with the advanced hydraulic piston corer (APC) to 48.7 meters below seafloor (mbsf) into upper Miocene sediments, with 104% recovery. Hole 804B was cored with the APC to 137.7 mbsf into middle Miocene sediments, with 103% recovery. The hole was abandoned when a core barrel became stuck and required 80,000 lb of overpull to free it after drilling 5 m over it. A major unconformity occurs near this level. Hole 804C was cored with the APC to 120.3 mbsf for an average recovery rate of 100%, as over- and under-recovery just balanced over the cored interval. Below this depth, coring with the extended core barrel (XCB) proceeded to 312.5 mbsf, at which point it ended in lower Oligocene sediments; the upper Oligocene was not represented. Average recovery for the XCB section was 80%. There was no logging at this site.

---

[1] Kroenke, L. W., Berger, W. H., Janecek, T. R., et al., 1991. *Proc. ODP, Init. Repts.*, 130: College Station, TX (Ocean Drilling Program).

[2] Shipboard Scientific Party is as given in the list of participants preceding the contents.

The entire sequence encountered is considered as one lithologic unit, consisting of nannofossil ooze and chalk with varying abundances of foraminifers. Below 158 mbsf (ca. 11 Ma), the sediments contain significant abundances of radiolarians. The ooze/chalk transition was placed at 181 mbsf in the middle Miocene (ca. 13 Ma).

Two lithostratigraphic subunits were recognized, as follows:

Subunit IA (0–181 mbsf): Pleistocene to middle Miocene nannofossil ooze with foraminifers, nannofossil ooze, and nannofossil ooze with radiolarians. Colors are light brown in the top 20–40 m, grading into white with color banding below. The color banding (green and reddish hues) is best expressed between 44 and 59 mbsf (uppermost Miocene and lowermost Pliocene). It is well developed between 71 and 90 mbsf, and persists to about 100 mbsf. Disturbed layers, which include disrupted and distorted color banding, occur over a wide interval (42–110 mbsf) in the upper Miocene. These features are prominent between 70 and 80 mbsf in the uppermost Miocene (ca. 8 Ma). Two turbidites near 93 mbsf attest to redeposition within the middle upper Miocene (ca. 11 Ma).

Subunit IB (181–313 mbsf): middle Miocene to upper lower Oligocene nannofossil chalk and nannofossil chalk with radiolarians. Colors are yellowish white, pale brown, and white. The main difference from the overlying unit is the greater lithification. Also, radiolarian-bearing sediments are more common in this subunit. At depths near 200 mbsf, there are indications of ooze/chalk clasts (glide breccia?) and distorted bioturbation features.

The sediments in the deepest core (130-804C-33X, 303.30–312.50 mbsf) were well indurated but posed no problem for XCB coring, which recovered a nearly full core of chunks and chips, with evidence of chalk grinding on chalk. This type of recovery was typical for the lowermost 100 m of the section. Sedimentation rates for this chalk are between 10 and 15 m/m.y. The Oligocene/Miocene boundary was located near 270 mbsf, with foraminifer-poor, low-carbonate, lower Miocene chalk overlying lower Oligocene chalks. There is evidence for the presence of microbreccia and fault gouge at this boundary.

In the lowermost Miocene, there are zones with greatly reduced foraminifer content. Thick layers of nannofossil chalk alternate with equally thick layers of nannofossil chalk containing radiolarians for much of the lower Miocene. A high radiolarian content was noted in the middle portion of this section (near 265 mbsf). The boundary between the lower and middle Miocene (near 200 mbsf) lies within a hiatus spanning the time from 20.0 to 14.7 Ma. The hiatus is bracketed by low-carbonate sediment highly enriched in radiolarians. The associated sediment (190–210 mbsf) also shows evidence of strong deformation, presumably by a gliding of the overlying section on the lower Miocene deposits. Pieces of nannofossil-radiolarite occur here. Foraminifers show signs of severe dissolution.

The ooze/chalk transition was located just a few meters above the glide zone, near the base of foraminifer Zone N12 (ca. 13.5 Ma). At Site 803, this transition was picked at a greater depth but at about the same age (ca. 13 Ma). Sedimentation rates between the hiatus at 197 mbsf (20–15 Ma) and the base of Zone NN9 at 154 mbsf (ca. 10.5 Ma) are near 18 m/m.y. Above this level, carbonate content increases (toward its maximum values of over 90%), as does foraminifer abundance. Radiolarians become less abundant. Sedimentation rates decline in upper Miocene time, dropping back to near 10 m/m.y. in the Pliocene and Pleistocene.

There is a condensed section (or a hiatus) in the lowermost Pliocene, marked by low carbonate values. After this event, carbonate values fluctuate greatly, and foraminifer abundance increases substantially. Detailed paleomagnetic stratigraphies for Pliocene-Pleistocene sediments in the three holes identified small changes in sedimentation rates and their between-hole variations.

Chemical gradients in interstitial waters at this site are generally similar to those at Site 803, reflecting the calcareous/siliceous nature of the sediments and the paucity of organic material. Calcium and magnesium gradients were influenced by basalt alteration reactions at depth and show the usual negative correlation ($R^2 = 0.97$). Strontium concentrations are lower than at Site 803, presumably reflecting diminished recrystallization intensity at Site 804. Dissolved silica increases with depth, indicating continuing dissolution of siliceous fossils. Near-maximum levels are reached at 100 mbsf, suggesting that below that level dissolution is reduced or balanced by precipitation.

Physical properties, including wet-bulk density and sound velocity, show greater variability at this site than at Site 803. Distinct minima in density occur near or within the intervals identified to include hiatuses. Clearly, this has implications for the positioning of associated reflectors within the seismic profiles.

BACKGROUND AND OBJECTIVES

Overview

Site 804, the deepest site of the Neogene depth transect on the Ontong Java Plateau, was drilled near target Site OJP-6 (3920 m), which was scheduled as an alternate to Site OJP-3 (4200 m) (Fig. 1). Both of these sites were expected to contain a record of the severe effects of varying dissolution on Neogene carbonates but at a level well short of complete removal. Thus, the saturation history of deep waters, and its ramifications for physical properties, would be contained in these sediments, as well as sufficiently preserved benthic foraminifers for bathyal paleoceanography. Triplicate APC-cored holes were planned at the site for the upper portion of the section (Quaternary and Neogene): two holes to 250 mbsf, and a third hole to 50 mbsf. Triple APC coring provides overlap between cores and sufficient material for concurrent high-resolution studies.

Background

The general background to this site is contained in the "Introduction" chapter (this volume; also see Kroenke, 1972). The Ontong Java Plateau is a broad, shallow, mid-ocean highland in the western equatorial Pacific. Its shallowest regions lie above 2000 m, and its flanks reach depths in excess of 4500 m. With an area greater than 1.5 million km^2, it is the largest of the "classic" Pacific plateaus. The plateau has a crustal thickness on the order of 40 km. Apparently, it maintained its present depth over much of its history, indicating isostatic equilibrium. Crustal seismic velocities are in the range of that of oceanic crust (Hussong et al., 1979).

The pelagic sediment cover of the Ontong Java Plateau is uniquely suited for paleoceanographic studies. The maximum thickness of the sediment cover is over 1200 m and occurs below the top of the plateau, in water depths between 2000 and 2500 m. The cover thins by roughly 100 m for every 200 m of water depth increase below 2200 m (Berger and Johnson, 1976). At Site 804 (3861 m) the sediment is approximately 500 m thick.

Site 804 is the deep-water end member of a depth transect along the equatorial portion of the Ontong Java Plateau, designed for the study of paleoceanographic events of global significance (Fig. 2). Two sites were proposed for drilling (OJP-3 and OJP-6). After drilling Site 803, we realized that considerable disturbance and/or the presence of unconformities were to be expected at both of the proposed deep-water sites, but that the shallower of the two might hold the better record. Thus, the alternate site, OJP-6, was chosen for drilling. Drilling continued to just below 300 mbsf, revealing several substantial hiatuses, and ended within early Oligocene sediments.

Unfortunately, problems arising from the creep of large sediment bodies are ubiquitous at these depths, because of a combination of tectonic and stratigraphic factors. The site location is close to a significant offset in basement levels between the plateau and the deep ocean floor (Fig. 2). Occasional earthquakes are to be expected in such a setting. Episodic shaking, basement relief, and perhaps increased mobility of deep-water sediments, from the presence of carbonate-poor layers, apparently create large-scale slumping and debris flow on the flanks of the plateau. Removal of support at greater water depths also may play

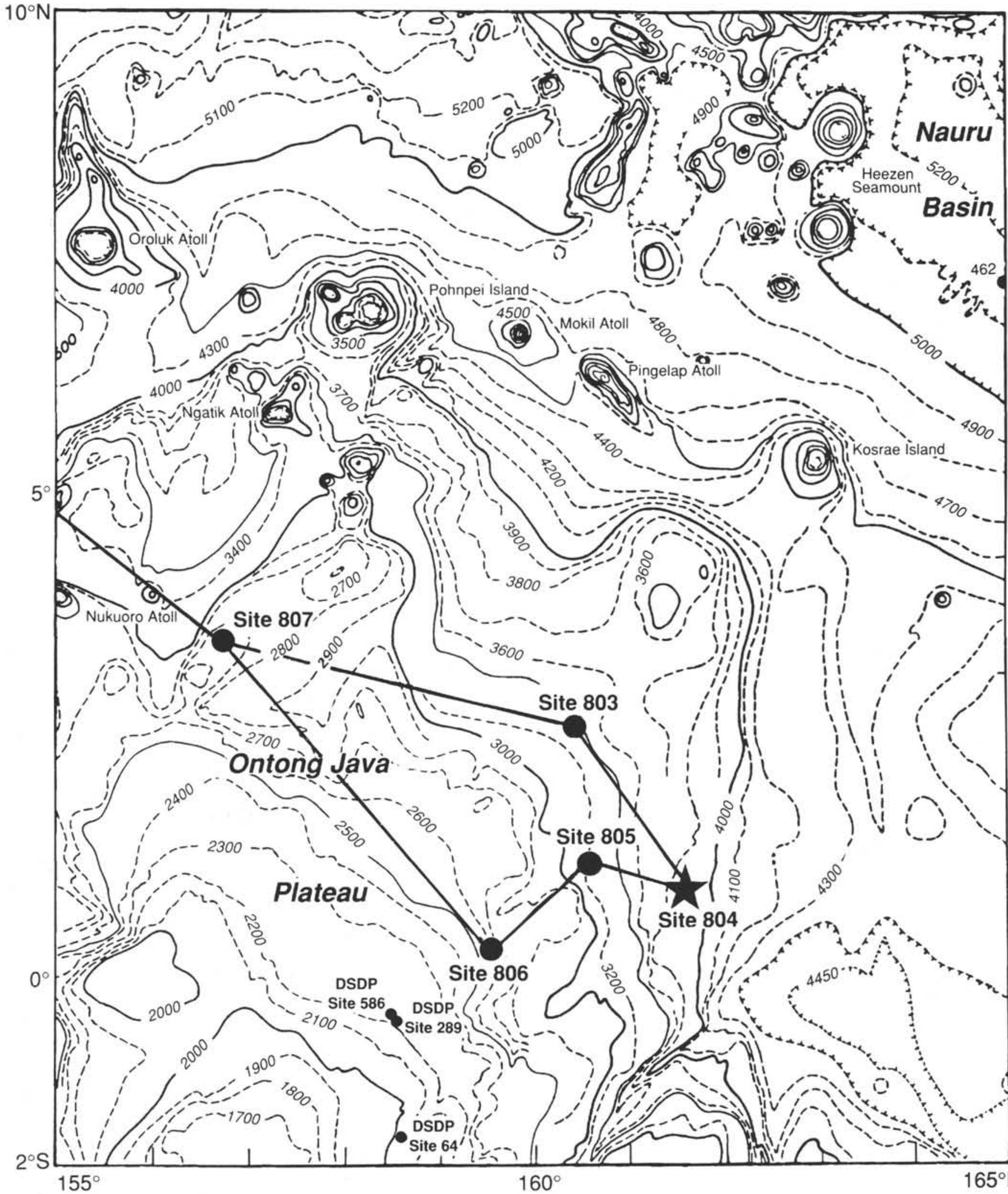

Figure 1. Bathymetry in meters of the northwestern part of the Ontong Java Plateau (after Mammerickx and Smith, 1985). The location of the Leg 130 sites and DSDP Sites 64 and 289/586 is shown. Contour interval is 100 m.

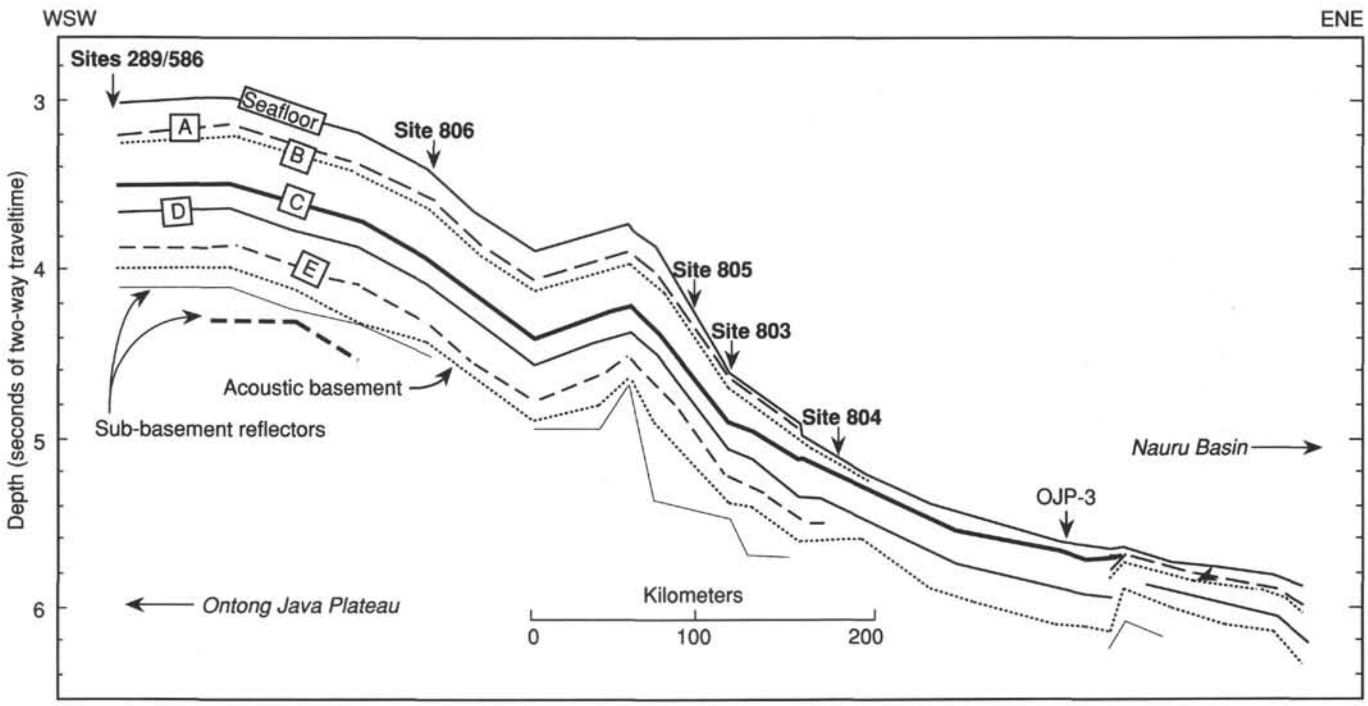

Figure 2. Simplified acoustic stratigraphy for the flank of the Ontong Java Plateau, and approximate location of Sites 803–806 (the depth transect).

a role in fostering mass movement (Berger and Johnson, 1976). Selection of a suitable site to drill was difficult under these conditions.

The seismic profiles across the proposed deep-water sites show the effects of mass movement. They exhibit crenulate reflectors ("crinkly horizons") at several levels, as well as evidence for wedging along the basin margins. The crenulate reflectors grade into transparent layers in places, implying the loss of energy return from disruption or tilting of the reflecting units (Fig. 3).

Indications exist that disturbance is associated preferentially with certain layers. Thus, we hypothesized that such layers may be predisposed, through conditioning during deposition, to serve as glide strata later. Furthermore, even with disturbance by mass movement, paleoceanographic (dissolution) events may be linked by acoustic stratigraphy. If we can establish such a connection, it will allow three-dimensional mapping and correlation into distant sediment sections throughout the Pacific basin.

The plateau has long been the focus of paleoceanographic studies based on conventional coring and on seismic profiling. Leg 130 is the fourth drilling expedition to sample the sediment cover here: four DSDP sites were drilled earlier on the plateau. Participants on Leg 7 drilled Site 64 (Shipboard Scientific Party, 1971), and those on Leg 30 drilled Sites 288 and 289 (Shipboard Scientific Party, 1975a, 1975b). All three of these sites were rotary-drilled and spot-cored. The upper 969 m in Site 289 consisted of late Eocene to Pleistocene nannofossil foraminifer chalks and oozes. The section was found to be continuous from the lower Oligocene on, the top of which was reached at 890 mbsf. Semilithified chalk first appears near 250 mbsf (late Miocene). The fourth site (Site 586, drilled on Leg 89 next to Site 289) was hydraulically piston cored to 305 mbsf and reached upper Miocene sediments (Shipboard Scientific Party, 1986a, 1986b). Well-preserved nannofossil ooze was recovered at this site.

Objectives

Site 804, roughly 375 km northeast of DSDP Sites 289/586 on the northeastern margin of the Ontong Java Plateau, was planned as the deepest of the four Leg 130 sites that constitute a Neogene depth transect (Sites 803–806; Fig. 1). The general objective of this transect was to detect and reconstruct depth-related paleoceanographic signals, such as the changing gradients of carbonate dissolution intensity and the deep-water $\delta^{13}C$ signals in benthic foraminifers. The sediments sampled along the transect are produced in the same surface-water conditions and thus arrive on the seafloor in the same pelagic rain, so that differences can be attributed to depth-related effects.

The depth sampled at Site 804 (Fig. 1), between the lysocline and the carbonate compensation depth (CCD), is that which shows the effects of dissolution most dramatically, yet preserves enough carbonate to study these effects. Thus, all physical properties should be severely affected by carbonate dissolution at this level (Johnson et al., 1977). In turn, this imprint should be detectable in the acoustic stratigraphy. Our hope was that the effects of dissolution would be strata-bound, so that a clear linkage could be established between paleoceanographic events and acoustic stratigraphy (Mayer et al., 1986). In the case of severe dissolution pulses, one would expect hiatus formation, presumably also linked to paleoceanographic events (Barron and Keller, 1982). The combination of dissolution effects (which apparently decreases resistance to shear) and the local tectonics (which provide for tilting and earthquakes) is inimical to these objectives regarding acoustic stratigraphy. Thus, it is necessary to find and sample minimally disturbed sediments. As it turned out, sediment disturbances identified as minor when studying seismic profiles proved to be quite substantial upon drilling. Nevertheless, the objectives regarding acoustic linkage and hiatus formation remain valid.

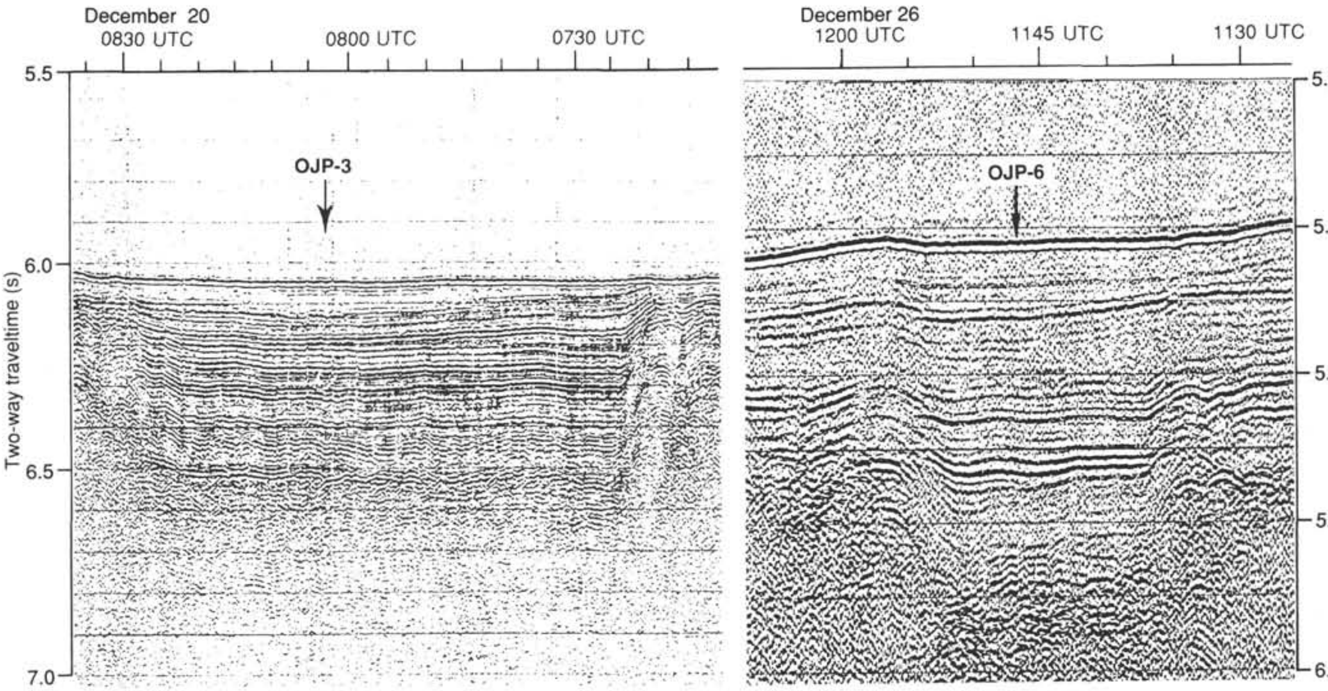

Figure 3. Seismic profiles across proposed drilling sites for Site 804, showing evidence of planar disturbance (crinkly horizons) and debris flow (wedges next to basin rim). Site OJP-3 was not drilled.

Regarding biofacies objectives, we expected that changes in the preservation of calcareous fossils would provide clues to changes in the intensity of dissolution, with wide implications for the study of deep-water history and the oceanic carbon cycle (e.g., Berger, 1981). In addition, we hypothesized that preserved benthic foraminifers would record deep-water properties directly in their abundances and chemical composition. The effects of partial dissolution on biostratigraphic zonation (by selective removal of marker species) also is important.

OPERATIONS

Site 804

The transit to Site 804 (proposed Site OJP-6) started at 1730 hr, 6 February 1990, and covered 98 nm over 7.5 hr at an average speed of 13.0 kt. Upon arrival, a 47-nmi pre-site seismic survey was run over the proposed site (for more details of the survey, see the "Underway Geophysics" chapter, this volume). The beacon was dropped at 0537 hr, 7 February 1990, initiating Site 804.

Hole 804A

The ship was positioned 20 m east of the beacon. Core 130-804A-1H was spudded at 1520 hr, 7 February 1990, in a water depth of 3861.7 m. Cores 130-804A-1H through -6H were taken from 0 to 48.7 mbsf, with 48.7 m of sediment cored and 50.52 m recovered (103.74% recovery; see Table 1). We conducted orientation surveys during Cores 130-804A-3H through -6H. Hole 804A was ended when the depth objective of 50 mbsf was reached.

Hole 804B

The ship was offset 40 m east of the beacon. Core 130-804B-1H was taken at 2215 hr, 7 February 1990, in a water depth of 3860.7 m. Cores 130-804C-1H through -15H were taken from 0 to 137.7 mbsf, with 137.7 m of sediment cored and 141.61 m recovered (102.84% recovery). Orientation surveys were taken on Cores 130-804-3H through -15H. Hole 804B was terminated when Core 130-803B-15H required 80,000 lb of overpull to free it after drilling 5 m over the core barrel.

Hole 804C

The ship was offset 60 m east of the beacon. Core 130-804C-1H was taken at 1500 hr, 8 February 1990, in a water depth of 3861.1 m. Cores 130-804C-1H through -13H were taken from 0 to 120.3 mbsf, with 120.3 m of sediment cored and 120.27 m recovered (99.98% average recovery).

The breakaway piston head was tested in Cores 130-804C-9H through -11H, but the piston came off in all three cores, in spite of passing deck tests with the outside and inner holes plugged. Recovery for the three cores was reduced from an average of 9.95 to 8.34 m. Orientation surveys were taken on Cores 130-804C-3H through -13H. Cores 130-804C-14X through -33X were taken from 120.3 to 312.5 mbsf with 192.2 m of sediment cored and 153.51 m recovered (79.92% recovery). Hole 804C was terminated after reaching the depth/age objectives.

The drill string was pulled out of the hole, and the bit cleared the rotary table at 0830 hr, 10 February 1990, ending Hole 804C. Before departing Site 804, the vibration-isolated television (VIT) frame was run to the seafloor to test the televiewer (TV) camera and coaxial cable. After successful completion of this test, the TV was pulled, and the ship got underway at 1200 hr, 10 February 1990.

LITHOSTRATIGRAPHY

Introduction

Three holes were drilled at Site 804. Holes 804A and 804B were cored with the APC to 49 mbsf and 138 mbsf, respectively.

Table 1. Coring summary, Site 804.

Core no.	Date (Feb. 1990)	Time (UTC)	Depth (mbsf)	Cored (m)	Recovered (m)	Recovery (%)
130-804A-						
1H	7	1520	0–1.2	1.2	1.26	105.0
2H	7	1620	1.2–10.7	9.5	9.83	103.0
3H	7	1725	10.7–20.2	9.5	10.03	105.6
4H	7	1825	20.2–29.7	9.5	9.92	104.0
5H	7	1925	29.7–39.2	9.5	9.98	105.0
6H	7	2100	39.2–48.7	9.5	9.50	100.0
Coring totals				48.7	50.52	103.7
130-804B-						
1H	7	2215	0–4.7	4.7	4.64	98.7
2H	7	2315	4.7–14.2	9.5	9.95	105.0
3H	8	0015	14.2–23.7	9.5	10.03	105.6
4H	8	0220	23.7–33.2	9.5	9.91	104.0
5H	8	0310	33.2–42.7	9.5	10.12	106.5
6H	8	0400	42.7–52.2	9.5	9.85	103.0
7H	8	0500	52.2–61.7	9.5	9.82	103.0
8H	8	0545	61.7–71.2	9.5	9.89	104.0
9H	8	0630	71.2–80.7	9.5	9.70	102.0
10H	8	0730	80.7–90.2	9.5	9.87	104.0
11H	8	0810	90.2–99.7	9.5	10.01	105.3
12H	8	0900	99.7–109.2	9.5	9.78	103.0
13H	8	0950	109.2–118.7	9.5	7.95	83.7
14H	8	1050	118.7–128.2	9.5	10.01	105.3
15H	8	1215	128.2–137.7	9.5	10.08	106.1
Coring totals				137.7	141.61	102.8
130-804C-						
1H	8	1500	0–6.3	6.3	6.31	100.0
2H	8	1600	6.3–15.8	9.5	10.00	105.2
3H	8	1710	15.8–25.3	9.5	9.78	103.0
4H	8	1815	25.3–34.8	9.5	9.98	105.0
5H	8	2030	34.8–44.3	9.5	10.05	105.8
6H	8	2130	44.3–53.8	9.5	10.07	106.0
7H	8	2230	53.8–63.3	9.5	9.99	105.0
8H	9	0000	63.3–72.8	9.5	9.79	103.0
9H	9	0100	72.8–82.3	9.5	8.14	85.7
10H	9	0200	82.3–91.8	9.5	7.98	84.0
11H	9	0300	91.8–101.3	9.5	8.91	93.8
12H	9	0400	101.3–110.8	9.5	9.77	103.0
13H	9	0500	110.8–120.3	9.5	9.50	100.0
14X	9	0545	120.3–129.8	9.5	6.92	72.8
15X	9	0630	129.8–139.3	9.5	4.75	50.0
16X	9	0715	139.3–148.8	9.5	2.51	26.4
17X	9	0800	148.8–158.3	9.5	9.26	97.5
18X	9	0920	158.3–168.0	9.7	8.60	88.6
19X	9	1045	168.0–177.7	9.7	8.30	85.5
20X	9	1130	177.7–187.4	9.7	8.10	83.5
21X	9	1230	187.4–197.1	9.7	6.58	67.8
22X	9	1310	197.1–206.8	9.7	9.06	93.4
23X	9	1355	206.8–216.5	9.7	8.38	86.4
24X	9	1505	216.5–226.2	9.7	4.84	49.9
25X	9	1610	226.2–235.8	9.6	9.31	97.0
26X	9	1715	235.8–245.4	9.6	9.15	95.3
27X	9	1820	245.4–255.1	9.7	8.58	88.4
28X	9	1920	255.1–264.7	9.6	8.95	93.2
29X	9	2020	264.7–274.4	9.7	7.81	80.5
30X	9	2130	274.4–284.0	9.6	8.49	88.4
31X	9	2230	284.0–293.7	9.7	7.98	82.2
32X	9	2340	293.7–303.3	9.6	7.47	77.8
33X	10	0045	303.3–312.5	9.2	8.47	92.0
Coring totals				312.5	273.78	87.6

At Hole 804C, the interval from 0 to 120 mbsf was cored with the APC and the interval from 120 to 313 mbsf was cored with the XCB. Recovery was near 100% in the intervals cored with the APC and near 80% in the intervals cored with the XCB.

The entire sedimentary sequence consists of nannofossil ooze and chalk with varying abundances of foraminifers. Significant abundances of radiolarians (10%–25%) are noted below 158 mbsf. The oldest sediment recovered is of late early Oligocene age.

The sediments are relatively homogeneous in composition; thus, they were grouped into one lithostratigraphic unit and divided into two subunits based on the degree of lithification (Fig. 4). Subunit IA is composed of nannofossil ooze and nannofossil ooze with varying abundances of foraminifers and radiolarians. Subunit IB contains nannofossil chalk and nannofossil chalk with varying abundances of radiolarians. The ooze/chalk transition is located at 181 mbsf, in Section 130-804C-20X-3, and is of middle Miocene age.

Description of Units

Unit I

Intervals: Hole 804A, Cores 130-804A-1H to -6H; Hole 804B, Cores 130-804B-1H to -15H; Hole 804C, Cores 130-804C-1H to -33X
Age: Pleistocene–late early Oligocene
Depth: 0–313 mbsf

The sediments recovered at Site 804 consist of nannofossil ooze and chalk. Foraminifers and radiolarians generally are present in abundances of less than 25%. The sequence was divided into two subunits to distinguish between oozes and chalks.

Subunit IA

Intervals: Hole 804A, Cores 130-804A-1H to -6H; Hole 804B, Cores 130-804B-1H to -15H; Hole 804C, Core 130-804C-1H to Section 130-804C-20X-3
Age: Pleistocene–middle Miocene
Depth: 0–181 mbsf

Subunit IA is 181 m thick and is composed of (in decreasing order of abundance) nannofossil ooze, nannofossil ooze with foraminifers, nannofossil ooze with radiolarians, foraminifer nannofossil ooze, and nannofossil foraminifer ooze.

Drilling disturbance was generally minor, although several sections in Cores 130-804C-4H through -6H contained flow-in.

Nannofossil ooze with foraminifers and foraminifer nannofossil ooze were found at the top of Subunit IA; they graded into nannofossil ooze at approximately 20–40 mbsf. Foraminifer abundances remain near 5% in the interval from 40 to 120 mbsf and increase below 120 mbsf, whereas radiolarian abundances increase to 10% or more below 158 mbsf. As a result, nannofossil ooze with foraminifers alternates with nannofossil ooze with radiolarians on a scale of 5–10 m between 120 and 182 mbsf.

The dominant sediment color is white (2.5Y 8/0), except for the uppermost Pleistocene section (the first two cores in each hole), which is pale brown (10YR 6/3). Most cores of Subunit IA also contain pale yellowish green (10GY 7/2), light gray (5Y 7/1), and reddish gray (5R 7/1), millimeter- to centimeter-scale, diffuse color bands of varying intensity. Between 42 and 110 mbsf (Cores 6H through 12H in each hole), numerous color bands are dipping and show evidence of microfaulting and contortion. These characteristics do not appear to be caused by the drilling process or bioturbation and may be evidence of mass displacement.

Other evidence for mass movement is the presence of three graded beds 10, 12, and 50 cm thick that are interpreted to be turbidites. The first graded bed is located in the interval dominated by nannofossil ooze approximately 93 mbsf (upper Miocene) in both Holes 804B and 804C (Sections 130-804B-11H-2 and 130-804C-11H-2, respectively); it consists of sand-rich nannofossil foraminifer ooze (Fig. 5). The other two graded beds are located in Sections 130-804C-19X-1 and -3, respectively (middle Miocene), within an interval of nannofossil ooze with foraminifers between 168 and 174 mbsf. They consist of nannofossil foraminifer ooze.

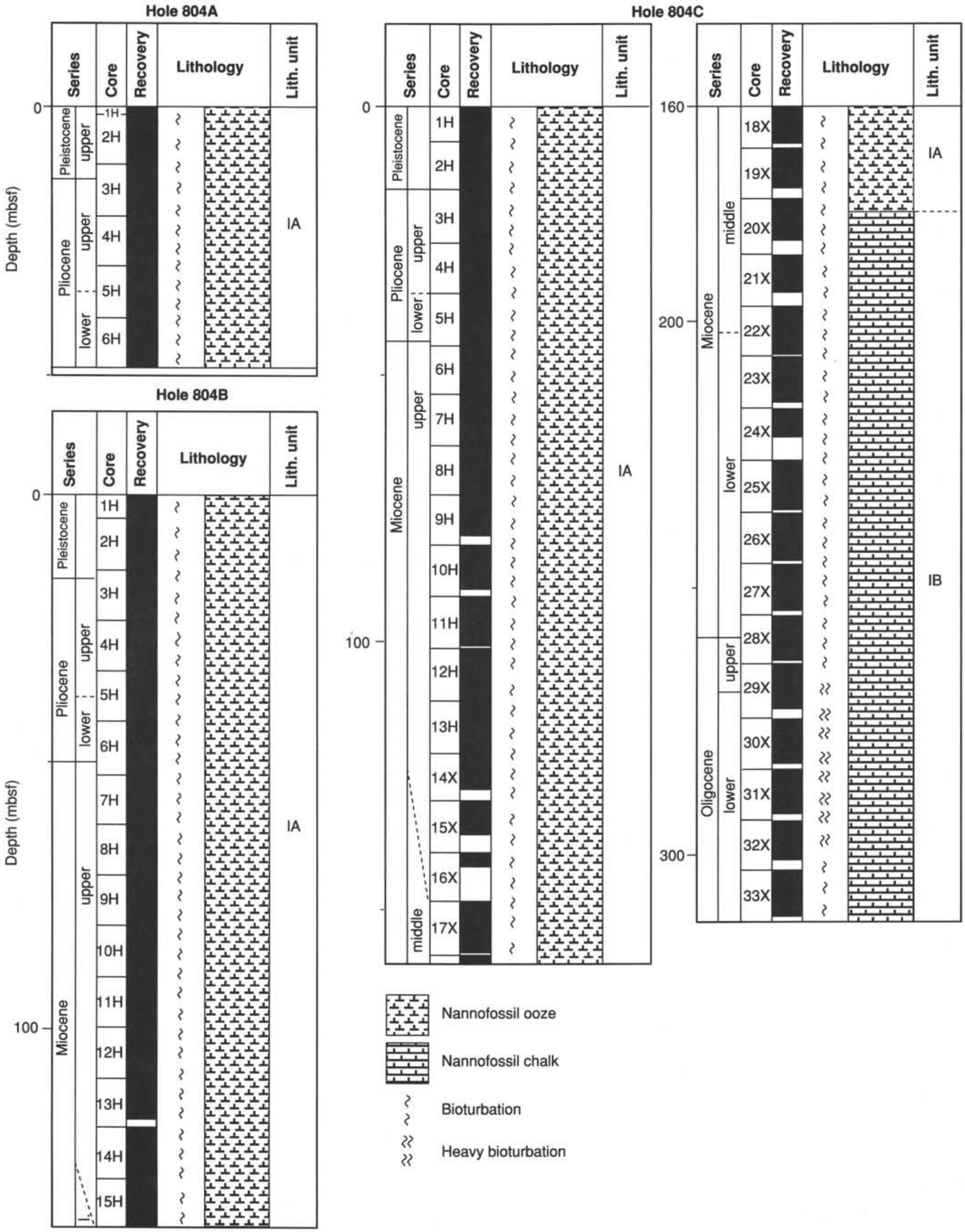

Figure 4. Lithologic summary, Site 804.

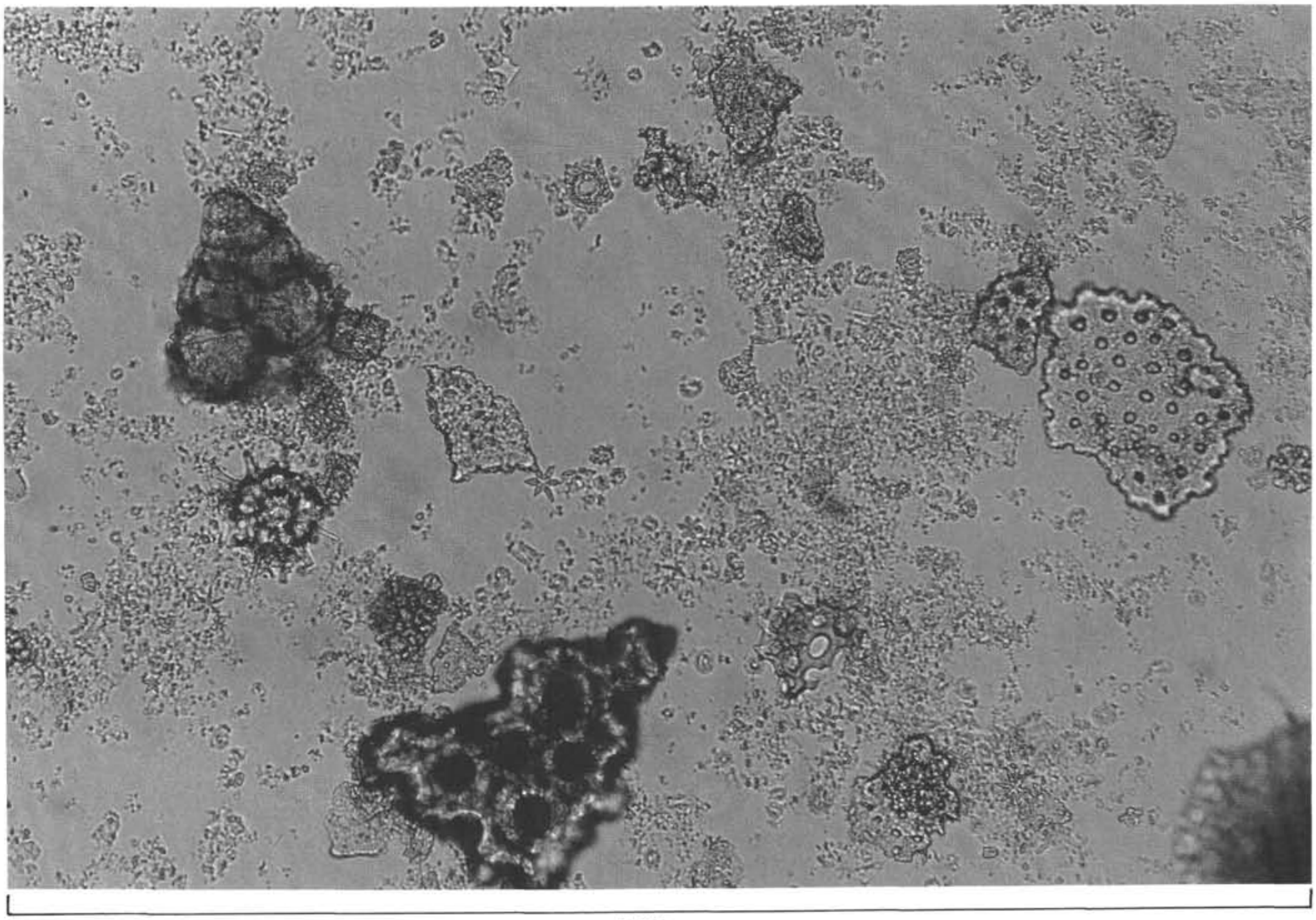

Figure 5. Photomicrograph of turbidite sediment (Section 130-804C-11H-2).

The sediments of Subunit IA generally are slightly to moderately bioturbated, but they are heavily bioturbated in a few intervals. Bioturbation is indicated by burrow mottles of a material that exhibits a different color and is often coarser grained than the surrounding sediments; the burrows and trace structures sometimes are filled by pyrite.

As estimated from visual observation and smear slide descriptions (Fig. 6), texturally these sediments are silts with a few intervals of clayey silts; the sand content rarely exceeds 5%. Carbonate contents generally range between 78% and 93% (Fig. 7). The transition from nannofossil ooze with foraminifers to nannofossil ooze at 40 mbsf is marked by an average increase of approximately 7% in carbonate content. The interval composed of nannofossil ooze shows fairly constant and high carbonate values (around 91%). Fluctuations in the carbonate content increase below 158 mbsf as radiolarians become a significant component of the sediment.

The siliceous biogenic components, mainly radiolarians and diatoms, make up less than 5% of the sediment in Subunit IA, except in the intervals of nannofossil ooze with radiolarians. Abundances of nonbiogenic components identified in smear slides (zeolite, quartz, volcanic ash) are always below 3%. X-ray diffraction (XRD) scans indicate the dominance of calcite throughout Subunit IA, but also record the more detailed variations described previously. Above 40 mbsf, the terrigenous fraction is abundant and includes illite, 7Å and 14Å clays, quartz, and feldspar. Below approximately 40 mbsf, the terrigenous fraction is less abundant and consists predominantly of mixed-layer clays and quartz. The presence of opal is indicated in an XRD sample taken below 158 mbsf.

Subunit IB

Intervals: Hole 804C, Section 130-804C-20X-4 to Core 130-804C-33X
Age: middle Miocene–late early Oligocene
Depth: 181–313 mbsf

Subunit IB is 132 m thick and is composed of nannofossil chalk, nannofossil chalk with radiolarians, radiolarian nannofossil chalk, and nannofossil radiolarite, in order of decreasing abundance. Drilling disturbance is seen as moderately fractured to highly fragmented cores with a few brecciated sections (especially Sections 130-804C-26X-2 through -6).

Nannofossil chalk in the upper part of this subunit graded into radiolarian nannofossil chalk at 197 mbsf (top of Core 130-804C-22X) in the middle Miocene. Within the interval of radiolarian nannofossil chalk, two minor sediment types were encountered that appeared only once and in very small quantities: (1) a drilling fragment of nannofossil radiolarite was found in Section 130-804C-22X-5, and (2) very stiff and structureless nannofossil ooze, heavily disturbed by drilling, was located in Sections 130-804C-23X-5 and -6.

Three intervals of nannofossil chalk, each several meters to several tens of meters thick, alternate with 10- to 25-m-thick in-

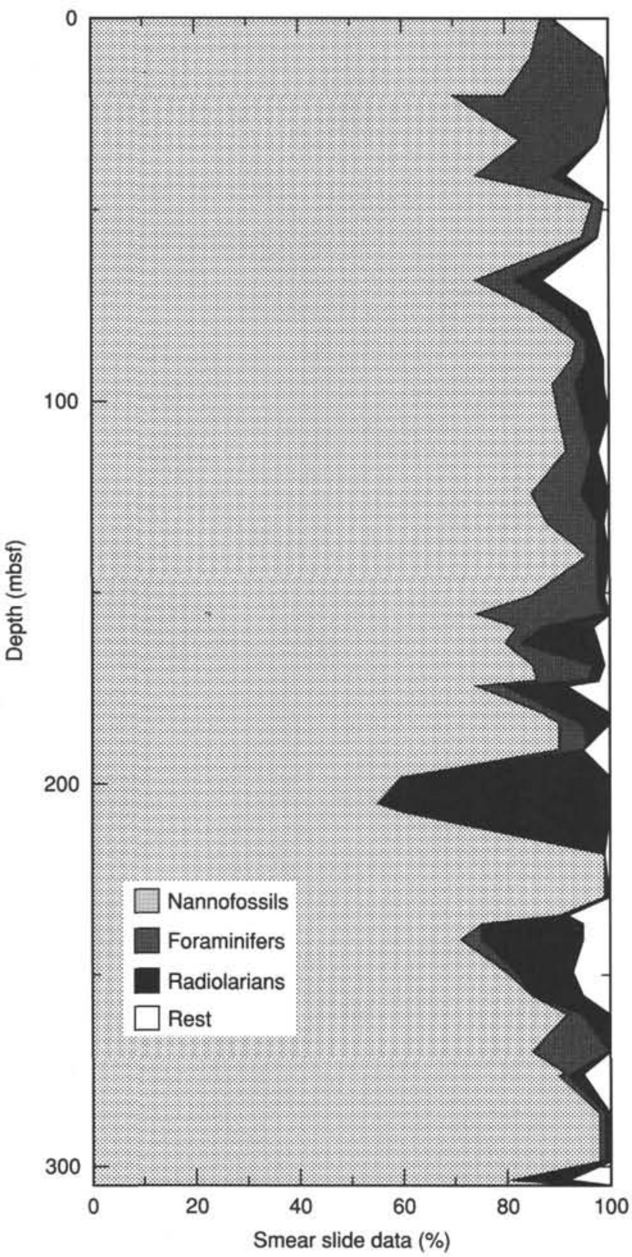

Figure 6. Composition of sediments at Hole 804C, as compiled from smear slide data.

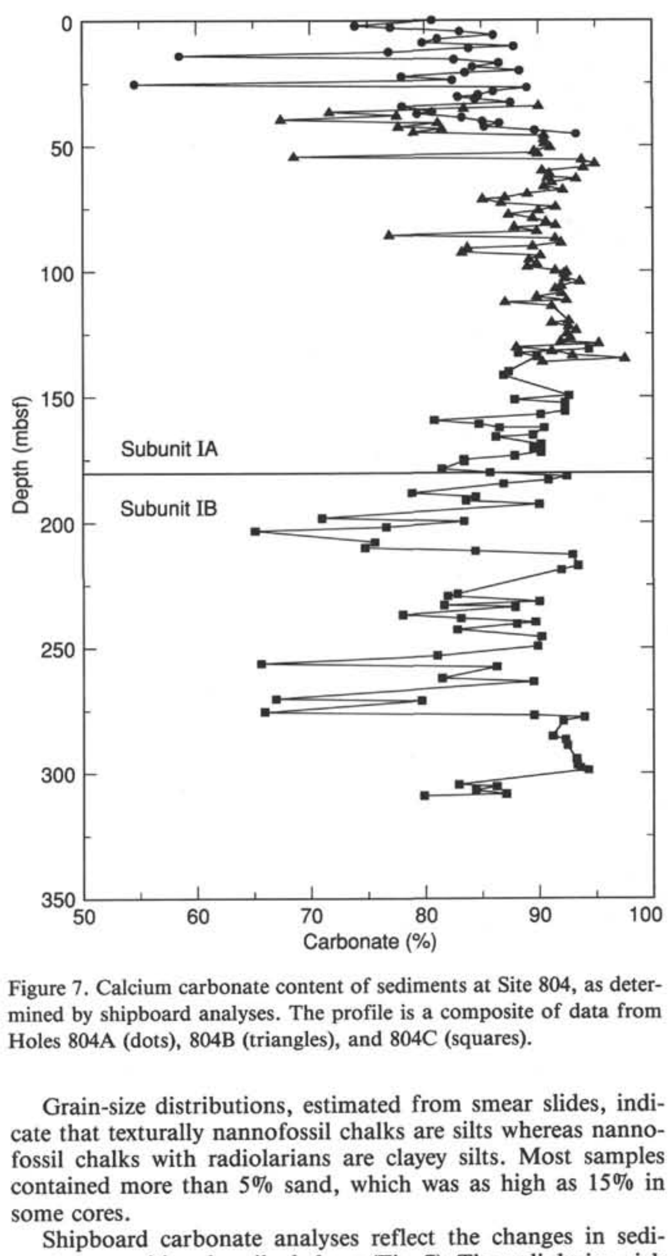

Figure 7. Calcium carbonate content of sediments at Site 804, as determined by shipboard analyses. The profile is a composite of data from Holes 804A (dots), 804B (triangles), and 804C (squares).

tervals of nannofossil chalk with radiolarians below 226 mbsf in lower Miocene sediments. The base of Subunit IB consists of nannofossil chalk with radiolarians and is of late early Oligocene age.

Bioturbation is generally moderate throughout the subunit, but it is heavy in a few sections. Bioturbation is indicated by color mottles, simple discrete burrows, and well-developed *Zoophycos* trace fossils (e.g., Section 130-804C-33X-1). In Section 130-804C-24X-2, a few centimeter-long pieces of a pyritized burrow fill (around 1 cm in diameter) were noted. Color differences helped us to distinguish between nannofossil chalk and nannofossil chalk with radiolarians in Subunit IB. Pure nannofossil chalk is white (2.5Y 8/0) to light gray (5Y 7/1), whereas nannofossil chalk with radiolarians is white (5Y 8/2, appears yellowish) to very pale brown (10YR 7/3).

Grain-size distributions, estimated from smear slides, indicate that texturally nannofossil chalks are silts whereas nannofossil chalks with radiolarians are clayey silts. Most samples contained more than 5% sand, which was as high as 15% in some cores.

Shipboard carbonate analyses reflect the changes in sediment composition described above (Fig. 7). The radiolarian-rich interval at the top of Subunit IB (197–226 mbsf) appears as a minimum in the carbonate profile, with concentrations between 65% and 75%. The underlying interval of alternating nannofossil chalk and nannofossil chalk with radiolarians is apparent in both the smear slide and the carbonate profiles (Figs. 6 and 7).

Siliceous biogenic components other than radiolarians include diatoms, siliceous sponge spicules, silicoflagellates, and unidentified fragments, each of which contributed less than 5% to the sediments. The XRD scans of samples from Subunit IB indicate the continued importance of calcite, together with the presence and variable abundances of clays, quartz, feldspar, and opal.

Cores 130-804C-21X and -22X are unique in Subunit IB for the evidence of sediment disturbance that they contain. In Core 130-804C-21X, this included elongate (2–5 cm long) features and irregularly shaped mottles with faint outlines that are slightly different in color than the surrounding sediment. Some of these features appear to be compressed burrow fills, but others may be poorly defined sediment clasts. Core 130-804C-22X contained several disturbed zones, with highly contorted, swirled, or fragmented trace fossils and sediment clasts (Fig. 8); distorted (stretched, microfaulted, rotated) thin color bands or laminae (Fig. 9); and angular, centimeter-scale, slightly darker clasts distributed irregularly throughout the core (Fig. 10).

Discussion

The sedimentary sequence at Site 804 is composed of fairly homogeneous nannofossil oozes and chalks with varying abundances of foraminifers and radiolarians. The lithostratigraphic sequence at this site consists of one lithologic unit divided into two subunits (IA and IB) to distinguish between ooze and chalk. The primary sedimentary process that produced the interval cored at Site 804 is interpreted to be pelagic, biogenic sedimentation.

The sedimentary column between the upper Oligocene and the middle Miocene (Subunit IB and the lower part of Subunit IA) is characterized by alternating radiolarian-rich and -poor intervals, implying variations in surface-water productivity and/or dissolution. Carbonate preservation generally is poor in the radiolarian-rich intervals, as indicated by the low abundances of foraminifers and their poor state of preservation (see "Biostratigraphy" section, this chapter). Calcium carbonate values in these intervals are 10%–20% lower than in the pure nannofossil chalks. Intervals with significant radiolarian abundances (>10%) also are recognized by their color; nannofossil chalks are generally white, as compared with the yellowish or pale brown appearance of the nannofossil chalks with radiolarians. The combination of low foraminifer abundances, poor foraminifer preservation, and darker color can be interpreted as an indication of extensive dissolution because of deposition close to the CCD, resulting in the relative enrichment of radiolarians and clays.

Evidence for sediment disturbance (slump blocks, microfaults, dipping, and contorted color bands) is concentrated in Cores 130-804C-21X and -22X (187–207 mbsf). The elongate features in Core 130-804C-21X can be interpreted as clasts that were transported, perhaps only a short distance, and redeposited when both the clasts and the matrix were still soft (ooze). The distortion of trace fossils and color bands or laminae observed in Core 130-804C-22X may represent a shear zone between semilithified sediment packages. Seismic reflection profiles from this area (see "Seismic Stratigraphy" section, this chapter) indicate the effects of major slumping at approximately 80 and 200 mbsf, which coincide with the disturbed intervals in the cores described above. Biostratigraphic data indicate the presence of a hiatus at the top of Core 130-804C-22X (197 mbsf; see "Biostratigraphy" section, this chapter); this hiatus encompasses the time interval from 15 to 20 Ma and occurs at an interval of low measured sonic velocities (see "Physical Properties" section, this chapter). Based on the evidence for mass failures and dissolution and the presence of stratigraphic hiatuses, sedimentation in Subunit IB is considered to be noncontinuous.

The upper portion of Subunit IA appears to be a complete section of upper middle Miocene to Pleistocene sediments (see "Biostratigraphy" section, this chapter), which are dominated by nannofossils with varying abundances of foraminifers. Evidence for some carbonate dissolution is seen in foraminifer test preservation, but the carbonate content remains high (Fig. 7) and radiolarian abundances are insignificant.

Microfaulting and distortion of color bands in the upper Miocene interval (42–110 mbsf) and the presence of turbidites at 93, 178, and 180 mbsf indicate the effects of sediment mass-movement processes. Further evidence for mass-wasting and reworking comes from the mixing observed in the biostratigraphic record (see "Biostratigraphy" section, this chapter) and from the incoherent and transparent zones on the seismic reflection

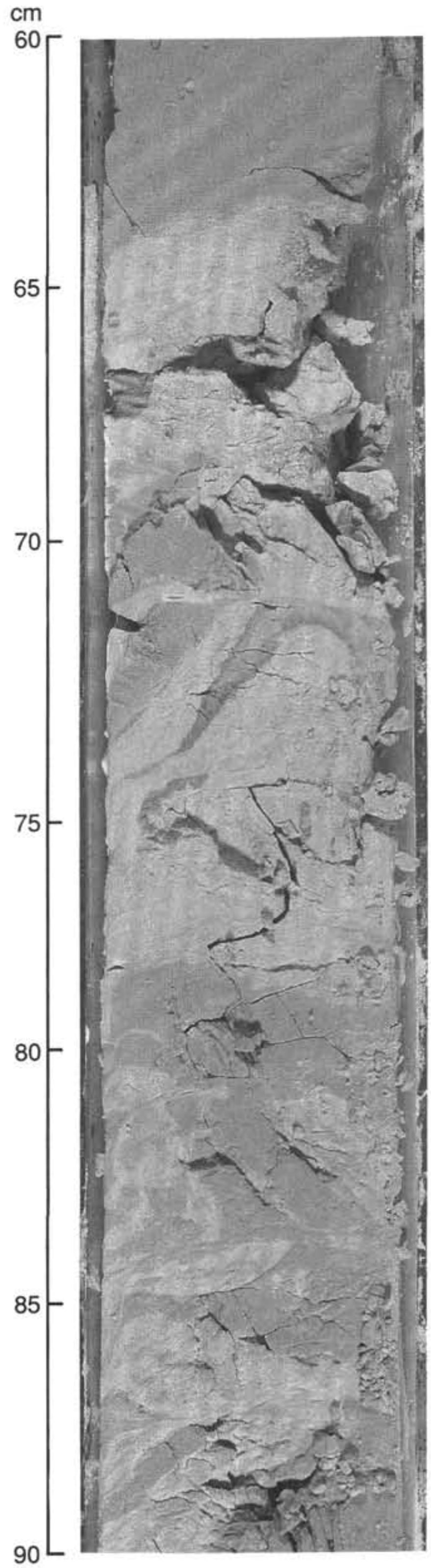

Figure 8. Photograph of disturbed sediment clasts and contorted trace fossils (Section 130-804C-22X-1, 60–90 cm).

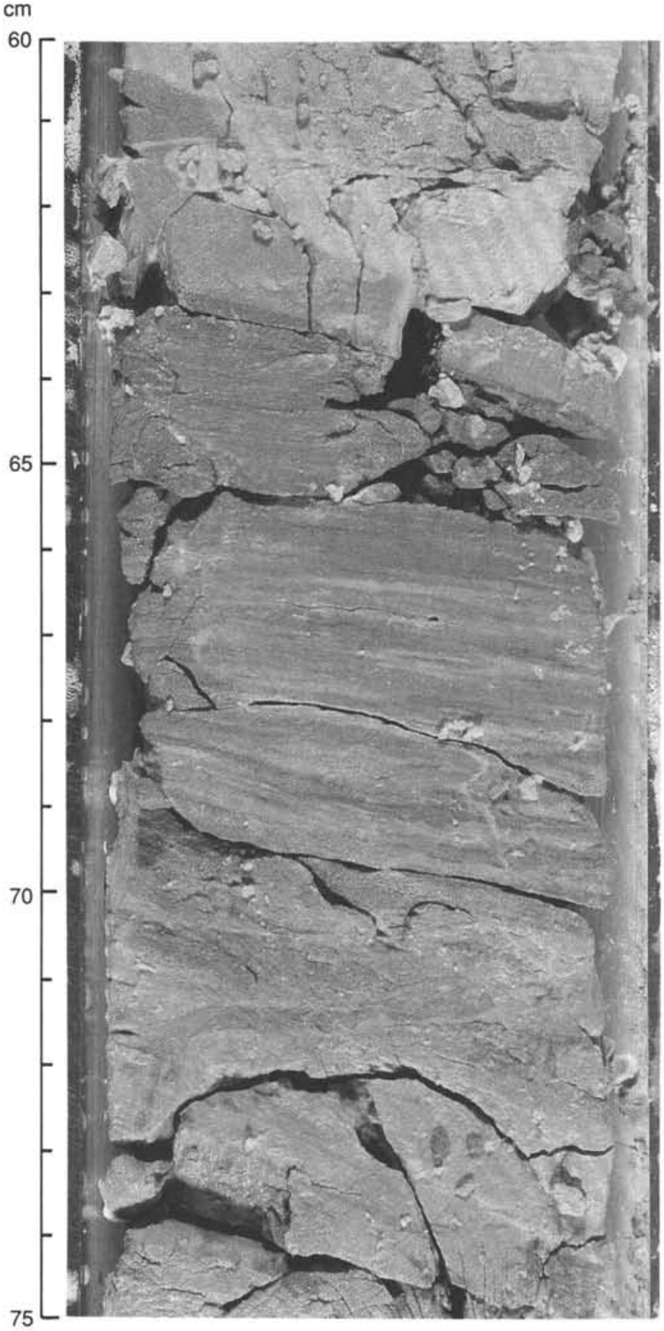

Figure 9. Photograph of distorted color bands or laminae (Section 130-804C-22X-4, 60–75 cm).

profiles taken through the site (see "Seismic Stratigraphy" section, this chapter).

The lithologic and microfossil evidence indicates that carbonate dissolution may have been less severe since the late middle Miocene than before that time. The style of sedimentation, however, which was largely pelagic, biogenic deposition with infrequent slope failures and resedimentation events, remained constant from the late early Oligocene to the Pleistocene.

BIOSTRATIGRAPHY

Introduction

Of the three holes drilled at Site 804, Hole 804A penetrated sediments of Pliocene and Pleistocene age. An apparently com-

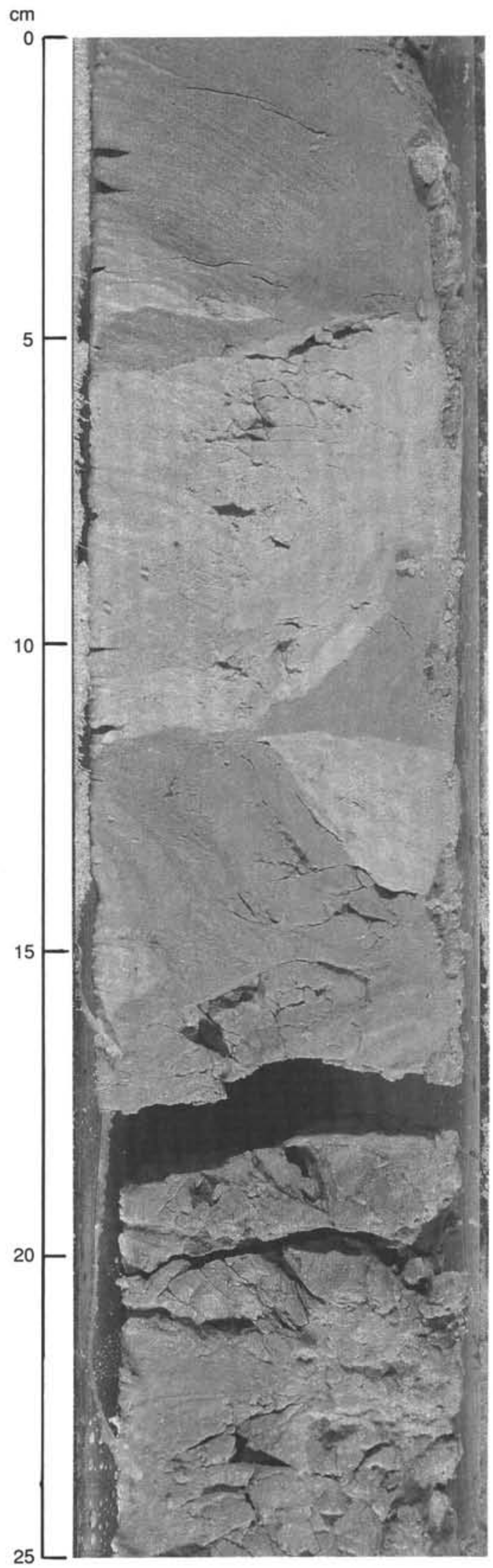

Figure 10. Photograph of angular sediment clasts (Section 130-804C-22X-2, 0–25 cm).

plete sequence was retrieved (Fig. 11). We placed the Pliocene/Pleistocene boundary in Core 130-804A-3H on the basis of planktonic foraminifer, calcareous nannofossil, radiolarian, and diatom evidence.

Hole 804B was drilled to a depth of 137.7 mbsf and penetrated into sediment of late middle Miocene age (Fig. 11). Evidence of downhole contamination and reworking was found in Hole 804B based on evidence from all four fossil groups.

The deepest hole at this site, Hole 804C, penetrated strata of early Oligocene age (Fig. 11). However, we recognized a hiatus at the lower/middle Miocene boundary in this section. The selective dissolution of planktonic foraminifers across this critical interval has removed several important time-diagnostic taxa. The Oligocene/Miocene boundary lies within the interval from Cores 130-804C-27X to -29X (255.1–274.4 mbsf).

Calcareous Nannofossils

Neogene and Oligocene calcareous nannofossil assemblages were recovered from the three holes drilled at Site 804.

Hole 804A

Pleistocene

Sample 130-804A-1H-CC, 0–1 cm, contains abundant *Emiliania huxleyi* together with *Calcidiscus leptoporus, Gephyrocapsa oceanica, Syracosphaera,* and *Umbilicosphaera;* it was placed in Zone NN21. Because of the absence of *E. huxleyi* and *Pseudoemiliania lacunosa,* we assigned Sample 130-804A-1H-CC to Zone NN20. The presence of *P. lacunosa* in Sample 130-804A-2H-CC indicates the Pleistocene Zone NN19. This sample also contains *Reticulofenestra asanoi* (see Sato et al., 1991), which is concentrated in the middle part of Zone NN19, and thus has its range in the upper half of the Matuyama reversed epoch. *Coccolithus pelagicus* and *Discoaster brouweri* were found as high as Samples 130-804A-3H-4, 36–37 cm, and -3H-5, 110–111 cm, respectively. Therefore, the Pliocene/Pleistocene boundary was placed in Core 130-804A-3H.

Pliocene

Sample 130-804A-3H-CC contains *Discoaster brouweri* together with *D. triradiatus;* therefore, this sample was assigned to the uppermost Pliocene Zone NN18. *Discoaster* species in Sample 130-804A-4H-CC consist of *Discoaster brouweri, D. pentaradiatus,* and *D. asymmetricus* and a single specimen of *D. tamalis.* Consequently, we placed this sample in Zone NN17. In contrast to this sample, a diverse discoaster assemblage consisting of such species as *D. asymmetricus, D. brouweri, D. challengeri, D. pentaradiatus, D. surculus, D. triradiatus,* and *D. variabilis* was recognized in Sample 130-804A-5H-CC. This discoaster assemblage, together with the presence of abundant *Reticulofenestra pseudoumbilica* and the absence of *Amaurolithus* species, places Sample 130-804A-5H-CC in Zone NN15. A few beautiful specimens of *D. tristellifer* are also present in this sample. The co-occurrences of *Discoaster quinqueramus, D. berggrenii,* and *Triquetrorhabdulus rugosus* place Sample 130-804A-6H-CC, which is the deepest sample from Hole 804A, in Zone NN11.

Hole 804B

Pleistocene

The nannofossil assemblages of the upper Pliocene and Pleistocene in Hole 804B are similar to those observed in Hole 804A. The extinction of *P. lacunosa* was observed between Sample 130-804B-1H-3, 75 cm, and the core-catcher sample of this core. *Calcidiscus macintyrei* disappears between Samples 130-804B-2H-1, 75 cm, and -3H-1, 74 cm.

Pliocene

Discoaster brouweri and *D. triradiatus* disappear between the 74- and 94-cm levels in Section 130-804B-3H-4, thus placing the Pliocene/Pleistocene boundary in the upper part of Core 130-804B-3H. The NN18/NN17 and NN17/NN18 zonal boundaries fall within Core 130-804B-4H; *D. asymmetricus, D. tamalis,* and *D. variabilis* were observed in Sample 130-804B-4H-CC, placing this sample in the lower half of Zone NN16 (2.9–3.5 Ma). Sample 130-804B-5H-CC contains *Ceratolithus rugosus* and *Discoaster asymmetricus,* together with abundant *Reticulofenestra pseudoumbilica* and sphenoliths, placing this sample in the lower Pliocene. The rare and/or inconsistent occurrences of *D. asymmetricus* and *Amaurolithus* spp. prevent a reliable subdivision of the Zone NN13–NN15 interval in the lower Pliocene. *Cyclicargolithus floridanus* was observed in Sample 130-804B-5H-CC, indicating reworking from Miocene or Oligocene strata.

Miocene

Discoaster quinqueramus was observed from Sample 130-804B-6H-CC through -9H-CC, placing these samples in Zone NN11. The presence of *Discoaster asymmetricus* and several species of ceratoliths, such as *Ceratolithus rugosus* and *C. acutus,* was considered to be the result of downhole contamination. The absence of both *Discoaster quinqueramus* and *Discoaster hamatus* in the two next underlying samples (130-804B-9H-CC and -10H-CC) places these samples in Zone NN10. Sample 130-804B-9H-CC also shows signs of downhole contamination because Pliocene species like *Discoaster tamalis* and *Ceratolithus acutus* are observed within the Miocene Zone NN10 assemblage. One noteworthy character of the Zone NN10 assemblages is the bloomlike, high abundances of small sphenoliths (*Sphenolithus neoabies*?).

Sample 130-804B-11H-CC contains both *Discoaster hamatus* and *Discoaster neohamatus,* whereas Sample 130-804B-12H-CC lacks the latter species. These samples were placed, therefore, in the upper and lower parts of Zone NN9, respectively. Sample 130-804B-13H-CC contains neither *Catinaster coalitus* nor *Sphenolithus heteromorphus,* placing this sample in the NN7–NN6 zonal interval. *Discoaster kugleri* was not observed. The rare and inconsistent occurrences of this species, however, prevent a reliable separation of the NN6 and NN7 Zones. Reworked forms (*Reticulofenestra umbilica* and *Dictyococcites bisectus*) from Eocene or Oligocene strata also occur in Sample 130-804B-13H-CC.

Samples from the two deepest cores of Hole 804B (130-804B-14H-CC and -15H-CC) show mixed assemblages of varying ages. *Discoaster hamatus, Discoaster neohamatus, Catinaster coalitus,* and *Discoaster bellus* represent the late Miocene, whereas *Discoaster druggii* represents the early Miocene, and *Dictyococcites bisectus* must have had an Oligocene or Eocene origin. These taxa are all mixed into sediment of middle Miocene age (Zones NN6/NN7).

Hole 804C

Miocene

The nannofossil assemblages from the Pleistocene to the upper Miocene are similar to those observed in Hole 804B.

We assigned Samples 130-804C-8H-CC through -10H-CC to Zone NN10 because *Discoaster quinqueramus* and *Discoaster hamatus* are both absent in an otherwise early late Miocene assemblage that contains exceptionally abundant sphenoliths, for example. The underlying Zone NN9 interval is remarkably thick, lasting from Samples 130-804C-11H-CC through -16H-CC. The last occurrence (LO) of *Catinaster* spp. was observed between

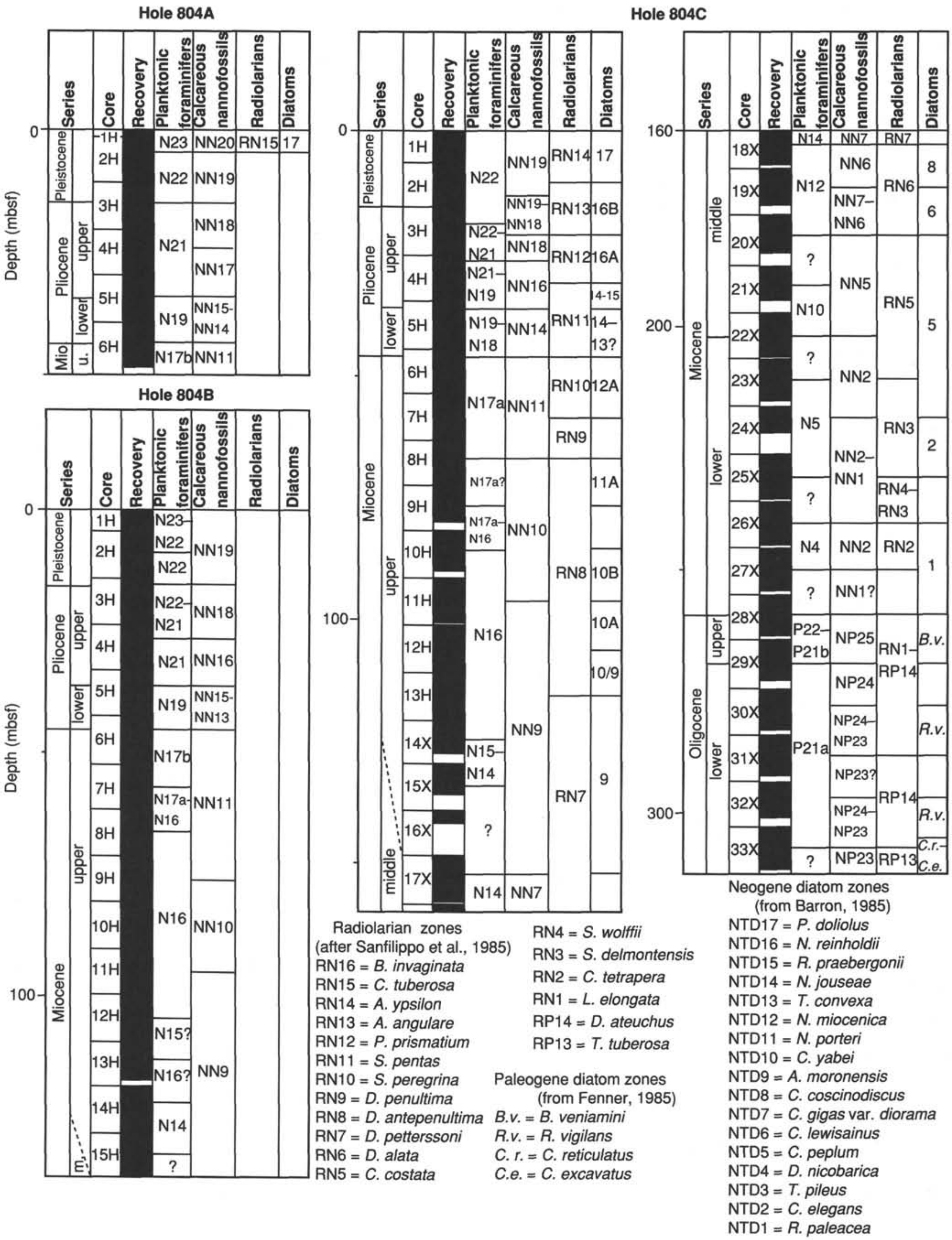

Figure 11. Biostratigraphic hole summaries, Site 804. RN = radiolarian Neogene zone, NTD = Neogene tropical diatom zone, RP = radiolarian Paleogene zone, and NN = nannofossil Neogene zone.

Samples 130-804C-10H-CC and -11H-CC, the first occurrence (FO) of *Discoaster neohamatus* was observed between Samples 130-804C-14X-CC and -15X-CC, and the FO of *Catinaster calyculus* was observed between Samples 130-804C-16X-CC and -17X-CC.

Sample 130-804C-16X-CC is characterized by strong dissolution. The fairly dissolution-resistant discoasters, therefore, are concentrated in abundance and show little or no evidence of secondary overgrowth. Rare *Discoaster kugleri* were observed in Sample 130-804C-17X-CC, placing this sample within Zone NN7. The two next deeper samples (130-804C-18X-CC and -19X-CC) were placed in Zone NN6, not so much because of the absence of *Discoaster kugleri*, which clearly is an unreliable biostratigraphic marker in the Ontong Java Plateau area, but rather because of the LO of *Coronocyclus nitescens* in Sample 130-804C-18X-CC.

Sample 130-804C-20X-CC contains abundant *Sphenolithus heteromorphus* and common *Cyclicargolithus floridanus*, together with other typical early middle Miocene assemblage components, such as *Discoaster deflandrei, Coccolithus miopelagicus*, and *Reticulofenestra pseudoumbilica*. The presence of the last species together with *S. heteromorphus* indicates that this sample belongs to the uppermost part of Zone NN5, because the top of this zone contains the evolutionary FO of "normal-sized" *Reticulofenestra pseudoumbilica* (>7 μm).

We also observed that sphenoliths, including *S. heteromorphus*, were abundant in Sample 130-803C-21X-CC. The lack of *Helicosphaera ampliaperta* in Miocene sediments in the Ontong Java region (see also Shafik, 1973) prevents the subdivision of the NN4/NN5 zonal interval. The presence of *Reticulofenestra pseudoumbilica* in Sample 130-803C-21X-CC, however, suggests that this sample represents the upper part of Zone NN5.

Sample 130-803C-22X-CC lacks *Sphenolithus heteromorphus* and *Sphenolithus belemnos*, but it does contain such characteristic lower Miocene species as *Triquetrorhabdulus carinatus* and *Triquetrorhabdulus milowii*, as well as the ubiquitous lower Neogene taxa, *Discoaster deflandrei* and *Cyclicargolithus floridanus*. This implies that perhaps as much as 10% of the lower Neogene is represented in Core 130-803C-22X or that a hiatus is present. The latter seems to be true because *Sphenolithus heteromorphus* is missing already 8 cm into the top of that core. This hiatus across the lower/middle Miocene boundary in Hole 804C has a similar extension to that observed in Hole 803D.

Triquetrorhabdulus carinatus increases in abundance in Core 130-803C-24X, and *Discoaster druggii* was observed in Sample 130-803C-26X-CC, indicating a position within Zone NN2 and above the Oligocene/Miocene boundary. Reliable nannofossil markers for the Oligocene/Miocene boundary are missing in the Ontong Java region. When considering the position of the FO of *Discoaster druggii* and the fact that *Sphenolithus ciperoensis* has its LO in Core 130-803C-29X, which gives this core a position well into the Oligocene, it follows that the Oligocene/Miocene boundary must lie within the two intervening cores.

The presence of intergrading morphotypes within the sphenolith lineage used in Oligocene zonal schemes usually results in poor biostratigraphic precision when determining zonal boundaries (see recent reviews by Okada, 1990; Fornaciari et al., 1990). Unfortunately, this problem also affects the Oligocene biostratigraphy of Leg 130 sediments. Thus, the NP24/NP25 zonal boundary was tentatively placed in Core 130-804C-31X because of the presence of *Sphenolithus distentus* in the core-catcher sample. *Sphenolithus* cf. *S. ciperoensis* was observed in Sample 130-804C-32X-CC, together with *Sphenolithus distentus*, suggesting a position within Zone NP24.

Hole 804C reached its terminal depth at Sample 130-804C-33X-CC, a sample that also contains *Sphenolithus predistentus* and *Sphenolithus pseudoradians*, abundant *Coccolithus pelagicus, Cyclicargolithus floridanus*, few *Discoaster tanii*, and *Coccolithus eopelagicus*. This sample was assigned to Zone NP23 of the lower Oligocene.

Planktonic Foraminifers

The preservation of the abundant planktonic foraminifers in Hole 804A ranges between moderate and poor. The time span represented in the six cores retrieved covers the interval from Zone N22 (Pleistocene) to Zone N17b (just below the Miocene/Pliocene boundary). Figure 11 illustrates the stratigraphic distribution of the planktonic foraminifers recovered from Site 804.

The Pleistocene section in this site is characterized by a diverse assemblage of planktonic foraminifers with clear tropical affinities. Sample 130-804A-1H-CC does not contain *Globorotalia tosaensis* and so is of latest Pleistocene age (upper N22). The co-occurrence of *G. tosaensis* and *Globorotalia truncatulinoides* in Sample 130-804A-2H-CC indicates a lower Pleistocene age within Zone N22.

The Pliocene/Pleistocene boundary, as defined by the presence of planktonic foraminifers, is within Core 130-804A-3H as Sample 130-804A-3H-CC does not contain specimens of *G. truncatulinoides*. We referred Samples 130-804A-3H-CC and -4H-CC to Zone P21 in the upper Pliocene, and we placed Sample 130-804A-5H-CC in Zone N18 on the basis of the presence of *G. tumida* in the absence of *Sphaeroidinella dehiscens*. Sample 130-804A-6H-CC was assigned to Zone N17b based on the presence of *Pulleniatina primalis*. Given the distribution of this species, it appears that part of the Pliocene (Zones 19/20) is missing in the recovered section or has failed to be resolved with a sampling density of one sample per core.

The abundance and preservation of planktonic foraminifers in Hole 804B is highly variable. The total age range of the 15 cores retrieved at this hole covers the time interval from the early Pleistocene (N22) to the late middle Miocene (N14). The fauna in Sample 130-804B-1H-CC lacks *G. truncatulinoides* and *G. tosaensis;* however, Sample 130-804B-2H-CC is placed in Zone N22 (Pleistocene). The co-occurrence of *G. truncatulinoides* and *Globigerinoides fistulosus* indicates a latest Pliocene age for Sample 130-804B-3H-CC, although it is still within Zone N22. Sample 130-804B-4H-CC was assigned to Zone N21. It is not possible to assign a zone to Sample 130-804B-5H-CC.

Sample 130-804B-6H-2, 135–137 cm, was placed within Zone N19, whereas the core catcher from the same section was assigned to Zone N17. This implies either the presence of a hiatus covering much of the Pliocene within Core 130-804B-6H or insufficient sampling resolution, as noted in Hole 804A. Zone N16 was expanded in this hole, and time-diagnostic fossils of this interval (the absence of *Globorotalia plesiotumida* and the presence of *Neogloboquadrina acostaensis*) were found from Samples 130-804B-7H-CC through -13H-CC. Sample 130-804B-12H-CC was difficult to date because of the poor preservation. We assigned Sample 130-804B-14H-CC to Zone N14 based on the presence of *Globorotalia siakensis*. Hence, the implication is that Zone N15 is either missing in this hole or was missed in our preliminary core-catcher examination.

Hole 804C is the deepest hole drilled at this site and covers the interval from the Pleistocene (N22) to the early Oligocene (P21b). The abundance of planktonic foraminifers declines downhole, reaching a minimum between Samples 130-804C-21X-CC and -28X-CC. Further downhole, the abundance of the planktonic foraminifers increases. The preservation of planktonic foraminifers is variable in Hole 804C, but it is best between Samples 130-804C-12H-CC and -15H-CC. The poorest preservation occurs between Samples 130-804C-16H-CC and -24X-CC.

Samples 130-804C-1H-CC through -3H-CC are of Pleistocene age within Zone N22. Sample 130-804C-4H-CC was placed in lower Zone N21 or upper Zones N19–N20. As was the case with the previous two holes at this site, much of the Pliocene of Zone N19/N20 appears to be missing or condensed. Sample 130-804C-5H-CC was assigned to Zone N18 because of the presence of *Globorotalia tumida* and the lack of *Sphaeroidinella dehiscens.* Zone N17a occupies Samples 130-804C-6H-CC through -9H-CC because the index species for Zone N17b (*Pulleniatina primalis*) was not observed. Samples 130-804C-10H-CC to -13H-CC were assigned to Zone N16 based on the absence of *G. plesiotumida* and the presence of *N. acostaensis.*

It was not possible to assign an age to Sample 130-804C-14X-CC because of the downhole contamination that is evident (the presence of *Neogloboquadrina humerosa* and *N. acostaensis* in a sample containing *G. siakensis* is particularly revealing in this regard). Sample 130-804C-15X-CC is partially dissolved and devoid of age-diagnostic planktonic foraminifer taxa, and Sample 130-804C-16X-CC is barren of foraminifers, implying that dissolution intensified. Sample 130-804C-17X-CC also shows evidence of downhole contamination with the co-occurrence of *G. siakensis* and *N. acostaensis.* Sample 130-804C-18X-CC is of Zone N12 age, based on the presence of *Globorotalia fohsi lobata,* and Sample 130-804C-19X-CC was assigned to Zone N12 based on the presence of *Globorotalia fohsi.* The poor preservation in Sample 130-804C-20X-CC precluded a zonal assignment.

The poor preservation inherent in this portion of Hole 804C probably has selectively removed more delicate morphotypes, as suggested by the low diversity of foraminifers in Sample 130-804C-21X-CC. Hence, the presence of *Globorotalia* cf. *peripheroacuta* suggests an age range of Zones N10 through N12, but the more delicate *Globorotalia praefohsi,* which would indicate Zone N11, may have been dissolved out of the sample. Poor preservation in Sample 130-804C-22X-CC has reduced species diversity to only the most robust members of the fauna. This sample contained only single specimens each of the species *Globorotalia venezuelana* and *Sphaeroidinella disjuncta.* It was not possible, therefore, to assign an age to it.

Samples 130-804C-23X-CC and -24X-CC were assigned to Zone N5. The lack of age-diagnostic fossils in 130-804C-25X-CC precluded an age assignment for this sample. Sample 130-804C-26X-CC was assigned to Zone N4 based on the presence of *Globorotalia kugleri.* Samples 130-804C-27X-CC and -28X-CC are barren of planktonic foraminifers. Samples 130-804C-29X-CC to -32X-CC are of early Oligocene age (Zone P21a), based on the presence of *Globorotalia opima.* Sample 130-804C-33X-CC is barren. Much of the upper Oligocene is missing at this site.

Diatoms

We also examined diatoms in Hole 804C and found that Quaternary through Oligocene specimens were present. The assignment of samples to low-latitude diatom zonation is summarized in Figure 11.

Above 101.3 mbsf (Cores 130-804C-1H to -11H), diatoms are common to abundant, and preservation is generally good. Below Sample 130-804C-11H-CC, diatoms are less abundant and preservation is generally poor to moderate. Diatoms decreased sharply in abundance and preservation from Samples 130-804C-27X-CC (lowest early Miocene) through -30X-CC (early Oligocene). This interval contains only sparse, poorly preserved diatoms that are difficult to assign to any particular zone. Thereafter, diatoms increase in abundance again, and preservation is good from Sample 130-804C-32X-CC to the base of the hole.

As at Site 803, the sequence is complete from the Quaternary NTD 17 *Pseudoeunotia doliolus* Zone (Sample 130-804C-1H-CC) through the lower middle Miocene NTD 5 *Cestodiscus peplum* Zone (Sample 130-804C-22X-CC). At this point, we observed a break in the sequence, and Sample 130-804C-24X-CC was assigned to the NTD 2 *Craspedodiscus elegans* Zone. The sequence is complete from the lower middle Miocene through the early Oligocene (Sample 130-804C-33X-CC). Two diatom zones, NTD 4 *Denticulopsis nicobarica* and NTD 3 *Triceratium pileus,* are completely missing at Site 804; therefore, a hiatus in the early Miocene has been suggested to account for this gap (see "Biostratigraphy" section, "Site 803" chapter, this volume).

Sample 130-804C-1H-CC was assigned to the NTD 17 Zone. The Pliocene/Pleistocene boundary is located in the NTD 16 *Nitzschia reinholdii* Zone (Samples 130-804C-2H-CC and -3H-CC) and is coincident with a peak in the abundance of *Thalassiosira oestrupii.*

Sample 130-804C-4H-CC was placed in the late Pliocene TD 15 *Rhizosolenia praebergonii* Zone (Subzone A). The LO of *Nitzschia jouseae* falls within Subzone A. Sample 130-804C-4H-CC is contaminated with Pleistocene specimens. The Miocene species *Coscinodiscus nodulifer* var. *cyclopus* is present in Samples 130-804C-5H-CC and -6H-CC and is probably reworked. The Pliocene/Miocene boundary could not be identified with the present sampling resolution.

The presence of *Nitzschia miocenica* and the absence of members of the *Thalassiosira convexa* group allowed us to assign Sample 130-804C-6H-CC to the NTD 12 *N. miocenica* Zone, Subzone A. The overlap between the FO of *N. miocenica* and the LOs of *Nitzschia porteri* and *Rossiella paleacea* and the presence of *Thalassiosira burckliana* is noted in Sample 130-804C-8H-CC. This sample was assigned to the NTD 11 *N. porteri* Zone, base of Subzone A, with some uncertainty.

The NTD 10 *Coscinodiscus yabei* Zone extends over Cores 130-804C-10H (Subzone B: *T. burckliana* present) and 130-804C-11H (Subzone A: *Coscinodiscus temperei* var. *delicata* present). The LOs of *Actinocyclus moronensis* and *Denticulopsis hustedtii* and the FO(?) of *Coscinodiscus vetustissimus* var. *javanicus* were observed in Sample 130-804C-12H-CC. Samples 130-804C-13H-CC through -16X-CC were assigned to the NTD 9 *Actinocyclus moronensis* Zone (middle Miocene/late Miocene boundary). Sample 130-804C-18X-CC is contained in the NTD 8 *Craspedodiscus coscinodiscus* Zone. In Hole 804C the LOs of *Synedra jouseana, Actinocyclus ingens,* and *Actinocyclus ellipticus* var. *spiralis* also fall within this zone.

The LOs of *Coscinodiscus lewisianus* and *Cestodiscus pulchellus* were recorded in Sample 130-804C-19X-CC. Sample 130-804C-20X-CC falls within Subzone B of the NTD 5 *Cestodiscus peplum* Zone, and Sample 130-804C-22X-CC is within Subzone A, which contains *Annellus californicus.* The middle Miocene/early Miocene boundary is also contained within Subzone A.

The LO of *Craspedodiscus elegans* (NTD 2 Zone) was found in Sample 130-804C-24X-CC. In Sample 130-804C-26X-CC, the next downcore sample analyzed, *Rosiella paleacea* and *Borgorovia veniamini* are common, and *Coscinodiscus oligocenicus* and *C. lewisianus* var. *rhomboides* are present. *Thalassiosira primalabiata* is present in Sample 130-804C-27X-CC. The presence of this flora allowed us to assign this interval to the NTD 1 *Rosiella paleacea* Zone.

The *Rocella gelida* Zone seems to be missing or compressed at Hole 804C. Therefore, we could not identify the Miocene/Oligocene boundary. However, *Rocella vigilans* becomes abundant in Sample 130-804C-28X-CC and remains common throughout Sample 130-804-32X-CC. *Borgorovia veniamini* is also present in Sample 130-804C-28X-CC. Preservation in Cores 130-804C-28X through -30X is too poor to allow recognition of the subzones of the *R. vigilans* Zone.

Sample 130-804C-33X-CC contains lower Oligocene flora and was placed in the *Cestodiscus reticulatus–Coscinodiscus excavatus* Zones sensu Fenner (1985) and the *C. excavatus* Zone sensu Barron (1985).

Radiolarians

Radiolarians examined from core-catcher samples at Holes 804A and 804C range in age from the Pleistocene in the uppermost cores to the Oligocene at the base of Hole 804C (312.5 mbsf). The following discussion is based on the zonal assignment of stratigraphically important taxa examined in core-catcher samples. Also discussed is the state of radiolarian preservation. The radiolarian zonation of Hole 804C and the correlation of these zonations with other taxa is summarized in Figure 11. The radiolarian biostratigraphic data from this site show a sequential zonal succession throughout the Neogene and the Oligocene, except for one zone that was not recorded (between Samples 130-804C-22X-CC and -23X-CC).

Pleistocene

Sample 130-804A-1H-CC was assigned to the *Collosphaera tuberosa* Zone of the late Pleistocene as it contains *C. tuberosa, Lamprocyrtis nigriniae,* and *Theocorythium trachelium trachelium,* key taxa to this zone. Core 130-804C-1H-CC, however, does not contain either *C. tuberosa* or *T. t. trachelium,* but one specimen of *L. nigriniae* was found. Therefore, this sample belongs to the *Amphirhopalum ypsilon* Zone. The next lower sample (130-804C-2H-CC) was assigned to the *Anthocyrtidium angulare* Zone of the lower Pleistocene because *A. angulare, Lamprocyrtis neoheteroporos,* and *T. t. trachelium* are present.

Pliocene

The LO of *Pterocanium prismatium* was recorded in Sample 130-804C-3H-CC together with the presence of *Lamprocyrtis heteroporos* (FO) as well as *Spongaster tetras* and *Didymocyrtis tetrathalamus,* which lead us to assign this sample to the *P. prismatium* Zone. The specimen of *Calocycletta virginis* found in this sample is either the result of reworking or contamination. The LO of *Stichocorys peregrina* was located in Sample 130-804C-4H-CC. The presence of *D. tetrathalamus, P. prismatium,* and *Anthocyrtidium jenghisi* leads to an assignment of this sample to the *Spongaster pentas* Zone.

The next lower sample (130-804C-5H-CC) contains the LOs of *Phormostichoartus doliolum* and *Didymocyrtis avita* as well as the presence of *S. pentas* and *P. prismatium.* One specimen of *Diartus hughesi* and a few specimens of *Didymocyrtis avita* found in this sample are probably the result of reworking. This sample was placed in the *S. tetras* Zone. Sample 130-804C-6H-CC was placed in the *Stichocorys peregrina* Zone as it contains the LO of *Spongaster berminghami* and the presence of *S. peregrina, S. delmontensis, D. avita,* and *Solenosphaera omnitubus.* This zone extends from 4.3–4.4 to 6.1–6.7 Ma and contains the Miocene/Pliocene boundary.

Late Miocene

We assigned Sample 130-804C-7H-CC to the *Didymocyrtis penultima* Zone mainly because of the presence of *S. omnitubus,* although *Didymocyrtis antepenultima* and *D. laticonus* are also present, most likely the result of reworking. Sample 130-804C-8H-CC was unambiguously placed in the *Didymocyrtis antepenultima* Zone because abundant *S. peregrina, D. laticonus,* and *D. hughesi* as well as common *S. delmontensis* and rare *Dictyocoryne ontogenesis* are present. This zone continues through Sample 130-804C-12H-CC.

Middle Miocene

Sample 130-804C-13H-CC was placed in the *Diartus petterssoni* Zone based on the occurrences of *Lithopera thornburgi, Liriospyris elevata, Stichocorys wolffii,* and *D. petterssoni.* The specimen of *Lithopera renzae* found in this sample is considered to be reworked. Samples 130-804C-14H-CC and -16H-CC were also assigned to this zone. Sample 130-804C-18X-CC is considered to be in the *Calocycletta alata* Zone because of the presence of *D. laticonus, Lithopera neotera, L. renzae,* and *S. wolffii.*

Abundant specimens of *Stichocorys* cf. *peregrina* are present in this sample, but *S. peregrina* is thought to be extinct slightly before 7.2 Ma (Shipboard Scientific Party, 1989). Thus, it should not be placed in this sample but, rather, assigned to the *D. antepenultima* Zone or to a younger zone. An alternative explanation is that *Stichocorys* cf. *peregrina* is a form quickly evolved from *S. delmontensis,* which went extinct soon after. Therefore, this form is considered to be a variant of *S. delmontensis* or a taxon other than *S. peregrina.*

Early Miocene

Sample 130-804C-20X-CC belongs to the upper part of the *Calocycletta costata* Zone as *Dorcadospyris dentata* (LO), *D. forcipata* (LO), *Lithospyris parkerae,* and *Didymocyrtis violina* are present. This zone continues into Sample 130-804C-22X-CC. The *Stichocorys wolffii* Zone, the next sequential radiolarian zone, was not recorded in either Sample 130-804C-22X-CC or -23X-CC. Therefore, it is possible that a hiatus exists within Core 130-804C-23X. Sample 130-804C-23X-CC was placed in the *Stichocorys delmontensis* Zone, the next lower zone, as this sample contains the LO of *D. ateuchus* and the FO of *Cyclampterium leptetrum.* Sample 130-804C-24X-CC is also in the same zone.

The next lower sample examined (130-804C-26X-CC) is bracketed by the FO of *Cyrtocapsella cornuta* and the LO of *Theocyrtis annosa,* which leads to the *Cyrtocapsella tetrapera* Zone. It should be noted that the FOs of *S. delmontensis, D. violina,* and *Lychocanoma elongata* were all recorded in this sample, which indicates that the ranges of the former two taxa extend into this zone rather than end at the bottom of the *S. delmontensis* Zone (Sanfilippo et al., 1985).

Sample 130-804C-27X-CC contains *D. ateuchus, T. annosa,* and *Dendrospyris bursa* and the LO of *Artophormis gracilis,* which places this sample in the *Lychocanoma elongata* and/or *D. ateuchus* Zone. According to Nigrini and Lombari (1984), *D. bursa* ranges from the *L. elongata* Zone in the late Oligocene to the *D. alata* Zone in the middle Miocene, based on a study in the western tropical Pacific. However, several stratigraphically deeper samples, assignable to the Oligocene, contain this species. Therefore, we conclude that the range of this species is older than previously thought (see below for documentation of this taxon).

Sample 130-804C-28X-CC belongs to the lower part of the *L. elongata* Zone and to the upper part of the *D. ateuchus* Zone as four specimens of *Dorcadospyris papilio* were found, in addition to the presence of *Dorcadospyris forcipata, D. ateuchus,* and *D. praeforcipata* in the >250-μm size fraction. (Several samples of this age were specifically processed with either the 125- or 250-μm sieve in addition to a 63-μm sieve because of the large size of the species belonging to the genus *Dorcadospyris.*) Sample 130-804C-29X-CC cannot be differentiated from either the *L. elongata* or the *D. ateuchus* zones because this sample only contains such taxa as *A. gracilis, D. ateuchus, D. forcipata,* and *T. annosa.* Sample 130-804C-30X-CC was placed in the *L. elongata* or *D. ateuchus* zones based on the presence of *D. ateuchus, C. pegetrum,* and *D. bursa.*

Oligocene

Sample 130-804C-31X-CC was unambiguously placed in the *D. ateuchus* Zone because of the presence of *D. ateuchus, D. forcipata, Theocyrtis annosa,* and *Lithocyclia angusta.* One specimen of *Dorcadospyris triceros* recorded in this sample is present in the next older zone. This specimen is considered to be an evolutionary form because the change from *D. triceros* to *D. ateuchus* is an evolutionary transition. Sample 130-804C-32X-CC was assigned to the *D. ateuchus* Zone as it contains *D. ateuchus, D. forcipata, C. pegetrum,* and *T. annosa.* One specimen of *Dorcadospyris triceros* found in this sample is probably the result of evolutionary transition.

Abundant *Centrobotrys petrushevskayae* in this sample (observed continuously from Sample 130-804C-23X-CC downward) warrants further study in revising the ranges of this taxon, as it is should be present only in the lower part of the *Theocyrtis tuberosa* Zone of the Oligocene. Based on data from this site alone, the younger limit of *C. petrushevskayae* extends to the *S. delmontensis* Zone. Sample 130-804C-33X-CC, from the last core in the hole, was assigned to the *T. tuberosa* Zone because of the presence of *Dorcadospyris pseudopapilio* and *Lithocyclia crux. D. bursa,* also found in this sample, ranges from the *T. tuberosa* Zone (FO) to the *S. delmontensis* Zone (LO) and revises the published range of Nigrini and Lombari (1984).

Preservation

The preservation of radiolarians at this site is generally better than that of specimens studied at Site 803. Site 804 (3920 m) is 520 m deeper than Site 803 (3400 m), resulting in significantly greater dissolution of both calcareous nannoplankton and planktonic foraminifers at this site. This, in turn, may have provided higher concentrations of cations (e.g., Fe, Mn, and Al) remineralized from biogenic minerals in interstitial waters. Although the sedimentation rate at this site is less than that at Site 803, the predicted higher concentrations of these elements may have resulted in increased cation coating and, hence, a lower rate of silica dissolution; this hypothesis is supported by the better preservation of diatoms at Site 804 than at 803.

As at Site 803, the preservational state of radiolarians deteriorates in the older samples. Generally, Pleistocene and Pliocene radiolarians are well preserved and early Miocene and Oligocene radiolarians are poorly preserved. It appears that once the biogenic opal contents of the sediment decrease beyond a critical level, siliceous fossils start dissolving at a higher rate, thereby resulting in poorer preservation. This may be related to changes in paleoproductivity that controlled supply rates of biogenic opal to the seafloor.

PALEOMAGNETISM

Introduction

Pass-through cryogenic magnetometer measurements were conducted on all cores from the three holes drilled at Site 804. As at Site 803, the Pliocene-Pleistocene sequence yielded stable magnetizations after alternating field (AF) demagnetization, from which a detailed magnetostratigraphy was recognized (Fig. 12). Intensities diminished in all three holes from average values of 1–10 mAm^{-1} above Cores 130-804A-6H, 130-804B-6H, and 130-804C-6H to values generally <0.1 mAm^{-1} below Cores 130-804A-7H, 130-804B-7H, and 130-804C-7H; this drop in intensity corresponds to an age of about 5 Ma. Reduced natural remanent magnetization (NRM) intensities, and the presence of a steeply inclined viscous overprint probably originating during drilling, precluded any interpretation of the Miocene sequence.

Measurements were taken at 3- and 5-cm intervals throughout the Quaternary and Pliocene sequence, but the interval was increased to 10 cm in the weakly magnetized Miocene sequence. The NRM was measured on all cores as well as the magnetization after 15-mT AF demagnetization on all but the most weakly magnetized cores.

Multishot orientations were carried out on Cores 130-804A-3H to -6H, 130-804B-3H to -6H, and 130-804C-3H to -13H. Careful examination of the multishot tool by the drilling team after each use largely avoided the orientation problems encountered at Site 803, but orientation errors nevertheless appeared to affect Cores 130-804B-4H and 130-804C-13H. The declinations of intervals of the same polarity frequently increase by about 20°–30° from the top to the base of a core (e.g., Core 130-804A-3H; Fig. 13); this is evidently a result of rotation within the core barrel, either during or after drilling. An additional error arose through the formation of air bubbles within the multishot magnetic compass. Core orientations are based on a photographic image of this compass, and bubbles obscured this record to the extent that some core orientations were uncertain by as much as ±20°.

Section 130-804A-4H-2 was cut along the wrong orientation lines, resulting in an incorrect reference declination; this was corrected in constructing the magnetostratigraphy.

Pliocene-Pleistocene Magnetostratigraphy

Magnetostratigraphic columns were constructed for each of the three holes (Fig. 12) and were generally in good agreement with each other. Cores 130-804A-1H and -2H, 130-804B-1H and -2H, and 130-804C-1H and -2H were unoriented; their polarities were inferred by extension from the polarity sequence of the underlying oriented cores. No coherent polarity record could be recognized below Core 6H in all three holes. Holes 804A and 804B preserve nearly complete polarity records over the Brunhes, Matuyama, and Gauss chrons. Continuous magnetostratigraphy in Hole 804B may extend as far as the Nunivak Subchron in the Gilbert Chron. Interruptions to the magnetostratigraphic record in Hole 804C (the result of disturbed sections in Cores 130-804C-4H and -5H) limit the resolution of the Gauss and Gilbert chrons in this hole.

Preservation of major polarity events is good in all three holes. We identified the Jaramillo and Olduvai subchrons within the Matuyama Chron and the Kaena and Mammoth subchrons within the Gauss Chron in all three holes. Near the base of Core 130-804B-5H, we could also identify the Cochiti Subchron of the Gilbert Chron. A short but prominent normal polarity event occurs within the Matuyama Chron at a similar stratigraphic level in all three holes at this site; this probably represents one of the two normal events within the Réunion Subchron, but which one is not clear.

A short interval of intermediate polarity overlies the prominent Réunion Event in both Holes 804A and 804B (Fig. 13). This may correspond to the upper Réunion Event, but no corresponding event is present in Hole 804C. An interval of intermediate polarity, which may correspond to the lower Réunion Event, occurs between 23.8 and 24.5 mbsf in Hole 804C. Correct identification of the Réunion events is important, as they occur near the time a change in sedimentation rate is indicated by the magnetostratigraphy of Site 803. The correlation indicated in Figure 12 results in the simplest pattern of change in the sedimentation rate, and so is preferred here, at least for Holes 804A and 804B.

The oldest polarity event that can be definitely correlated among the holes is the Cochiti Subchron, between 42.5 and 41.7 mbsf in Hole 804B. Greater than 100% recovery leads to an overlap of about 30 cm between the sub-bottom depths indicated for the base of Core 130-804B-5H and the top of Core 130-804B-6H. Within this overlap, the polarity indicated in Core 130-804B-5H is reversed, whereas in Core 130-804B-6H it is normal. It is possible that a very short normal polarity event has been recovered here. Alternatively, either some recovery may have been lost, or the section is locally compressed, so that the Nunivak Subchron is represented by only a 50-cm interval, and the lowest interval recorded in this hole is the Sidufjall Subchron.

Intensities decrease rapidly below 43–45 mbsf in all three holes, dropping by an order of magnitude over a few meters. Core 130-804A-6H appears to record a pattern of continuous

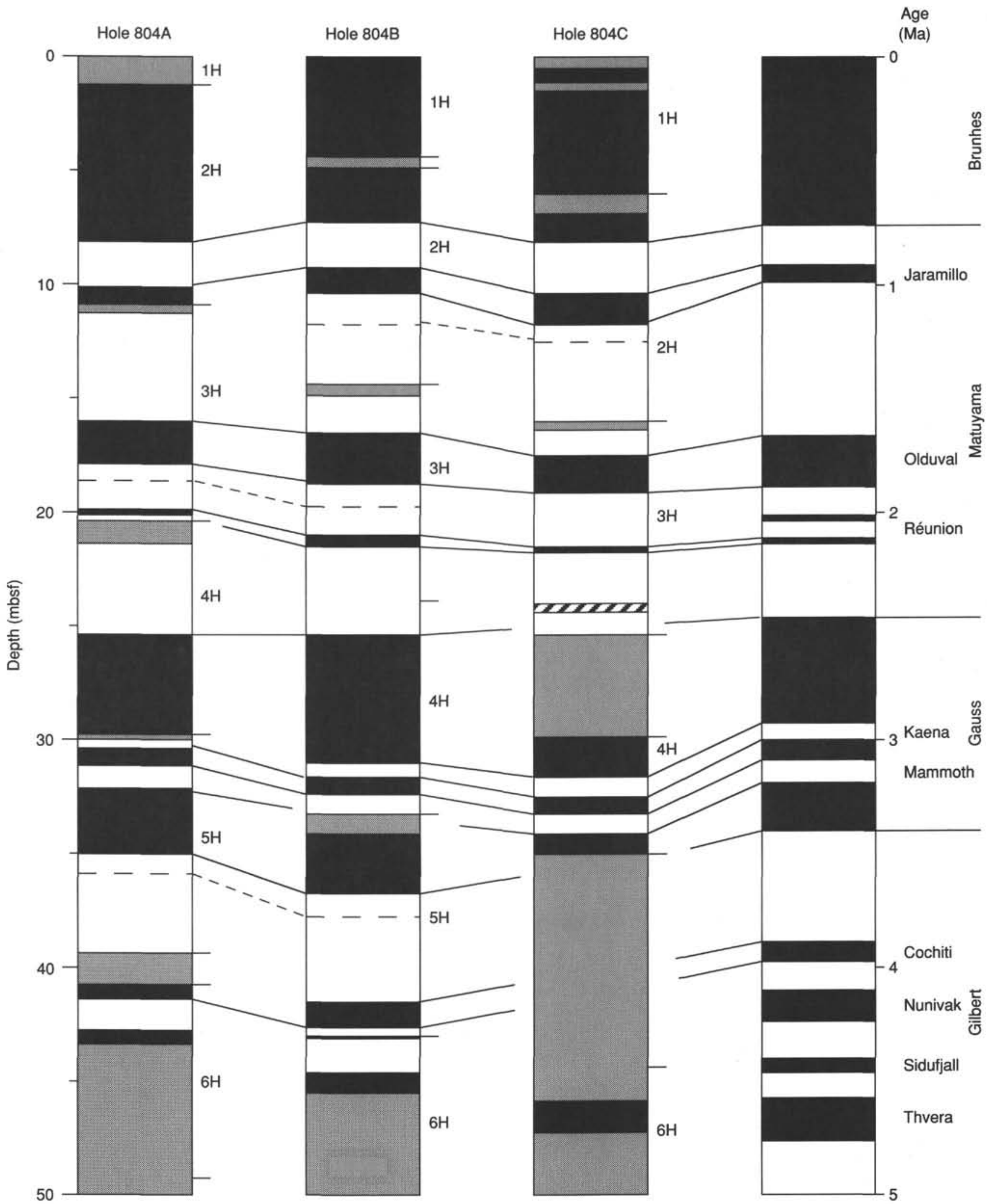

Figure 12. Magnetostratigraphic columns for holes at Site 804, with a reference magnetostratigraphy after Berggren et al. (1985). Black intervals indicate normal polarization; white, reverse polarization. Half-tone shading indicates unknown polarity. Dashed lines within columns are short events; diagonally hatched interval is of intermediate polarity. Confident ties between columns are shown by an unbroken line; dashed lines indicate ties between minor events.

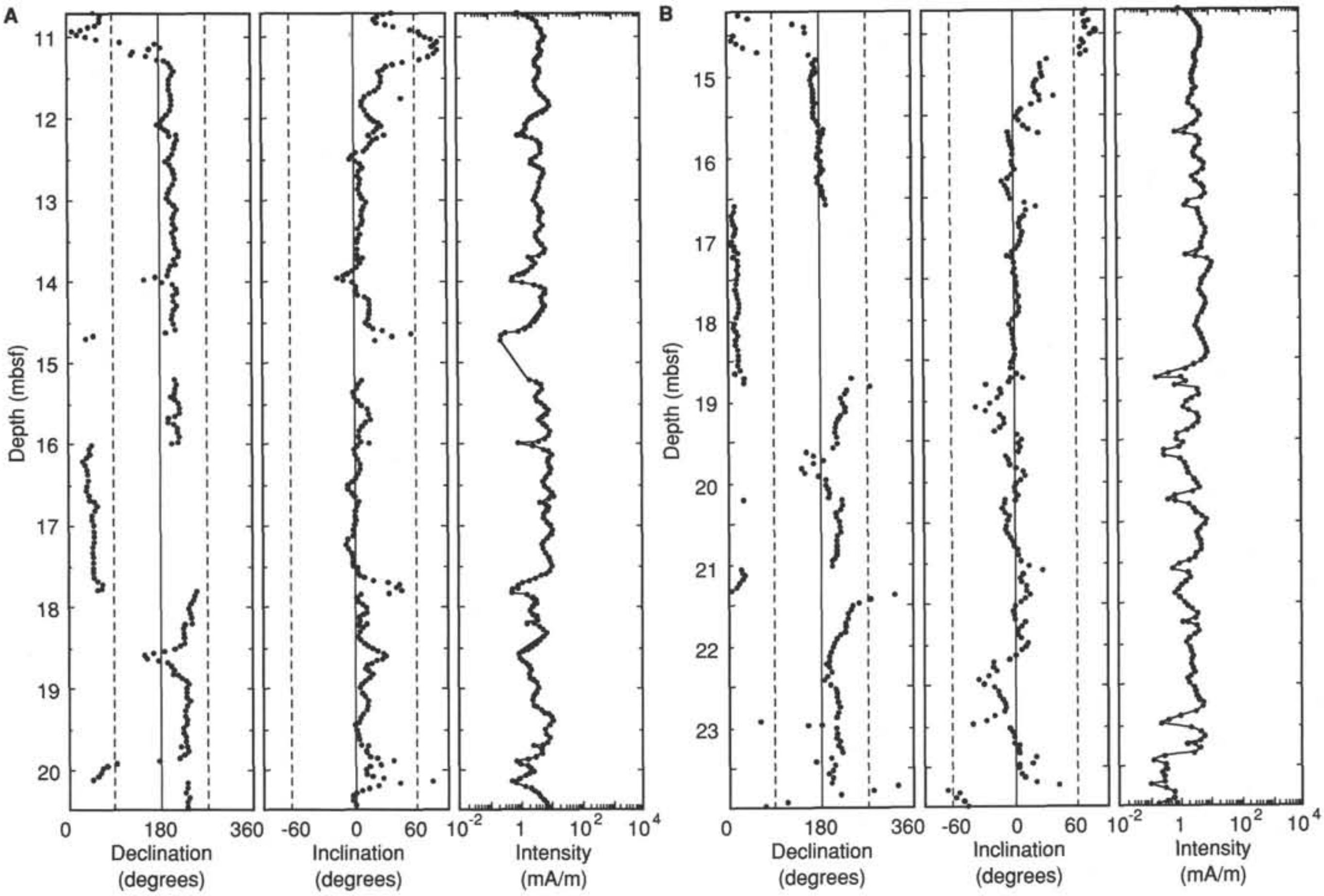

Figure 13. Oriented data from (A) Core 130-804A-3H and (B) Core 130-804B-3H. Note the prominent normal Réunion event at 20 mbsf in Hole 804A and at 21.2 mbsf in Hole 804B, and the weaker, intermediately polarized event at 18.6 mbsf in Hole 804A and 19.8 mbsf in Hole 804B.

normal polarity below 43.5 mbsf (Fig. 14). This normal interval is far too long to fit in with the rest of the Pliocene magnetostratigraphy and so is suspect. In addition, both the declination and inclination patterns through this interval are noisy, and the intensity record has a cyclic series of alternations with a spatial frequency of about 20 cm superimposed on the general decline in intensity. It is possible that this interval within Core 130-804A-6H represents remobilized material, perhaps a slump or mudflow, that was remagnetized when it was partially fluidized at the time of its redeposition. Alternatively, the cyclicity also may be related to depth variations in the concentration of pyrrhotite (see "Site 806" chapter for a further discussion of pyrrhotite generation).

Pliocene-Pleistocene Sedimentation Rates

Comparative age vs. depth plots of the three holes at this site are shown in Figure 15. Some variation between the three holes is evident, but this does not exceed about 2 m and probably reflects only imprecision in sub-bottom depth measurement. Age-depth picks from Holes 804A and 804C cluster around the trend of Hole 804B, which represents the most complete and internally consistent record.

Age-depth data from Hole 804B fall into two intervals, which are characterized by linear sedimentation rates that intersect at about 2 Ma (Fig. 16). As was the case at Site 803, sedimentation rates at Site 804 declined at this time, but the change is less marked at Site 804. Sedimentation rates over the interval from 0 to 2 Ma average 10 m/m.y. at Sites 803 and 804, but the rates for the earlier Pliocene are lower at Site 804 (11.6 m/m.y. at Site

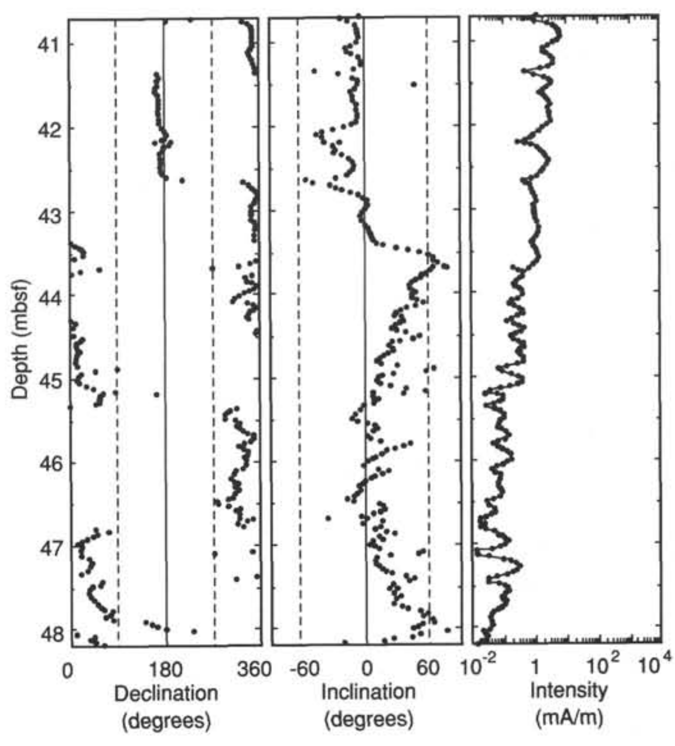

Figure 14. Oriented data from Core 130-804A-6H.

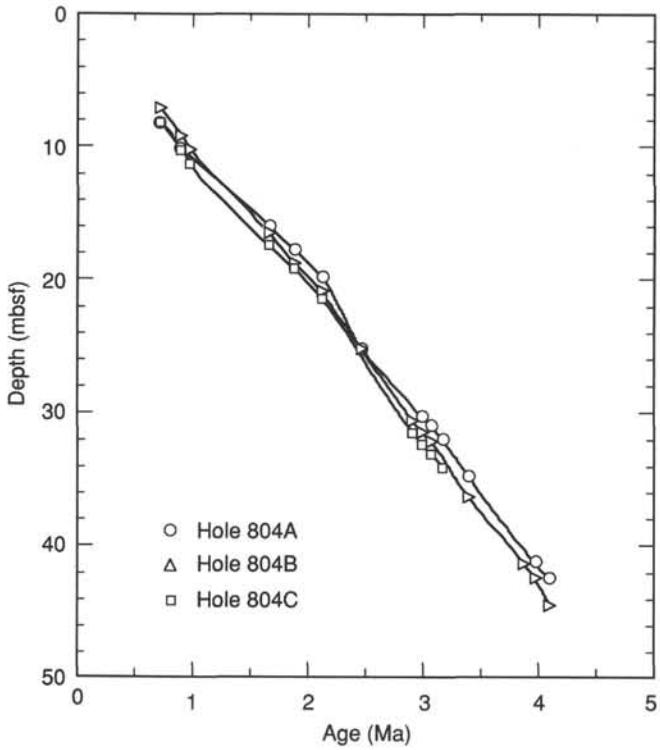

Figure 15. Plot of age vs. depth for polarity events, Site 804.

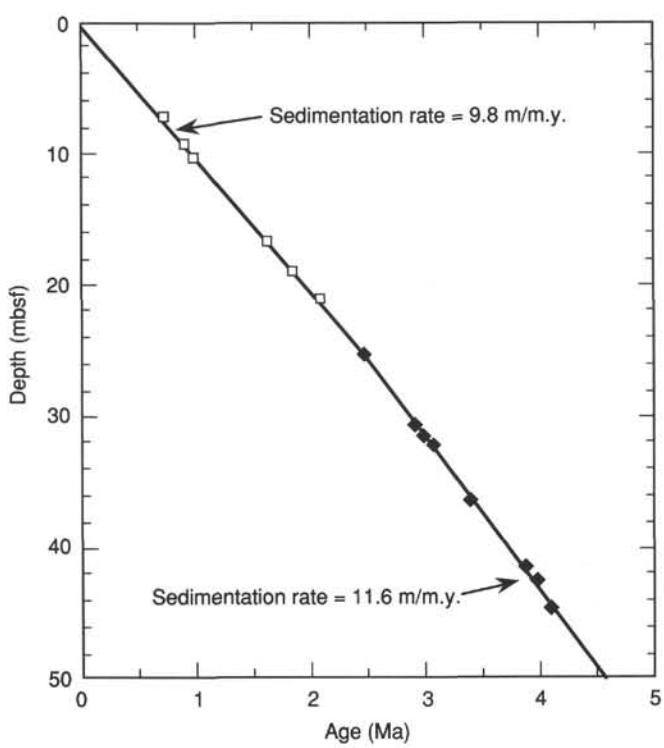

Figure 16. Age vs. depth for events from Hole 804B, showing alignment of events on two linear trends. Corresponding sedimentation rates are indicated.

804 compared with 15.4 m/m.y. at Site 803). This difference may reflect dissolution processes at the greater water depth of Site 804, which lies at 3861 m, compared with 3410 m at Site 803.

SEDIMENTATION RATES

Lower Oligocene through Holocene sediments were recovered at the three holes cored at Site 804. Interpretable geomagnetic reversal histories were obtained in the Pleistocene–lower Pliocene interval, to the Nunivak Subchron of the Gilbert Chron (see "Paleomagnetics" section, this chapter). All shipboard bio- and magnetostratigraphic age-depth indicators are listed in Table 2. The series of control points that were chosen for the sedimentation rate calculations in each of the three holes at Site 804 are presented in Table 3.

The Pliocene through Pleistocene interval is presented graphically in Figure 17, which presents age-depth data from the entire sequence (0–48.7 mbsf) of Hole 804A. The magnetostratigraphic data indicate one sedimentation rate change at the termination of the Jaramillo Subchron, and another change at the onset of the Olduvai Subchron. The two oldest biostratigraphic points clearly suggest a major change in sedimentation rate at the termination of the Nunivak Subchron. The lower Pliocene interval is condensed at Hole 804A.

The results from Hole 804B are presented graphically in Figure 18. This graph shows that the condensed lower Pliocene interval that ended at 4.1 Ma has its onset at about 5.0 Ma, almost precisely at the Miocene/Pliocene boundary. Two age-depth indicators from Hole 804A have been included in Figure 18, namely, the appearance of *Ceratolithus rugosus* (44.6–45.8 mbsf in Hole 804A; 4.6 Ma) and the disappearance of *Discoaster quinqueramus* (45.8–47.3 mbsf in Hole 804A; 5.0 Ma), because these events were determined with closer sample intervals in Hole 804A, and because they constrain sedimentation rates in the pertinent interval. These two events occur with the Gilbert/Nunivak boundary within a single core in Holes 804A (130-804A-6H) and 804B (130-804B-6H). This reversal boundary lies exactly 2 m deeper in Hole 804B than in Hole 804A; therefore, 2 m are added to the depths of the two biostratigraphic events as observed in Hole 804A to derive their depths in Hole 804B. Both of these inferred depths are within the uncertainty ranges of the events as determined in Hole 804B. The extra points taken from Hole 804A argue for a somewhat condensed, but continuous Miocene/Pliocene transition interval rather than for the presence of a hiatus.

Plots of age-depth indicators from Hole 804C are shown in Figure 19, and the plots are shown at enlarged scales in Figures 20 (0–9 Ma) and 21 (8–22 Ma). The scatter of points, particularly those represented by radiolarian events, is wide in the upper Miocene through Holocene interval (Fig. 20), but throughout that scatter the trend from Holes 804A and 804B is clearly recognizable. Several species events representing widely distributed middle to early Miocene ages were observed at a single depth level around 200 mbsf (Fig. 21), thus indicating the presence of a hiatus. This hiatus was placed in the center of Core 130-804C-22X (197.1–206.8 mbsf). An age estimate of 14.7 Ma was obtained for the young side of the hiatus through extrapolation of the sedimentation rate from the nearest overlying control point (LO of *Sphenolithus heteromorphus;* 182.55 mbsf, 13.6 Ma; see Table 3).

The older side of the Miocene hiatus is less well constrained biostratigraphically. Nevertheless, it is obvious that the entire range of *Sphenolithus belemnos* is masked by the hiatus, implying that the youngest possible age estimate for the old side of the hiatus is identical to the age estimate of the first evolutionary appearance of *S. belemnos* (20.0 Ma). The LO event of *Glo-*

Table 2. Bio- and magnetostratigraphic events determined at Site 804.

Event	Upper depth (mbsf)	Lower depth (mbsf)	Age (Ma)
Hole 804A:			
FO *E. huxleyi* (N)	0	1.2	0.28
LO *P. lacunosa* (N)	1.2	10.7	0.46
LO *G. tosaensis* (F)	1.2	10.7	0.60
Brunhes (O)	8.2	8.2	0.73
Jaramillo (T)	10.15	10.2	0.91
Acme *R. asanoi*	10.7	10.7	1.00
LO *C. macintyrei* (N)	10.7	15.2	1.45
Olduvai (T)	16.0	16.0	1.66
Olduvai (O)	17.8	17.8	1.88
LO *D. brouweri* (N)	15.2	20.2	1.89
FO *G. truncatulinoides* (F)	10.7	20.2	1.90
LO *D. surculus* (N)	20.2	29.7	2.45
Gauss (T)	25.3	25.3	2.47
LO *G. altispira*	29.7	39.2	2.90
Kaena (O)	30.4	30.4	2.99
LO *Sphaeroidinellopsis* spp. (F)	29.7	39.2	3.00
FO *Sphaeroidinella dehiscens* (F)	29.7	39.2	3.00
Mammoth (T)	31.2	31.2	3.08
Mammoth (O)	32.2	32.2	3.18
Gauss (O)	35.0	35.0	3.40
LO *R. pseudoumbilica* (N)	29.7	39.2	3.56
Cochiti (O)	41.4	41.4	3.97
Nunivak (T)	42.7	42.7	4.10
FO *C. rugosus*	44.6	45.8	4.60
LO *D. quinqueramus*	45.8	47.3	5.00
Hole 804B:			
LO *P. lacunosa* (N)	3.8	4.7	0.46
LO *G. tosaensis* (F)	4.7	14.2	0.60
Brunhes (O)	7.2	7.2	0.73
Jaramillo (T)	9.3	9.3	0.91
Jaramillo (O)	10.3	10.3	0.98
LO *C. macintyrei* (N)	14.2	15.0	1.45
LO *G. fistulosus* (F)	14.2	23.7	1.60
Olduvai (T)	16.6	16.6	1.66
LO *G. extremus* (F)	4.7	14.2	1.80
Olduvai (O)	18.8	18.8	1.88
LO *D. brouweri* (N)	19.4	19.6	1.89
FO *G. truncatulinoides* (F)	23.7	33.2	1.90
LO *D. surculus* (N)	23.7	33.2	2.45
Gauss (T)	25.4	25.4	2.47
LO *D. variabilis* (N)	23.7	33.2	2.90
LO *G. multicamerata* (F)	33.2	42.7	2.90
LO *G. altispira* (F)	23.7	33.2	2.90
FO *G. fistulosus* (F)	23.7	33.2	2.90
Kaena (T)	30.8	30.8	2.92
Kaena (O)	31.6	31.6	2.99
LO *Sphaeroidinellopsis* spp. (F)	33.2	42.7	3.00
FO *S. dehiscens* (F)	42.7	45.6	3.00
Mammoth (T)	32.4	32.4	3.08
FO *G. tosaensis* (F)	23.7	33.2	3.10
Gauss (O)	36.6	36.6	3.40
LO *P. primalis* (F)	33.2	42.7	3.50
LO *R. pseudoumbilica* (N)	33.2	42.7	3.56
Cochiti (T)	41.6	41.6	3.88
LO *G. nepenthes* (F)	42.7	52.2	3.90
LO *P. spectabilis* (F)	33.2	42.7	3.90
Cochiti (O)	42.7	42.7	3.97
Nunivak (T)	44.7	44.7	4.10
LO *C. acutus* (N)	42.7	52.2	4.6
LO *D. quinqueramus* (N)	42.7	52.2	5.0
FO *S. dehiscens* (F)	42.7	52.2	5.1
FO *G. tumida* (F)	45.6	52.2	5.2
FO *P. spectabilis* (F)	45.6	52.2	5.2
LO *G. dehiscens* (F)	33.2	42.7	5.3
FO *P. primalis* (F)	52.2	61.7	5.8
FO *D. quinqueramus* (N)	71.2	80.7	7.5
LO *D. hamatus* (N)	90.2	99.7	8.7
LO *G. siakensis* (F)	118.7	128.2	10.4

Table 2 (continued).

Event	Upper depth (mbsf)	Lower depth (mbsf)	Age (Ma)
Hole 804C:			
LO *P. lacunosa* (N)	0	6.3	0.46
Brunhes (O)	8.2	8.2	0.73
Jaramillo (T)	10.3	10.3	0.91
Jaramillo (O)	11.3	11.3	0.98
LO *A. angulare* (R)	6.3	15.8	0.99
LO *L. neoheteroporos* (R)	6.3	15.8	1.11
LO *C. macintyrei* (N)	11.5	15.8	1.45
LO *R. praebergonii* var. *robusta* (D)	15.8	25.3	1.55
FO *A. angulare* (R)	15.8	25.3	1.58
Olduvai (T)	17.5	17.5	1.66
Olduvai (O)	19.2	19.2	1.88
LO *D. brouweri* (N)	24.1	25.3	1.89
LO *T. convexa* var. *aspinosa* (D)	25.3	34.8	2.10
LO *D. surculus* (N)	30.3	31.9	2.45
FO *L. neoheteroporos* (R)	15.8	25.3	2.52
LO *N. jouseae* (D)	25.3	34.8	2.60
LO *S. peregrina* (R)	25.3	34.8	2.63
LO *D. variabilis* (N)	31.9	33.4	2.90
LO *G. altispira* (F)	25.3	34.8	2.90
LO *G. multicamerata* (F)	44.3	53.8	2.90
Kaena (T)	31.7	31.7	2.92
Kaena (O)	32.5	32.5	2.99
LO *Sphaeroidinellopsis* (F)	34.8	44.3	3.00
FO *Sphaeroidinella dehiscens* (F)	34.8	44.3	3.00
FO *R. praebergonii* (D)	34.8	44.3	3.00
Mammoth (T)	33.2	33.2	3.08
FO *G. tosaensis* (F)	25.3	34.8	3.10
Mammoth (O)	34.2	34.2	3.18
LO *L. audax* (R)	44.3	53.8	3.34
LO *P. doliolum* (R)	34.8	44.3	3.54
LO *R. pseudoumbilica* (N)	34.8	46.1	3.56
FO *A. ypsilon* (R)	34.8	44.3	3.78
LO *S. pentas* (R)	34.8	44.3	3.78
LO *S. berminghami* (R)	44.3	53.8	3.86
FO *A. elegans* (D)	44.3	53.8	3.90
FO *S. pentas* (R)	44.3	53.8	4.25
LO *C. acutus* (N)	34.8	46.1	4.60
LO *S. omnitubus* (R)	44.3	53.8	4.75
LO *S. delmontensis* (R)	44.3	53.8	5.00
LO *D. quinqueramus* (N)	34.8	46.1	5.00
LO *S. corona* (R)	53.8	63.3	5.05
FO *G. tumida* (F)	44.3	53.8	5.20
FO *P. spectabilis* (F)	44.3	53.8	5.20
LO *G. dehiscens* (F)	44.3	53.8	5.30
LO *A. tritubus* (R)	53.8	63.3	5.35
FO *S. omnitubus* (R)	63.3	72.8	6.40
LO *C. caepa* (R)	72.8	82.3	6.40
FO *Amaurolithus* spp. (N)	63.3	72.8	6.70
LO *N. porteri* (D)	63.3	72.8	6.70
LO *R. paleacea* (D)	63.3	72.8	6.90
LO *T. burckliana* (D)	63.3	72.8	7.00
FO *G. plesiotumida* (F)	72.8	82.3	7.10
LO *D. hughesi* (R)	53.8	63.3	7.15
LO *N. porteri* (D)	63.3	72.8	7.20
LO *R. paleacea* (D)	63.3	72.8	7.40
LO *D. ontogenesis* (R)	63.3	72.8	7.45
FO *D. quinqueramus* (N)	63.3	72.8	7.50
FO *A. tritubus* (R)	53.8	63.3	7.74
FO *S. berminghami* (R)	91.8	101.3	7.95
LO *T. burckliana* (D)	63.3	72.8	8.00
LO *D. petterssoni* (R)	110.8	120.3	8.15
LO *D. laticonus* (R)	53.8	63.3	8.15
LO *S. wolffii* (R)	91.8	101.3	8.15
LO *C. temperei* var. *delicata* (D)	91.8	101.3	8.20
LO *D. hamatus* (N)	91.8	101.3	8.70
FO *D. hughesi* (R)	129.8	139.3	8.75
LO *A. moronensis* (D)	101.3	110.8	8.90
FO *T. burckliana* (D)	91.8	101.3	9.00
LO *C. temperei* var. *delicata* (D)	91.8	101.3	9.80
FO *N. acostaensis* (F)	120.3	129.8	10.20
LO *G. siakensis* (F)	120.3	129.8	10.40
FO *D. hamatus* (N)	148.8	158.3	10.50

Table 2 (continued).

Event	Upper depth (mbsf)	Lower depth (mbsf)	Age (Ma)
Hole 804C: (Cont.)			
LO *C. coscinodiscus* (D)	158.3	168.0	10.70
LO *D. punctata* f. *hustedtii* (D)	158.3	168.0	10.70
FO *L. thornburgi* (R)	110.8	120.3	10.95
FO *H. cuneiformis* (D)	158.3	168.0	10.20
LO *A. moronensis* (D)	101.3	110.8	11.30
LO *G. fohsi lobata* (F)	158.3	163.0	11.50
LO *C. cornuta* (R)	158.3	168.0	11.75
LO *C. coscinodiscus* (D)	158.3	168.0	12.20
LO *D. punctata* f. *hustedtii* (D)	158.3	168.0	12.20
FO *H. cuneiformis* (D)	158.3	168.0	12.60
FO *C. lewisianus* (D)	177.7	187.4	12.90
FO *G. fohsi lobata* (F)	168.0	177.7	13.10
FO *C. lewisianus* (D)	177.7	187.4	13.50
LO *S. heteromorphus* (N)	177.7	187.4	13.60
FO *G. praefohsi* (F)	177.7	187.4	13.90
LO *C. peplum* (D)	177.7	187.4	14.10
LO *G. peripheroronda* (F)	197.1	216.5	14.60
FO *C. peplum* (D)	206.8	216.5	16.30
LO *C. dissimilis* (F)	197.1	216.5	17.60
FO *S. heteromorphus* (N)	197.1	206.8	18.60
LO *C. elegans* (D)	216.5	226.2	18.70
LO *B. veniamini* (D)	226.2	235.8	19.90
FO *S. belemnos* (N)	197.1	206.8	20.00
LO *G. kugleri* (F)	226.2	245.4	21.80
FO *D. druggii* (N)	245.4	255.1	23.60
FO *G. kugleri* (F)	245.4	255.1	23.70
LO *S. ciperoensis* (N)	264.7	274.4	25.20
LO *G. opima* (F)	264.7	274.4	28.20

Notes: The depth uncertainty predominantly represents sampling intervals used. References for the age estimates are presented in the "Explanatory Notes" chapter (this volume). N = nannofossil, F = foraminifer, D = diatom, R = radiolarian, FO = first occurrence, and LO = last occurrence. Magnetostratigraphic reversal boundaries followed by the designation (T) or (O) refer to "termination" or "onset," respectively.

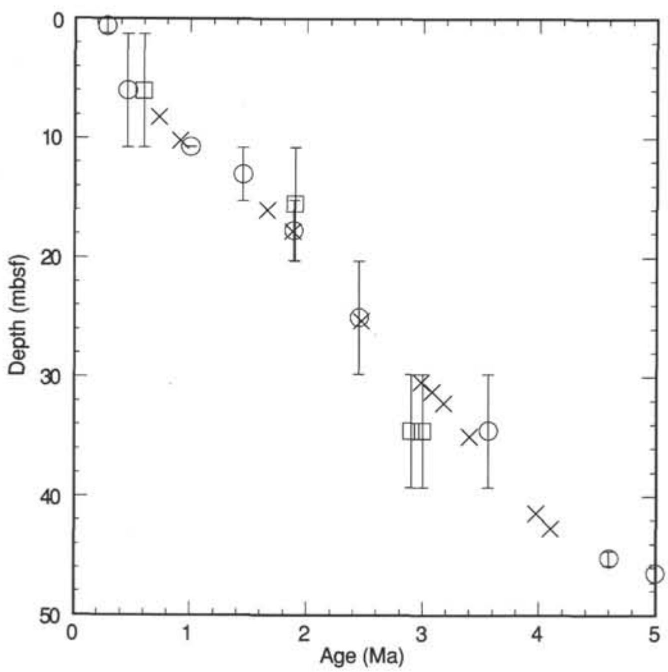

Figure 17. Age/depth relationships of bio- and magnetostratigraphic markers in Hole 804A. Error bars show sample interval uncertainties. Open circles = nannofossils, open squares = foraminifers, and × = magnetostratigraphic reversal boundary.

Table 3. Estimated sedimentation rates, Site 804, and the control points determining those rates.

Control point	Depth (mbsf)	Age (Ma)	Sedimentation rate (m/m.y.)
130-804A-			
Top section	0	0	
Jaramillo (T)	10.15	0.91	11.2
Olduvai (O)	17.80	1.88	7.9
Nunivak (T)	42.70	4.10	11.2
LO D. quinqueramus (N)	46.55	5.00	4.3
Terminal depth	48.70	5.50	
130-804B-			
Top section	0	0	
Brunhes (O)	7.20	0.73	9.9
Jaramillo (O)	10.30	0.98	12.4
Olduvai (O)	18.80	1.88	9.4
Nunivak (T)	44.70	4.10	11.7
LO D. quinqueramus (N)	47.45	5.00	3.1
LO D. hamatus (N)	94.95	8.70	12.8
Terminal depth	137.7	<10.5	>23.8
130-804C-			
Top section	0	0	
Brunhes (O)	8.20	0.73	11.2
Olduvai (O)	19.20	1.88	9.6
Mammoth (O)	34.20	3.18	11.5
Insufficient resolution	34.2–49.05	3.18–5.2	
LO P. spectabilis (F)	49.05	5.20	
LO D. hamatus (N)	94.95	8.70	13.1
LO S. heteromorphus (N)	182.55	13.60	17.9
Hiatus young side	201.95	14.69	
Hiatus old side	201.95	20.00	
FO S. belemnos (N)	201.95	20.00	
LO G. kugleri (F)	235.80	21.80	18.8
LO S. ciperoensis (N)	269.55	25.20	9.9
Hiatus young side	269.55	25.20	
LO G. opima (F)	269.55	28.20	
Hiatus old side	269.55	28.20	
Terminal depth	312.50	<33.8	?

Notes: N = nannofossil, F = foraminifer, D = diatom, R = radiolarian, FO = first occurrence, and LO = last occurrence. Magnetostratigraphic reversal boundaries followed by the designation (T) or (O) refer to "termination" or "onset," respectively. See "Explanatory Notes" chapter (this volume) for Leg 130 philosophy on sedimentation rates.

borotalia kugleri at 21.8 Ma lies well below the hiatus, implying that the old side of the hiatus begins between 20.0 and 21.8 Ma.

Another hiatus is implied in the upper Oligocene that encompasses the time interval from at least 25.2 (LO of *Sphenolithus ciperoensis*) to at least 28.2 Ma (LO of *Globorotalia opima*). The young side of the hiatus lies somewhere between the *S. ciperoensis* event and the FO of *G. kugleri* at 23.7 Ma. The youngest possible age for the old side of this Oligocene hiatus coincides with the *G. opima* event, although it appears likely that the old side of the hiatus is older than 28.2 Ma. About 43 m of sediment of early Oligocene age (<33.8 Ma) were cored below the hiatus. If they represent continuous deposition, these 43 m of sediments were deposited at a minimum rate of 7.7 m/m.y.

The sedimentation rates indicated for the lower Miocene/uppermost Oligocene interval that separates the two hiatuses are poorly constrained. Several alternatives to the sedimentation rates suggested in Table 3 can be deduced from the distribution of the available age-depth indicators.

The sedimentation rates for all three holes from Site 804 are plotted vs. age in Figure 22. The condensed lower Pliocene interval stands out clearly. Data from Hole 804C has been omitted above 5 Ma, simply because the data available do not permit us to identify the condensed lower Pliocene interval and because

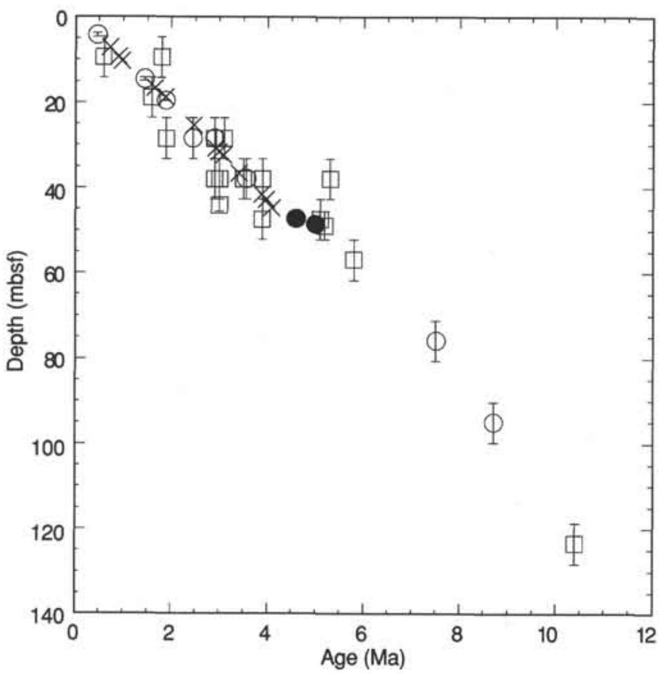

Figure 18. Age/depth relationships of bio- and magnetostratigraphic markers in Hole 804B. Error bars show sample interval uncertainties. Open circles = nannofossils, open squares = foraminifers, and × = magnetostratigraphic reversal boundary. Two nannofossil events (filled circles) are derived from Hole 804A (see explanation in text).

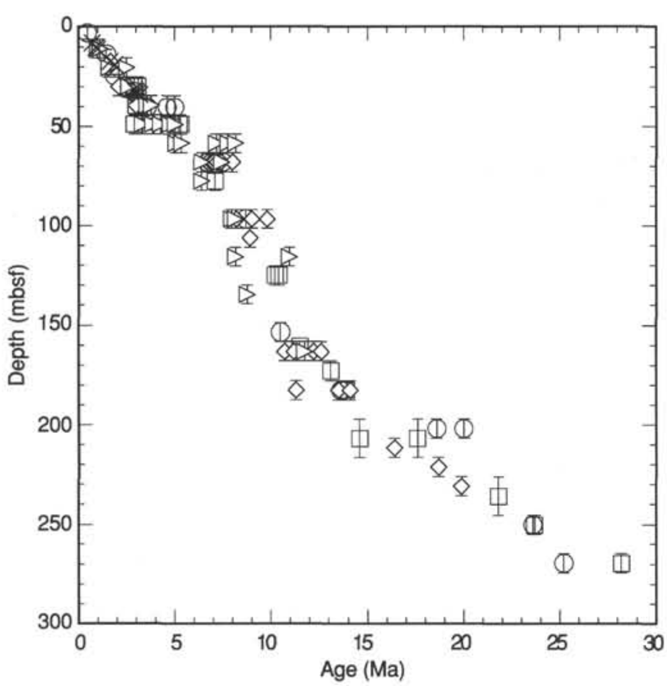

Figure 19. Age/depth relationships of bio- and magnetostratigraphic markers in Hole 804C. Error bars show sample interval uncertainties. Open circles = nannofossils, open squares = foraminifers, open diamonds = diatoms, open triangles = radiolarians, and × = magnetostratigraphic reversal boundary.

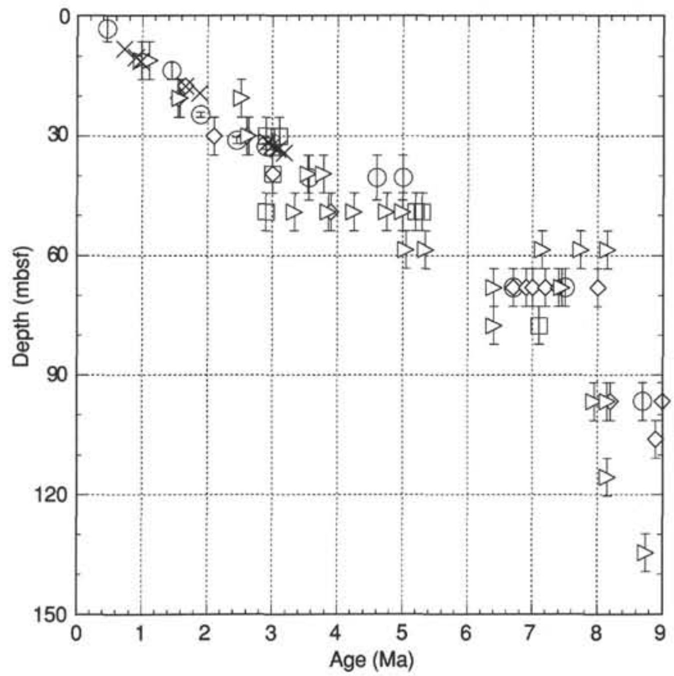

Figure 20. Late Miocene through Holocene age/depth relationships of bio- and magnetostratigraphic markers in Hole 804C. Error bars show sample interval uncertainties. Open circles = nannofossils, open squares = foraminifers, open diamonds = diatoms, open triangles = radiolarians, and × = magnetostratigraphic reversal boundary.

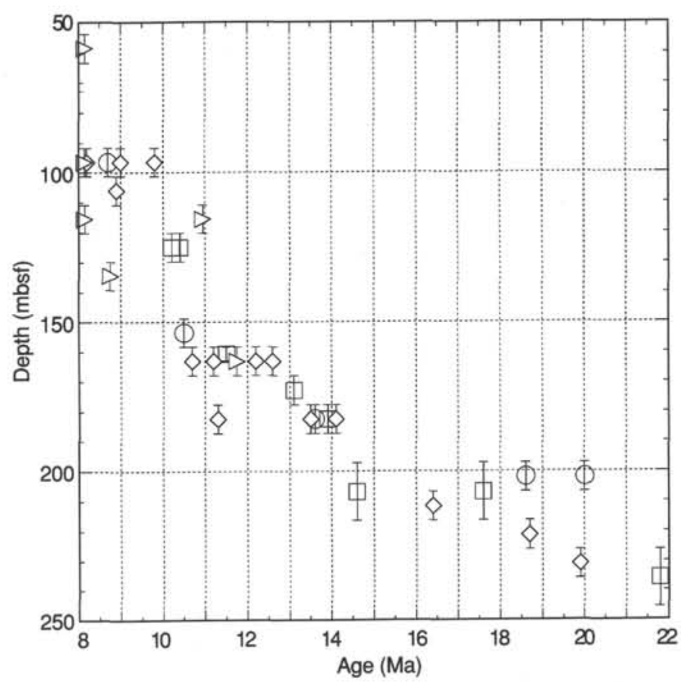

Figure 21. Early through late Miocene age/depth relationships of biostratigraphic markers in Hole 804C. Error bars show sample interval uncertainties. Open circles = nannofossils, open squares = foraminifers, open diamonds = diatoms, and open triangles = radiolarians.

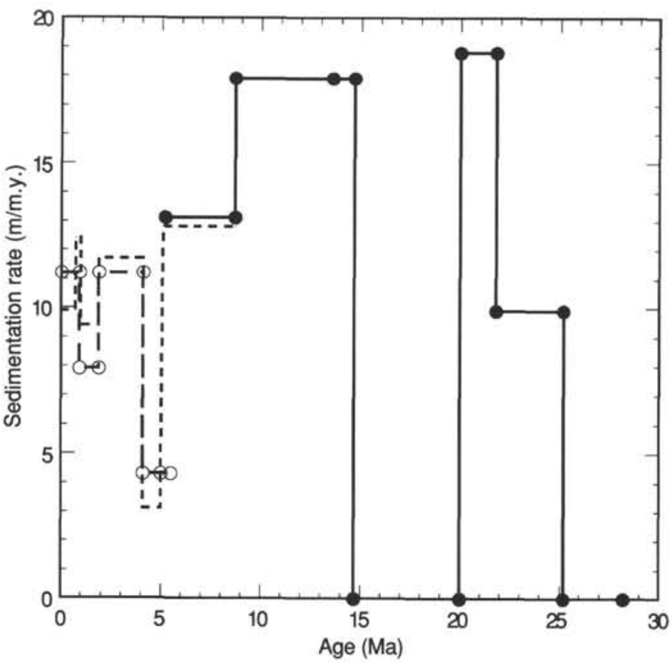

Figure 22. Sedimentation rate history, Site 804. Dashed line with open circles = Hole 804A, dashed line = Hole 804B, and solid line = Hole 804C.

the Pliocene and Pleistocene intervals are well represented by the sections from Holes 804A and 804B.

The sedimentation rate and its change in the 20- to 25-Ma interval (Fig. 22) should be regarded as but one possible way to connect four points.

INORGANIC GEOCHEMISTRY

We collected 15 interstitial water samples at Site 804: 9 from Hole 804B at depths ranging from 3.0 to 134.2 mbsf, and 6 from Hole 804C at depths ranging from 161.3 to 307.5 mbsf (Table 4). For this report, these are considered as constituting a single depth profile. Interstitial water samples span almost the entire drilled interval of the Unit I nannofossil oozes and chalks, the single lithologic unit recognized at Site 804 (see "Lithostratigraphy" section, this chapter). Chemical gradients in the interstitial waters at this site are generally similar to those at Site 803, being influenced by the biogenic-rich, organic-carbon-poor character of the sediments and by the diffusive influence of basalt alteration reactions at depth. However, the magnitudes of some chemical gradients and maxima are lower at Site 804 than at the shallower Site 803, as described below.

Chlorinity increases by <1% to values around 560 mM over the interval from 0 to 20 mbsf, with a small additional increase at depths greater than 250 mbsf (Fig. 23). Chlorinity values are similar to those at comparable depths at Site 803, as are salinity values, measured refractively as total dissolved solids (Table 4). Sodium concentrations measured by flame emission spectrophotometry (Table 4) and those estimated by charge balance calculations agree to within <1.5% and are approximately constant with increasing depth. Alkalinity is relatively constant at values around 3.6 mM, with small maxima at 10.7 mbsf in Core 130-804B-2H and at 246.9 mbsf in Core 130-804C-27X (Fig. 23).

Sulfate concentrations decrease by 10% to values around 25 mM at 100 mbsf and are approximately constant below that depth (Fig. 23). Sulfate concentrations at given depths and at comparable ages in Site 804 are higher than those at Site 803, suggesting that the rates and total extent of SO_4 depletion are even more limited at Site 804 by low organic carbon contents. The limited alkalinity increase as well as phosphate concentrations below the detection limit of 1–2 μM in all the samples (Table 4) support this interpretation. Ammonia concentrations are low, with the peak value observed in a single sample at 217.9 mbsf in Core 130-804C-24X similar to the maximum at Site 803. There are generally lower concentrations than at Site 803 throughout this profile (Fig. 23).

Dissolved silica concentrations increase with depth to around 900 μM (Fig. 23). The increase in dissolved Si concentrations, presumably a result of the continuous dissolution of biogenic silica, is similar to that observed at Site 803. Manganese concentrations are generally below the detection limit (<2–3 μM) in most samples, except for higher values in the upper 20 m and slightly elevated values around 217.9–246.9 mbsf in Cores 130-804C-24X and -27X (Table 4). Manganese profiles in interstitial waters often show complex structures with depth, probably caused by the occurrence of different zones in which Mn can be mobilized by reduction into its dissolved state (Gieskes, 1981).

Table 4. Interstitial water geochemical data, Site 804.

Core, section, interval (cm)	Depth (mbsf)	pH	Alk. (mM)	Sal. (g/kg)	Cl^- (mM)	Na (mM)	SO_4^{2-} (mM)	PO_4^{3-} (μM)	NH_4^+ (μM)	SiO_2 (μM)	Mn (μM)	Ca^{2+} (mM)	Mg^{2+} (mM)	Sr (μM)	Li (μM)	K (mM)	Rb (μM)
130-804B-																	
1H-2, 145–150	2.95	7.5	3.53	35.0	554	474	27.7	LD	8	450	21	10.7	51.4	108	25.9	10.5	1.77
2H-4, 145–150	10.65	7.4	4.55	35.5	557	475	27.4	LD	13	462	12	11.2	51.7	158	21.8	10.6	1.81
3H-4, 145–150	20.15	7.4	3.77	35.0	561	484	28.0	LD	19	531	4	11.6	51.6	201	20.9	11.2	1.74
4H-4, 145–150	29.65	7.8	3.53	35.5	559	485	27.7	LD	26	636	LD	11.9	50.8	242	20.9	11.2	1.89
5H-4, 145–150	39.15	7.6	3.54	35.5	561	481	27.2	LD	31	679	LD	12.2	50.2	272	20.4	11.1	1.83
6H-4, 145–150	48.65	7.6	3.64	35.5	560	477	26.4	LD	45	690	LD	12.5	49.8	300	19.5	10.9	1.82
9H-4, 145–150	77.15	7.8	3.77	35.0	558	480	26.5	LD	49	774	LD	13.5	48.8	392	17.2	10.6	1.76
12H-4, 145–150	105.65	7.6	3.75	35.0	560	483	25.7	LD	48	809	LD	14.7	47.5	460	15.9	11.9	1.78
15H-4, 145–150	134.15	7.6	3.56	35.5	561	481	25.1	LD	55	851	LD	15.8	46.1	514	15.0	10.8	1.81
130-804C-																	
18X-2, 145–150	161.25	7.6	3.39	35.5	561	479	25.7	LD	57	801	LD	16.2	45.8	521	15.9	9.91	1.69
21X-1, 145–150	188.85	ND	ND	ND	561	480	25.3	ND	79	836	ND	17.7	43.8	577	15.9	9.89	1.58
24X-1, 140–150	217.90	7.9	3.76	35.0	561	478	24.9	LD	113	843	7	18.5	43.6	573	18.7	9.40	1.54
27X-2, 0–10	246.90	7.8	4.28	35.5	561	495	26.6	LD	62	901	3	19.9	42.1	608	18.3	9.63	1.54
30X-3, 140–150	278.80	7.6	3.74	35.5	567	491	24.8	LD	62	930	LD	21.3	42.1	608	18.3	9.72	1.48
33X-3, 140–150	307.49	7.6	3.64	35.5	568	486	25.4	ND	67	909	ND	22.4	41.8	621	18.3	8.70	1.46

Notes: Alk. = alkalinity, Sal. = salinity, LD = concentration lower than detection limit, and ND = not determined.

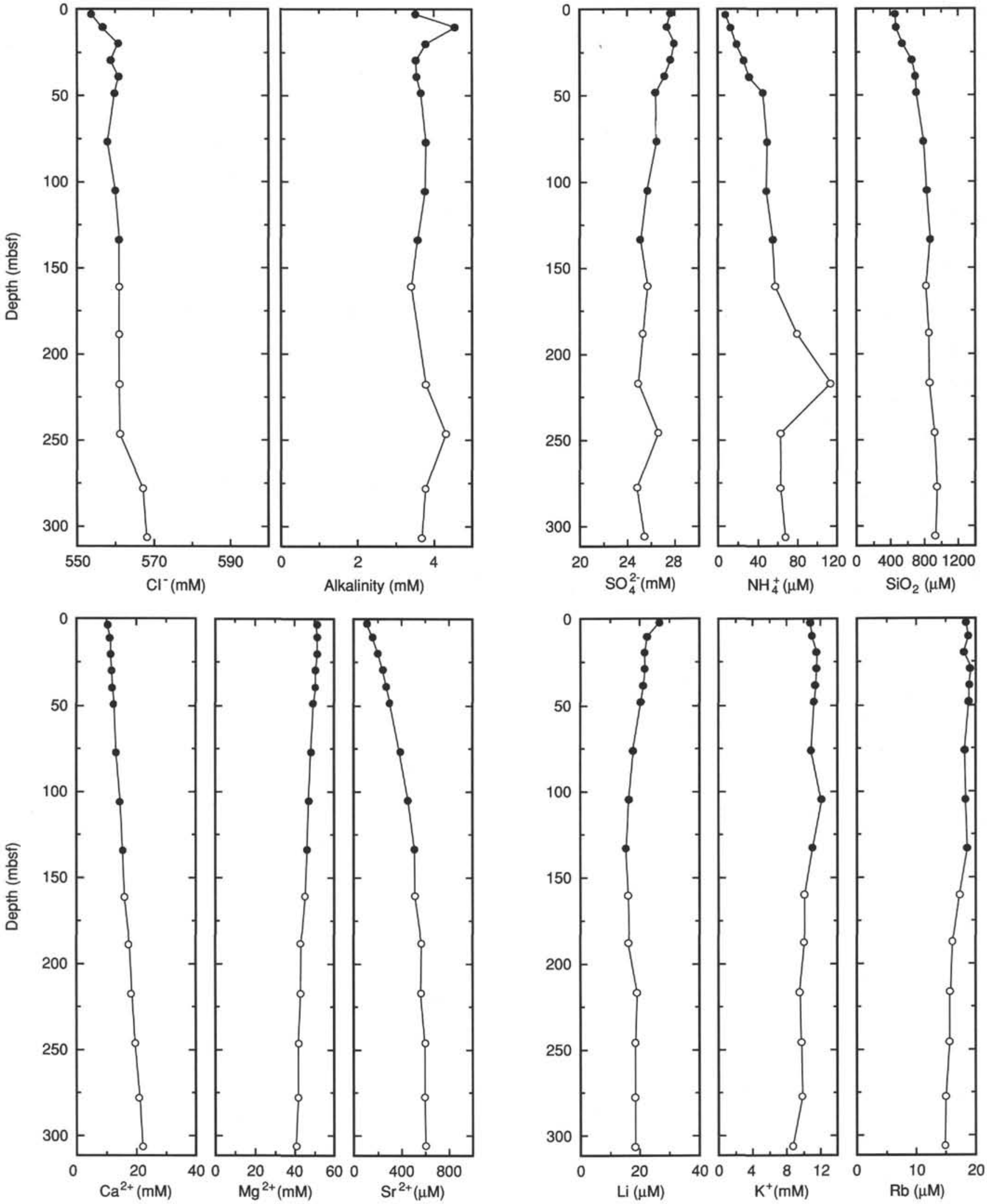

Figure 23. Interstitial water geochemical data vs. depth, Holes 804B and 804C. Closed circles indicate samples from Hole 804B; open circles, samples from Hole 804C. The depth at the base of the plots is that of the deepest sediment drilled.

Calcium concentrations increase with depth, with an average gradient of 4 mM/100 m (Fig. 23), approximately half that observed at Site 803. Magnesium concentrations decrease with depth, with a gradient of 4 mM/100 m (Fig. 23), similar to that observed at Site 803. Magnesium and calcium concentrations are linearly correlated (R^2 = 0.97), with a $\Delta Ca/\Delta Mg$ ratio approximately equal to -1, similar to those at Sites 288 and 289 (Leg 30) from the Ontong Java Plateau (Elderfield et al., 1982). The linear correlation is indicative of the conservative nature of these profiles, with Ca and Mg gradients primarily controlled by reactions in the underlying basalt and diffusion between this boundary and overlying seawater (McDuff and Gieskes, 1976; McDuff, 1981).

Strontium concentrations increase with depth to maximum observed values around 600 μM (Fig. 23). The character of the profile is consistent with the release of Sr to interstitial water during recrystallization of biogenic calcite to inorganic calcite (e.g., Gieskes, 1981). Strontium concentrations at Site 804 are lower than those at corresponding depths at Site 803, and the maximum observed concentrations at Site 804 are lower than the maximum concentrations observed at Sites 288 and 289 (Elderfield et al., 1982).

Lithium concentrations decrease from 26 μM near the top of the sediment column to minimum values around 15–16 μM from 105.7 to 188.9 mbsf and then slightly increase again with depth (Fig. 23). Potassium concentrations first increase slightly, then decrease with depth (Fig. 23), similar to the profile observed at Site 803. Rubidium concentrations also decrease with depth (Fig. 23), with this decrease linearly correlated with the Ca increase, implying that it is also caused by the diffusive influence of basalt alteration reactions on interstitial water composition.

CARBON GEOCHEMISTRY

Shipboard carbon geochemical analyses of samples from Site 804 include determinations of inorganic carbon (189 samples), volatile hydrocarbons in sediments (10 samples), and 8 Rock-Eval analyses. The NCS elemental analyzer was not operational at Site 804; therefore, there are no shipboard data for total carbon, sulfur, and nitrogen. The analytical methods are outlined in the "Explanatory Notes" chapter (this volume). More detailed descriptions of the methods are given by Emeis and Kvenvolden (1986). The sediments were routinely monitored for the presence of hydrocarbon gases as required by safety considerations. As in the sediments from Site 803, no volatile hydrocarbons were detected at Site 804.

Inorganic carbon (IC; see "Explanatory Notes" chapter, this volume) was measured on samples collected for physical properties analyses. The carbon data are presented in Table 5 (microfiche, back pocket) and plotted vs. depth in Figure 7. The sediments at Site 804 are characterized by carbonate values ranging from 55% to 95%. Lower carbonate contents (55%–70%) between 200 and 300 mbsf (upper Oligocene to lower Miocene) and between 0 and 100 mbsf (upper Miocene to Holocene) correlate with radiolarian-rich intervals and may reflect greater dissolution of carbonate in these sections.

Rock-Eval pyrolysis (Espitalié et al., 1977) was used for total organic carbon (TOC) determinations. The TOC values are below the detection limit of the shipboard Rock-Eval pyrolysis (0.05%; see "Site 803" chapter, this volume).

PHYSICAL PROPERTIES

Introduction

Physical properties were measured on whole rounds and split cores at Site 804. Whole-round analyses included gamma-ray attenuation porosity evaluator (GRAPE) and *P*-wave logger (PWL) measurements (using the multisensor track) as well as thermal conductivity. Index properties (wet-bulk density, porosity, grain density, and water content), undrained vane shear strength, and compressional wave velocity were measured on split cores. The digital sound velocimeter (DSV) was used in soft sediment sections, and the Hamilton Frame on discrete samples in indurated intervals. The methods of analyses are described in the "Explanatory Notes" chapter (this volume).

The intensive physical properties program conducted on Leg 130 concentrated on making closely spaced laboratory measurements and therefore provided little time for data processing. We recorded GRAPE and PWL data on board the ship but will process them on shore. No downhole measurements were made at Site 804; therefore, laboratory velocity and density measurements corrected to *in-situ* values were the only data available for the calculation of synthetic seismograms (see "Seismic Stratigraphy" section, this chapter).

Thermal Conductivity

Thermal conductivity was measured on whole-round sections using the needle-probe technique (see "Explanatory Notes" chapter, this volume). As at Site 803, problems caused by inaccurate needle calibration led to a high degree of scatter. For each core, the thermal conductivity reported is a mean value calculated by averaging the thermal conductivity values for Sections 3, 4, and 5 (see "Explanatory Notes" chapter, this volume). Results are given in Table 6, and Figure 24 shows changes in thermal conductivity with depth.

There is some indication that thermal conductivity increases with depth, presumably as a consequence of decreases in porosity and water content, but the measurements show little change between 40 and 240 mbsf.

Shear Strength

At Site 804, undrained shear strength was normally measured at an interval of one per split section, using a motorized minivane apparatus (see "Explanatory Notes" chapter, this volume). Measurements were made by inserting the vane in the soft sediment in the intervals cored with the APC and into undisturbed coherent blocks of sediment ("biscuits") in intervals cored with the XCB until the sediment became too stiff (at approximately 140 mbsf in Hole 804B and 160 mbsf in Hole 804C). The sediment at Site 804 is principally silt or clayey silt, similar to that at Site 803.

The vane shear test is designed for clay measurements, with cohesion being the main factor in the shear strength equation. The vane shear test, however, may be used as an estimate of undrained shear strength (see "Physical Properties" section, "Site 803" chapter, for a detailed discussion). Residual shear strength data were obtained wherever cracking did not dominate failure. Shear strength results are presented in Table 7 (microfiche, back pocket); mean grain size in the top of Hole 804B is presented in Table 8. Figure 25 shows the variations of shear strength with depth, and Figure 26 shows the changes with depth of mean grain size and shear strength in the upper portion of the sediment section at Hole 804B.

Shear strength values measured in the three holes range from approximately 5 to 50 kPa. There is a general increase with depth as a result of sediment consolidation (Fig. 25). Differences in the shear strength curves between Holes 804B and 804C below 80 mbsf may reflect coring disturbance.

From 0 to 80 mbsf, the shear strength curves from all three holes at Site 804 have the same basic shape (Fig. 25). Exact "peak-to-peak" correlations are very difficult, however, as coring-induced disturbance has considerable effect on the peak shear strength values (see discussion in "Physical Properties" section, "Site 803" chapter, this volume). The three curves show

Table 6. Thermal conductivity data, Site 804.

Core, section, interval (cm)	Depth (mbsf)	Thermal conductivity (W/m · K)	Corrected (mean per core)
130-804A-			
2H-3, 35	4.55	1.1567	
2H-4, 35	6.05	1.2426	1.2091
2H-5, 35	7.55	1.2280	
3H-3, 35	14.05	1.0420	
3H-4, 35	15.55	1.2043	1.1519
3H-5, 35	17.05	1.2095	
4H-3, 35	23.55	1.1338	
4H-4, 35	25.05	1.3144	1.2286
4H-5, 35	26.55	1.2375	
5H-3, 35	33.05	1.2387	
5H-4, 35	34.55	1.1817	1.2296
130-804B-			
2H-3, 35	8.05	1.2786	
2H-4, 35	9.55	1.2955	1.2531
2H-5, 35	11.05	1.1851	
4H-3, 35	27.05	1.3100	
4H-3, 35	28.55	1.2463	
4H-5, 35	30.05	1.1827	
6H-3, 35	46.05	1.2441	
6H-3, 35	47.55	1.3073	
6H-5, 35	49.05	1.3705	
8H-3, 35	65.05	1.3801	
8H-4, 35	66.55	1.2422	1.3010
8H-5, 35	68.05	1.2805	
9H-3, 35	74.55	1.2724	
9H-4, 35	76.05	1.1637	1.1600
9H-5, 35	77.55	1.0438	
10H-4, 35	85.55	1.2940	
	86.03	1.3730	
10H-5, 35	87.05	1.4520	
11H-3, 35	93.55	1.2525	
11H-4, 35	95.05	1.4145	1.3379
11H-5, 35	96.55	1.3466	
12H-3, 35	103.05	1.3372	
12H-4, 35	104.55	1.4353	1.4089
12H-5, 35	106.05	1.4543	
13H-3, 35	112.55	1.3003	
13H-4, 35	114.05	1.3947	1.2990
13H-5, 35	115.55	1.2021	
14H-3, 35	122.05	1.3805	
	122.80	1.3412	
14H-4, 35	123.55	1.3020	
15H-3, 35	131.55	1.3750	
15H-4, 35	133.05	1.4321	1.3538
15H-5, 35	134.55	1.2544	
130-804C-			
2H-3, 35	9.65	1.1854	
2H-4, 35	11.15	1.1280	1.1556
2H-5, 35	12.65	1.1535	
3H-3, 35	19.15	1.2286	
3H-4, 35	20.65	1.1654	1.2379
3H-5, 35	22.15	1.3198	
4H-3, 35	28.65	1.1949	
4H-3, 35	29.40	1.1750	
4H-4, 35	30.15	1.1552	
5H-3, 35	38.15	1.1882	
5H-4, 35	39.65	1.1215	1.1762
5H-5, 35	41.15	1.2190	
6H-3, 35	47.65	1.3962	
6H-4, 35	49.15	1.2984	1.3621
6H-5, 35	50.65	1.3918	
7H-3, 35	57.15	1.3010	
7H-4, 35	58.65	1.4224	1.3344
7H-5, 35	60.15	1.2798	
8H-3, 40	66.70	1.3698	
8H-4, 40	68.20	1.2739	1.2768
8H-5, 40	69.70	1.1867	
10H-3, 35	85.65	1.5051	
10H-4, 35	87.15	1.4132	1.4097
10H-5, 35	88.65	1.3108	
11H-3, 35	95.15	1.3116	

Table 6 (continued).

Core, section, interval (cm)	Depth (mbsf)	Thermal conductivity (W/m · K)	Corrected (mean per core)
130-804C- (Cont.)			
11H-4, 35	96.65	1.3322	1.3105
11H-5, 35	98.15	1.2878	
12H-4, 35	106.15	1.1912	
12H-4, 35	106.90	1.3249	
12H-5, 35	107.65	1.4586	
13H-3, 35	114.15	1.2298	
13H-4, 35	115.65	1.3117	1.3066
13H-5, 35	117.15	1.3784	
18X-3, 35	161.65	1.0240	
18X-4, 35	163.15	1.1899	1.2292
18X-5, 35	164.65	1.4736	
19X-3, 35	171.35	1.2268	
19X-4, 35	172.85	1.4120	1.2972
19X-5, 35	174.35	1.2528	
20X-3, 35	181.05	1.2091	
20X-3, 35	181.80	1.1826	
20X-4, 35	182.55	1.1561	
22X-3, 35	200.45	1.2620	
22X-3, 35	201.20	1.3086	
22X-4, 35	201.95	1.3553	
25X-3, 35	229.55	1.3429	
25X-4, 35	231.05	1.2136	1.2639
25X-5, 35	232.55	1.2352	
26X-3, 35	239.15	1.3305	
26X-3, 35	239.90	1.3595	
26X-4, 35	240.65	1.3885	
28X-3, 35	258.45	1.5486	
28X-4, 35	259.95	1.4803	1.4646
28X-5, 35	261.45	1.3651	
29X-3, 35	268.05	1.6781	
29X-3, 35	268.80	1.5562	
29X-4, 35	269.55	1.4343	
30X-3, 35	277.75	1.5816	
30X-4, 35	279.25	1.6533	1.5268
30X-5, 35	280.75	1.3456	

the same interval of anomalously high shear strength values (30 kPa) between approximately 20 and 45 mbsf. This interval is characterized by a marked increase in the mean grain size (Fig. 26). Smear slide examination reveals a greater abundance of foraminifers in this interval (see "Lithostratigraphy" section, this chapter). Enhanced grain-to-grain contact in this coarser sediment section may explain the higher shear strength values (through an increase in friction).

Index Properties

The sampling frequency for index properties at Site 804 was two samples per section in Holes 804A and 804B and one sample per section in Hole 804C (at the same locations as the velocity measurements). Intervals showing evidence of "flow-in" or any other coring disturbance were not sampled (usually, the top of Section 1 in many cores). Results of the index property measurements are presented in Table 9 (microfiche, back pocket). Figures 27 through 30 show the downhole profiles for bulk density, porosity, water content, and grain density in each hole; superimposed on Figure 31 are the merged porosity curve for Site 804 and a generalized porosity curve for calcareous sediments (Hamilton, 1976). On the whole, shipboard data appear to be of good quality. The very high bulk density (2.01 g/cm^3), low porosity, and low water content value at 125 mbsf is questionable. Comparison with GRAPE data will be necessary to check its validity.

The lithology at Site 804 is fairly uniform (see "Lithostratigraphy" section, this chapter). The mineralogical composition of the sediments is dominated by biogenic calcite, with variable,

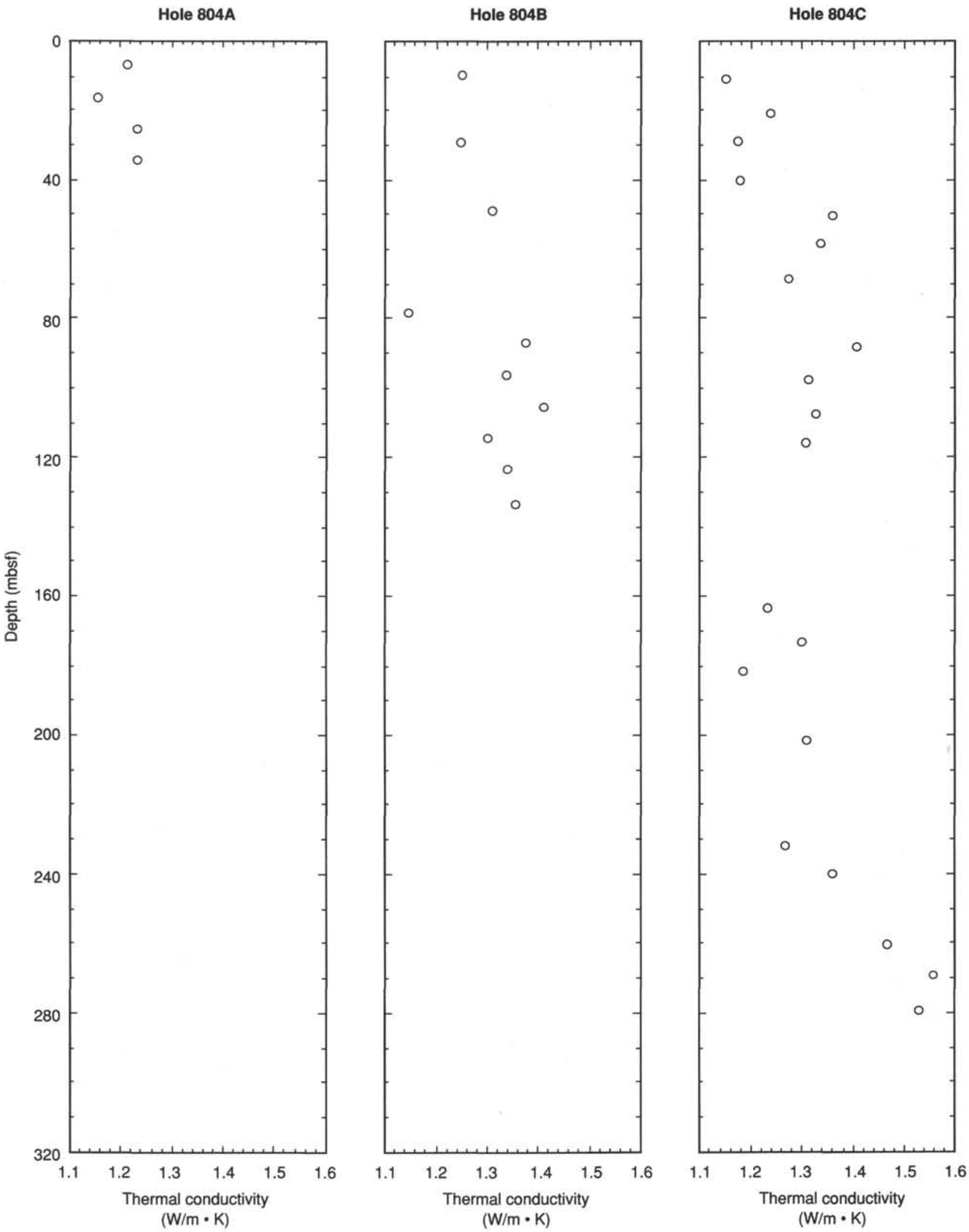

Figure 24. Thermal conductivity vs. depth, Site 804.

Table 8. Mean grain size data, Hole 804B.

Core, section, interval (cm)	Depth (mbsf)	Mean grain size (μm)
130-804B-		
1H-1, 28	0.28	15.2
1H-1, 99	0.99	13.6
1H-2, 22	1.72	20.0
1H-2, 101	2.51	26.8
1H-3, 37	3.37	13.3
1H-3, 121	4.21	13.5
2H-1, 43	5.13	24.6
2H-1, 104	5.74	6.9
2H-2, 30	6.50	21.5
2H-2, 110	7.30	10.6
2H-3, 22	7.92	17.8
2H-3, 123	8.93	11.2
2H-4, 28	9.48	10.5
2H-4, 101	10.21	9.8
2H-5, 33	11.03	11.2
2H-5, 126	11.96	12.1
2H-6, 27	12.47	13.1
2H-6, 112	13.32	13.1
2H-7, 53	14.23	9.0
3H-1, 110	15.30	9.0
3H-2, 31	16.01	11.7
3H-2, 111	16.81	8.9
3H-3, 42	17.62	9.8
3H-3, 114	18.34	12.2
3H-4, 37	19.07	37.1
3H-4, 103	19.73	20.3
3H-5, 38	20.58	25.8
3H-5, 111	21.31	17.2
3H-6, 43	22.13	18.6
3H-6, 107	22.77	15.5
3H-7, 49	23.69	21.8
4H-1, 46	24.16	25.5
4H-1, 105	24.75	25.8
4H-2, 36	25.56	48.4
4H-3, 38	27.08	18.6
4H-3, 109	27.79	17.5
4H-4, 36	28.56	14.2
4H-4, 111	29.31	24.0
4H-5, 27	29.97	19.7
4H-7, 33	33.03	25.3
5H-1, 122	34.42	10.0
5H-2, 38	35.08	9.3
5H-2, 111	35.81	14.7
5H-4, 38	38.08	63.8
5H-4, 107	38.77	25.8
5H-5, 32	39.52	61.6
5H-5, 112	40.32	58.3
5H-6, 31	41.01	56.4
5H-6, 106	41.76	72.7
5H-7, 41	42.61	61.0
6H-1, 39	43.09	39.4
6H-1, 117	43.87	41.8
6H-2, 44	44.64	21.5
6H-2, 108	45.28	22.6
6H-2, 109	45.29	12.6
6H-3, 110	46.80	27.0
6H-4, 112	48.32	23.4
6H-5, 33	49.03	22.8
6H-5, 108	49.78	16.9
6H-6, 33	50.53	13.7
6H-6, 38	50.58	27.5
6H-6, 107	51.27	17.3
6H-7, 37	52.07	15.6

but minor, amounts of biogenic silica; nonbiogenic components are always below 3% in abundance. Grain density reflects the contribution of these two end-members (calcite with a grain density of 2.7 g/cm^3 and silica with a grain density of 2.2 g/cm^3 [Fig. 30]); thus, there is a good correspondence of grain density to the carbonate profile (Fig. 30). Grain density values average 2.68 g/cm^3 when carbonate content is high (around 90%). They decrease to 2.55 g/cm^3 in intervals of lower carbonate content (65%–70%), presumably related to carbonate dissolution or to changes in productivity that result in an enrichment of siliceous microfossils (see "Lithostratigraphy" section, this chapter). Below 200 mbsf, fluctuations in the grain density curve reflect the alternation of nannofossil chalk sections with intervals of nannofossil chalk with radiolarians (see "Lithostratigraphy" section, this chapter).

Wet-bulk density at Site 804 appears to be controlled mainly by porosity changes (R^2 = 0.98; see Fig. 32). The reason for the high correlation can be seen from the equation relating wet-bulk density (D) to porosity (Θ) and grain density (D_g):

$$D = \Theta \cdot D_w + (1 - \Theta) \cdot D_g,$$

where D_w = density of interstitial water. The dominant effect of porosity on wet-bulk density at Site 804 can be readily appreciated when considering that the only variable showing large amplitude changes in the above equation is porosity (50%–70%).

Wet-bulk density values measured at Site 804 range from 1.42 g/cm^3 at about 39 mbsf to 1.97 g/cm^3 at 286.70 mbsf (Fig. 27), generally increasing with depth. This increase is not linear but overlain by steps and cycles. Porosity and water content have the same trends (but inverse from that of the wet-bulk density). Regions of anomalously low (or high) values are superimposed on these downhole trends. These anomalous regions are also characterized by marked anomalies in *P*-wave velocity, shear strength, and carbonate content.

In the uppermost 110 mbsf, consolidation effects lead to a constant decrease in porosity and water content (with a correlative increase in wet-bulk density). In a gross sense, the trend of the porosity-depth curve is similar to Hamilton's generalized consolidation curve for calcareous sediments (Fig. 31). The interval between 110 and 210 mbsf shows a marked difference from Hamilton's curve, with essentially no reduction of porosity or water content (increase of wet-bulk density) within that depth.

Several factors may explain this departure from the generalized trend. Beginning at 110 mbsf, sediment becomes stiff enough to create problems inserting the DSV transducers for *P*-wave velocity measurements, possibly a result of the onset of sediment induration. The ooze/chalk transition occurs at about 180 mbsf (see "Lithostratigraphy" section, this chapter), but chalk nodules in ooze were observed significantly shallower. Thus, the deviation of the Site 804 data from the Hamilton curve between 110 and 210 mbsf may be related to the progressive increase of cementation over this interval. Cementation increases the rigidity of the sediment framework, thereby improving its resistance to compaction.

Variations in radiolarian abundance may play a role in the absence of a porosity reduction with depth between 110 and 210 mbsf. Below approximately 150 mbsf, radiolarian abundance increases more or less continuously until about 200 mbsf (see "Lithostratigraphy" section, this chapter). In central equatorial Pacific sediments, porosity generally increases with increasing radiolarian content (Mayer, 1979). High porosities associated with radiolarian content may tend to cancel the reduction trend in the porosity profile by offsetting compaction effects.

Below 210 mbsf, high-amplitude fluctuations related to changes in sediment composition make it difficult to estimate a general trend in index property profiles. It seems, however, that porosity and water content decrease slightly with depth. This reduction is probably no longer an effect of consolidation but, rather, the results of pore-space infilling with calcite cementation.

Second-order, higher frequency fluctuations are superimposed on the general trend described above. These fluctuations take

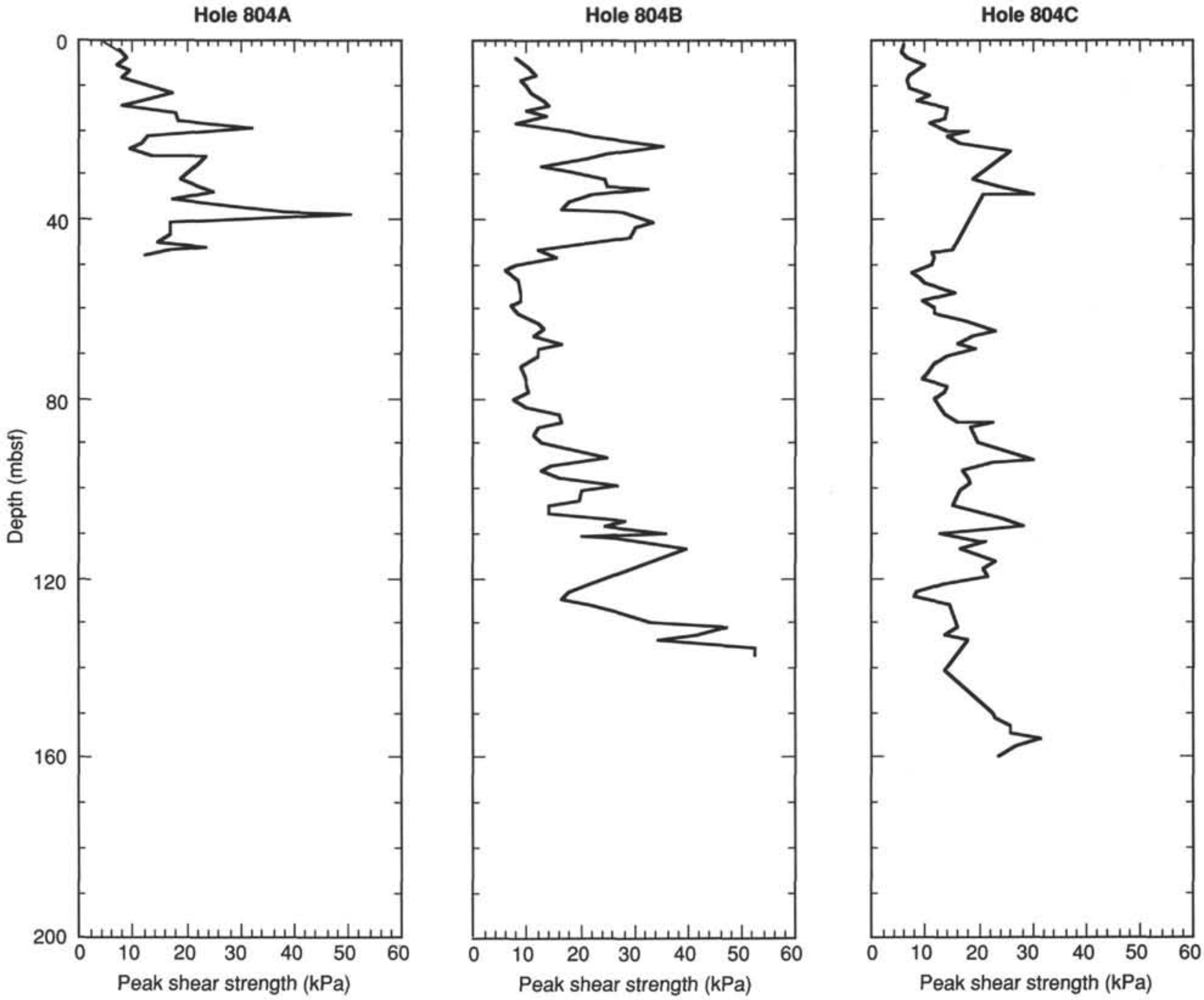

Figure 25. Laboratory vane peak shear strength vs. depth, Site 804.

place over intervals of a few meters to approximately 10 m. They appear to be related to changes in the carbonate content profile, with low porosities (high densities) measured in intervals of high carbonate content. The amplitude of these fluctuations increases with depth below 210 mbsf. Here, fluctuations in the index property profiles reflect the alternation between nannofossil chalk and nannofossil chalk with radiolarians (see "Lithostratigraphy" section, this chapter).

Two shallower intervals, 25–45 and 45–70 mbsf, depart from the Hamilton consolidation curve. The interval between 25 and 45 mbsf has high values of porosity and water content (low wet-bulk density). An increase in mean grain size was measured between 20 and 45 mbsf that corresponds to an increase in foraminifer content (Fig. 26). This increase in foraminifer content may lead to a more open sediment framework, with higher porosity and water content. Grain-to-grain contact between foraminifers also was proposed to explain the anomalously high shear strength values measured in this interval (see section on "Shear Strength" above). More detailed grain size analyses will be conducted post cruise to test these hypotheses.

The second anomalous interval, from 45 to 70 mbsf, shows a marked decrease in porosity and water content (increase in wet-bulk density), compared with the Hamilton consolidation curve (Fig. 31). This anomaly may reflect the effect of rapid consolidation caused by enhanced dewatering during slumping (see "Seismic Stratigraphy" section, this chapter).

Compressional Wave Velocity

Horizontal (parallel to bedding) and vertical (perpendicular to bedding) *P*-wave velocities were measured twice per section in all of Hole 804A and through 110 mbsf in Holes 804B and 804C (Cores 130-804B-13H and 130-804C-13H). Beginning at 110 mbsf, the sediment became stiff and insertion of the DSV probes created fractures along the bedding planes that made it difficult to transmit and receive the acoustic signal for vertical *P*-wave measurements. In Hole 804C, the DSV apparatus was replaced by the Hamilton Frame at the ooze/chalk transition near 180 mbsf (Section 130-804C-20X-2). Measurements were made on coherent and undisturbed blocks of chalk that were cut using the parallel-blade diamond saw. Good samples for Hamilton Frame measurements were sometimes difficult to obtain because of coring disturbance. Weakly cemented chunks also fractured easily when inserted between the Hamilton transducers, making measurements inaccurate or impossible. Results of velocity analyses are presented in Table 10 (microfiche, back pocket). Figure 33 shows the changes of velocity with depth.

The absence of downhole logging data at Site 804 makes it difficult to determine the validity of the anomalously high (or

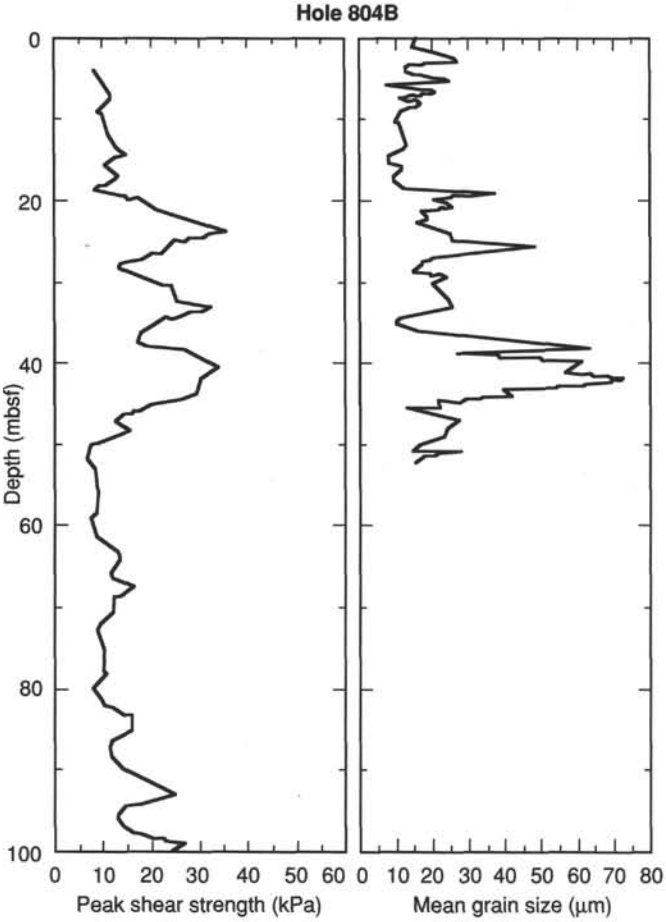

Figure 26. Vane shear strength and mean grain size vs. depth, Hole 804B.

low) laboratory velocity values. A cross correlation with PWL data within undisturbed intervals will be attempted on shore. Most of the velocity data recorded at Site 804 seem reliable; they compare well with those of Site 803. Two sharp decreases in the velocity values measured at Hole 804C (between 130 and 140 mbsf and at 160 mbsf) are, however, questionable. Signals transmitted between DSV transducers were weak, and we suspect that these low values are related to coring disturbance and/or internal fracturing caused by probe insertion.

Velocity values measured at Site 804 generally increase with depth, from 1530 m/s at the mud line to values greater than 1800 m/s at about 300 mbsf. In detail, between 0 and 50 mbsf, velocities do not appear to increase, with values averaging 1530 m/s. From 50 mbsf to the bottom of Hole 804C, velocities increase linearly with depth. Second-order fluctuations (changes occurring over intervals of a few meters to around 10 m) appear to be related to changes in the carbonate content, with high velocities measured in high carbonate content intervals. The amplitude of these fluctuations increases with depth.

Intervals of anomalous velocity values are superimposed on the depth trend. Beginning at approximately 170 mbsf, a decrease in *P*-wave velocity values correlates with a gradual decrease in the carbonate content (Fig. 33). Velocity values change from 1650 m/s at 170 mbsf to 1525 m/s at 200 mbsf. The base of this low velocity zone is difficult to determine because of the paucity of data. The vertical *P*-wave velocity data in Hole 804C (Fig. 33) implies that it may extend to 220 mbsf. It is interesting to note that the ooze/chalk transition boundary was placed at 180 mbsf (see "Lithostratigraphy" section, this chapter) and is located in the decreasing velocity interval, which begins at 170 mbsf. This result is opposite to what is expected, and the reason for it remains unexplained, at present.

SEISMIC STRATIGRAPHY

Site 804 is approximately 2 km northwest of proposed Site OJP-6, a site selected as a slightly shallower alternative to proposed Site OJP-3 (see "Underway Geophysics" chapter and Mayer et al., this volume). The location of proposed Site OJP-6 was chosen based on a single high-resolution seismic profile collected during the *Thomas Washington* site survey cruise (see Mayer et al., this volume), but the final position of Site 804 is off the site survey cruise line and based solely on the data collected by the *JOIDES Resolution* during its pre-beacon-deployment survey. Because the profile of the *JOIDES Resolution* is the only one that crosses the drilling site, discussion of seismic stratigraphy at Site 804 will be based on this line rather than the *Thomas Washington* line. A comparison of the *JOIDES Resolution* seismic line over Site 804 and a *Thomas Washington* line approximately 2 km from the site is presented in Figure 34.

At 3861 m, Site 804 represents the deepest site of the Ontong Java Plateau depth transect. As discussed in Mayer et al. (this volume), it is extremely difficult to find thick, undisturbed accumulations of sediment in this depth range; the only thick sequences present are found in a series of grabenlike features that are common on the plateau between about 3800 and 4200 m (see Mayer et al., this volume; Fig. 35). Both Site 804 and proposed Site OJP-3 (at 4200 m) are located in these grabenlike features and, although only limited surveying was done at Site 804, a detailed survey of OJP-3 revealed many of their characteristics. These small basins are typically oriented roughly north-south and are about 10–16 km wide and about 20–25 km long. They are full grabens in that the basement high completely encloses them (Fig. 36). The offset in acoustic basement between the "horst" and the graben is approximately 300 m at Site OJP-3 and 200 m at Site 804. Although it is not yet clear whether these features are original basement topography that has differentially filled or whether they are related to more recent tectonic activity, the ability to trace seismic units from graben to horst as well as clear evidence of erosion on top of the horst (e.g., OJP-3; Fig. 37) implies that fairly recent movement may, at least in part, be responsible for these structures.

In a gross sense, the seismic stratigraphy at Site 804, as at proposed Sites OJP-3 and OJP-6, can be tied together with the seismic stratigraphy of the rest of the plateau. These deep sites all show a thinned post-Miocene section (relative to the upper part of the plateau; see Mayer et al., this volume). Upon closer examination, however, it is clear that superimposed on this more general seismic stratigraphy is a clear signal of local sediment disturbance. This is particularly obvious in the north-south crossing of Site 804 where a lens of disrupted sediment can be seen between 0.051 and 0.250 sbsf (between Reflectors 4-1 and 4-7; 44–215 mbsf; Fig. 38). Both the upper and lower surfaces of this zone show a particularly incoherent (crenulate) reflector pattern; the upper surface is represented biostratigraphically as a condensed section (ca. 4.3 Ma), whereas the lower surface is a hiatus (ca. 20–15 Ma; see "Biostratigraphy" section, this chapter).

There are also several regions within the lens that have a more disturbed, incoherent reflector pattern (e.g., 0.051–0.103 sbsf at 44–85 mbsf and 0.120–0.190 sbsf at 100–160 mbsf). A number of small faults may be identified, implying that the mass has moved from the northwest to the southeast (from upslope) along a slip plane at about 207 mbsf. The movement does not appear to be large, but enough to cause internal deformation in the sedimentary section. This movement may represent

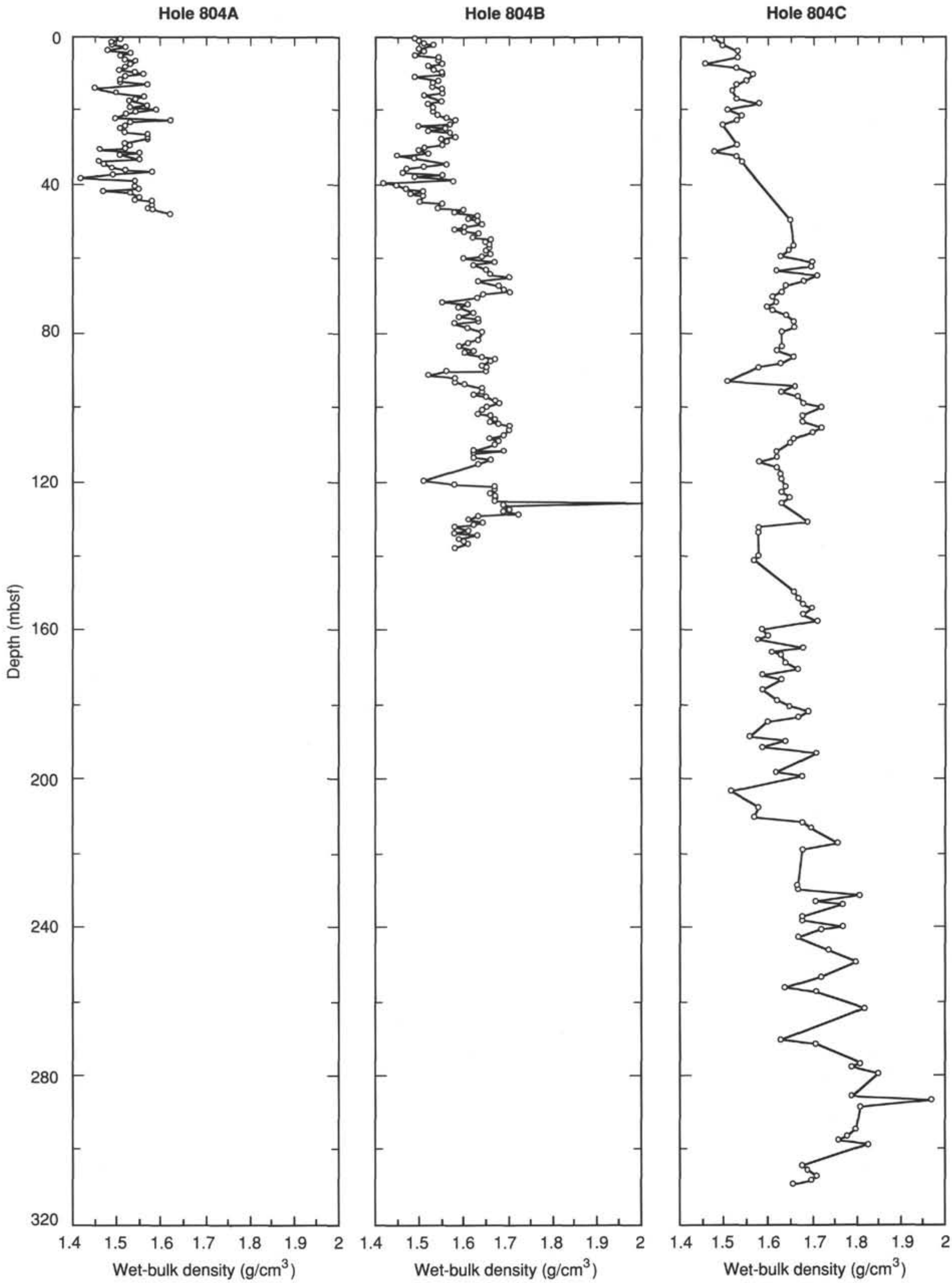

Figure 27. Laboratory wet-bulk density vs. depth, Site 804.

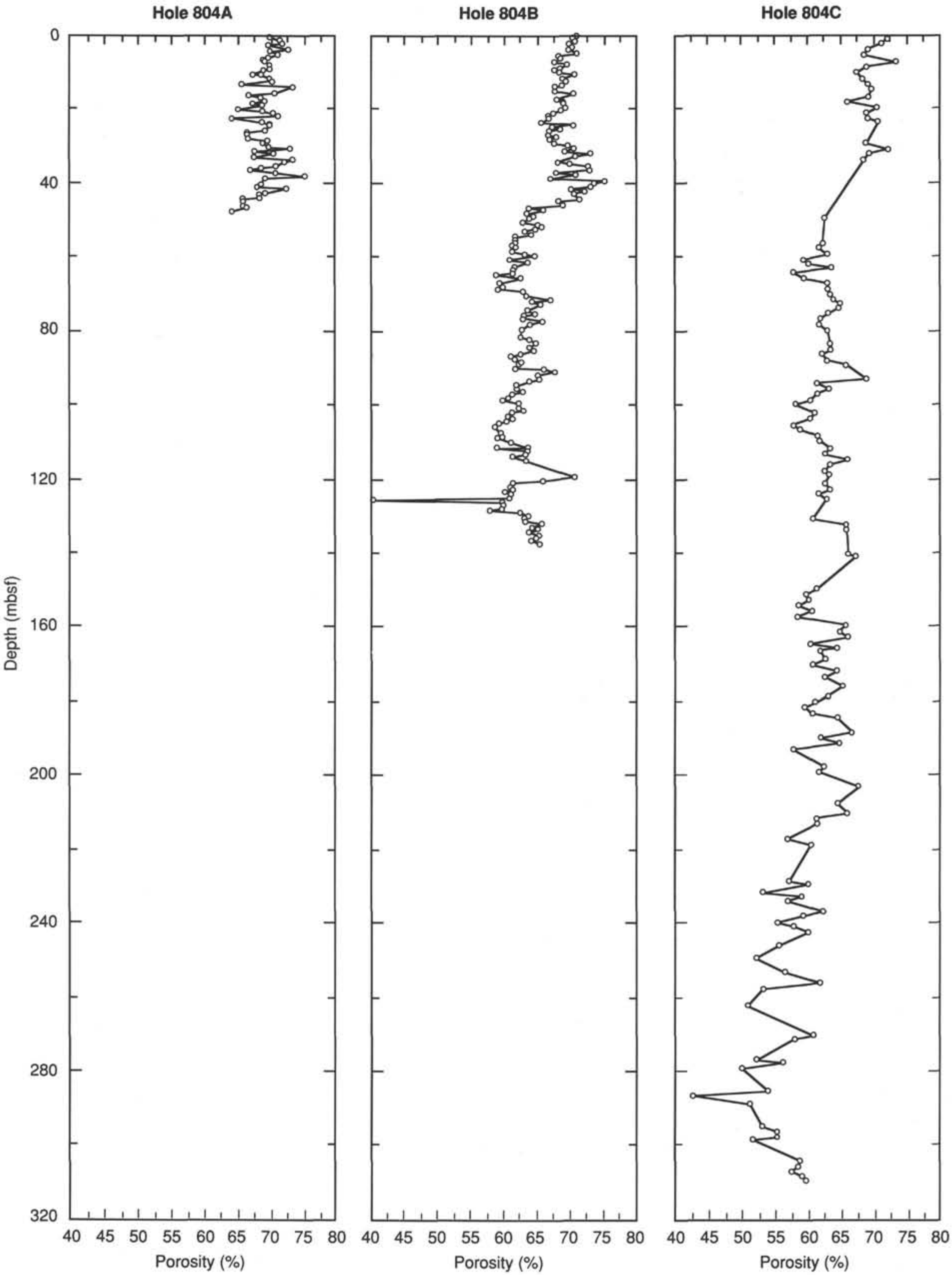

Figure 28. Laboratory porosity vs. depth, Site 804.

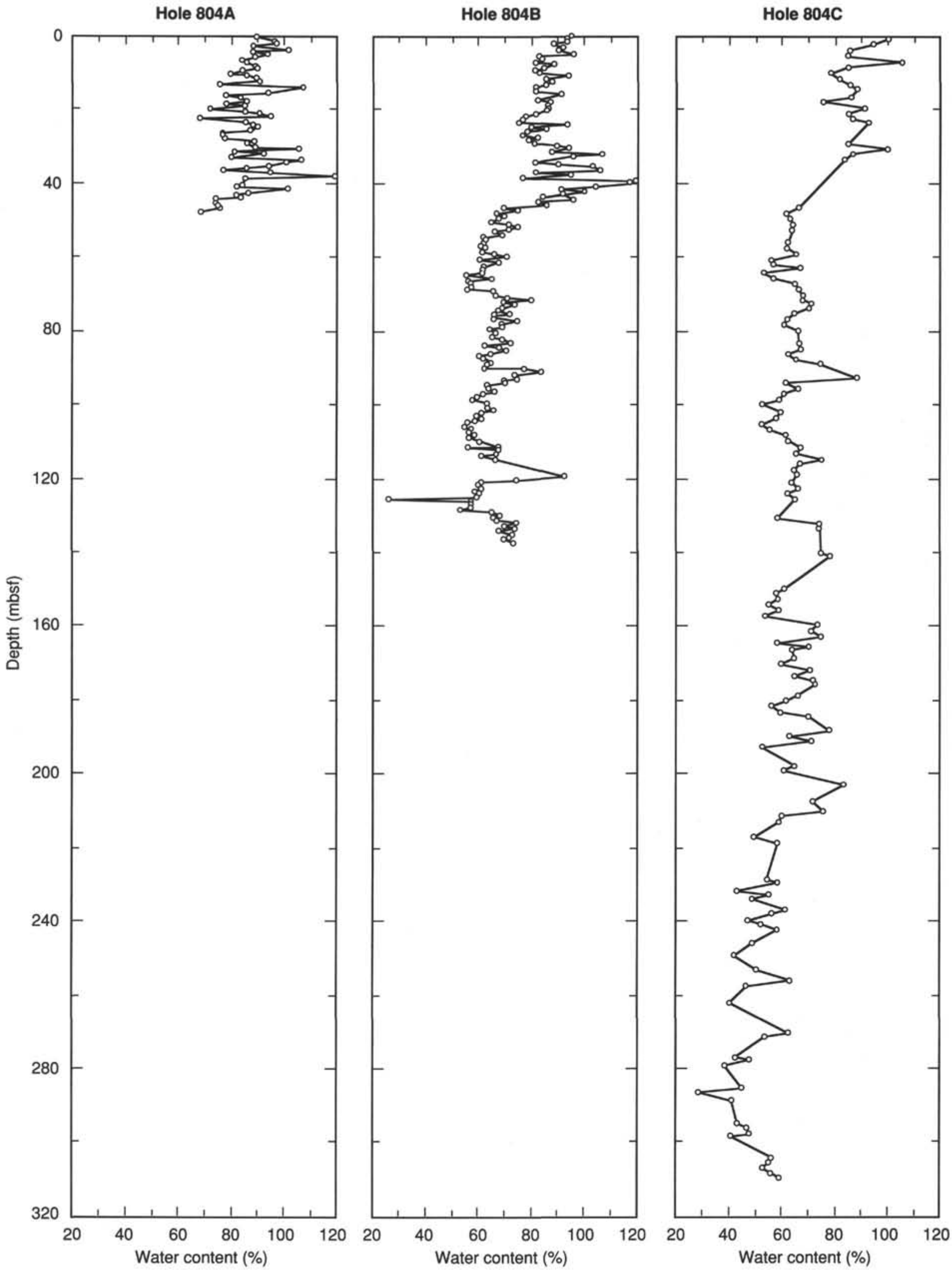

Figure 29. Laboratory water content vs. depth, Site 804.

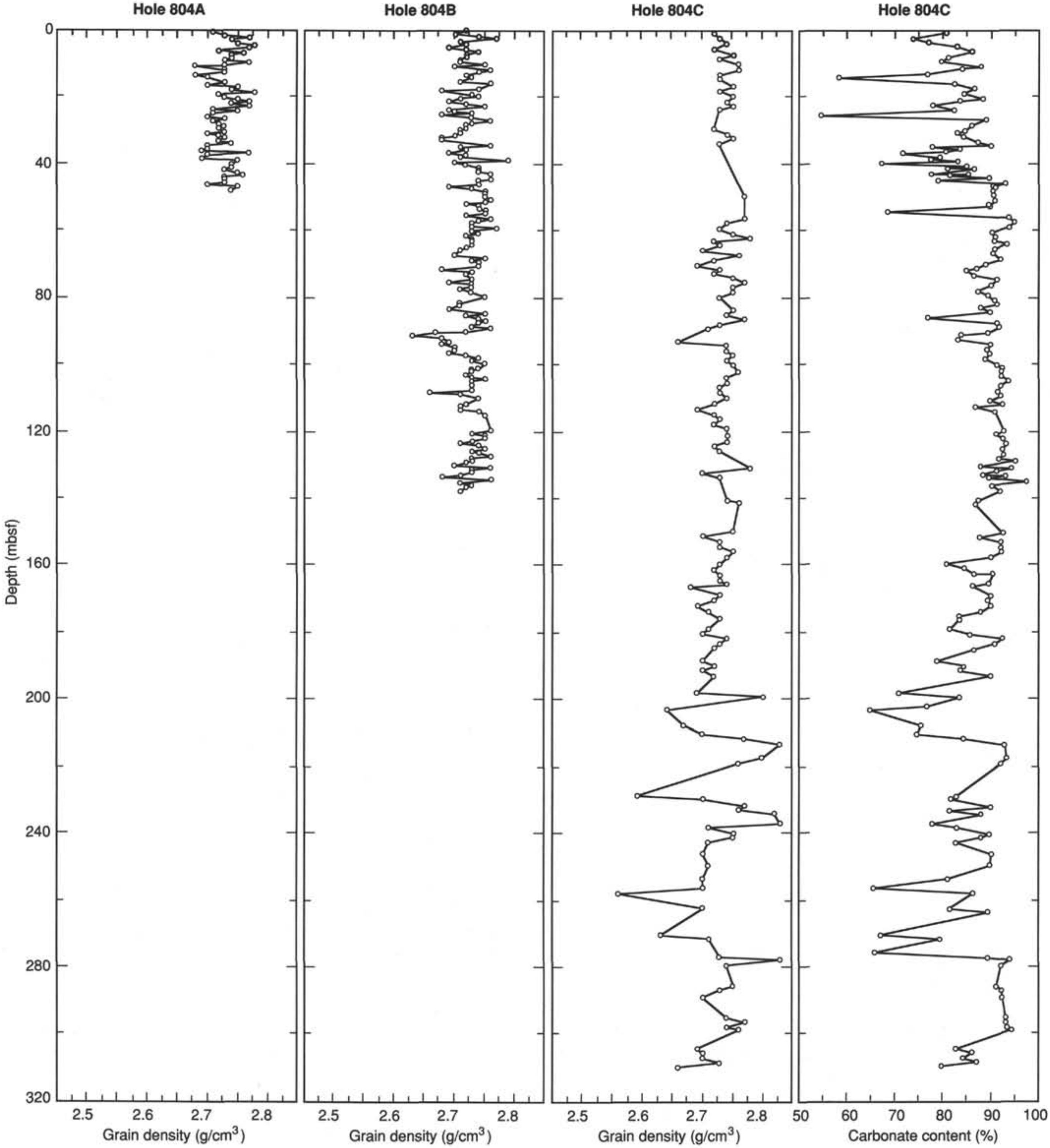

Figure 30. Grain density (Holes 804A, 804B, and 804C) and merged carbonate content vs. depth.

the response of the sediment column to earthquakes (e.g., Berger and Johnson, 1976), to differential compaction over pre-existing basement topography (e.g., Mayer, 1980), or to faulting. If faulting is the cause, the stratigraphic relationships within the disturbed lens imply that the faulting is fairly recent (see below).

Drilling results support the interpretation of mass movement within the sedimentary section. Microfaulted, dipping, and contorted beds are described in cores recovered between 42 and 110 mbsf (see "Lithostratigraphy" section, this chapter). Although there is clear evidence for movement and disruption within the sediment column, the section appears to be stratigraphically intact (see "Biostratigraphy" section, this chapter); thus, the conclusions drawn from the seismic stratigraphy should prove to be relevant to the more general questions of regional paleoceanography.

To relate drill hole results to the seismic record accurately, seismic modeling, as described in Mayer et al. (1985, 1986; see "Seismic Stratigraphy" section, "Site 803" chapter, this vol-

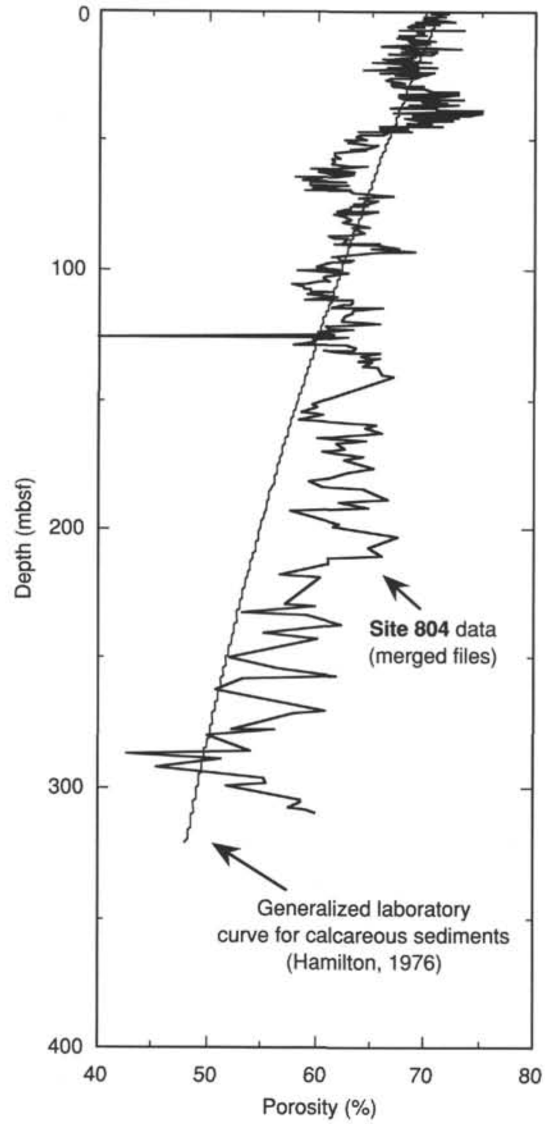

Figure 31. Merged porosity vs. depth, Site 804, and generalized laboratory curve for calcareous sediments (Hamilton, 1976).

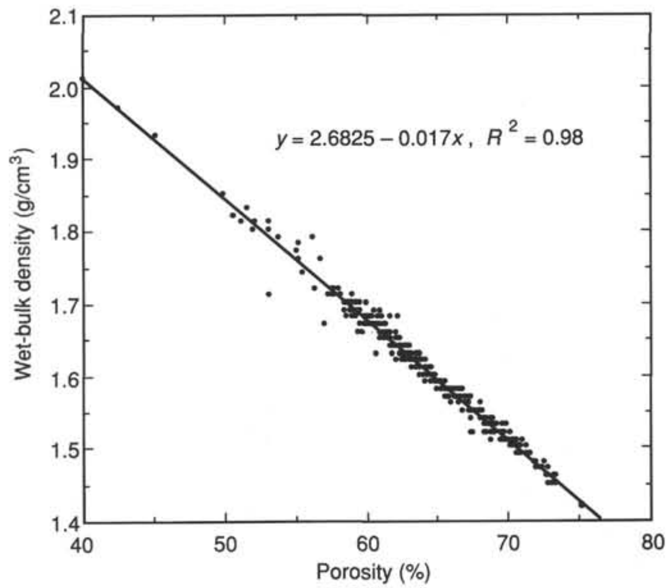

Figure 32. Regression of saturated bulk density vs. porosity for Site 804 (merged data sets from Holes 804A, 804B, and 804C).

ume) was conducted. Site 804 was not logged, and only laboratory measurements (converted to *in-situ* values, as described in the "Seismic Stratigraphy" section of the "Site 803" chapter, this volume) of velocity and density are available for synthetic seismogram generation. In addition, there is no seismic source signature available for the *JOIDES Resolution* seismic system; therefore, the signature of the *Thomas Washington*'s system was used for the modeling. The decrease in resolution resulting from the lack of logging data and the somewhat inappropriate source signature will inevitably degrade the synthetic seismogram. Nonetheless, there is still a reasonable match between the field record and the synthetic seismogram (Fig. 38), giving us some confidence in the traveltime-to-depth conversion.

Based on the *JOIDES Resolution* profile, nine reflectors (4-1 through 4-9; Table 11 and Fig. 39) were identified within the interval drilled (309 m). Most of these can be identified on the synthetic seismogram, with the exception of Reflector 4-8 (see discussion below).

As with Site 803 (and with all such analyses), the uppermost part of the section (upper 30 m/s) is dominated by the outgoing seismic pulse; the shallowest identifiable reflector beyond the outgoing pulse is 4-1 at 0.052 sbsf (42 mbsf; Figs. 34 and 39). This reflector, seen on both the *JOIDES Resolution* and *Thomas Washington* profiles, marks the upper boundary of the displaced lens of sediment. In the synthetic record, it appears as several closely spaced events; on the field record, it is a discontinuous (crenulate) surface. This reflector, dated at about 4.3 Ma, also marks the boundary of a 10-m-thick zone with low carbonate content, density, and velocity and generally high shear strength and large mean grain size (Figs. 39 and 40; see "Physical Properties" section, this chapter, for details). The unusual association of low carbonate with increased mean grain size and shear strength may imply an increased abundance of radiolarians, though this was not noted by the sedimentologists. This interval does, however, show an increased abundance of foraminifers (see "Lithostratigraphy" section, this chapter).

The reflector itself appears to be the result of closely spaced, large-amplitude changes from high to low velocity and density that may be the result of decreased sedimentation rates at this time (see "Sedimentation Rates" section, this chapter). Immediately below the depth of this reflector, we see a sharp change in the slope of the density vs. depth curve. Such slope breaks are to be expected with normal consolidation, but this change in slope is at a much shallower depth (and younger age) than the first change in slope at Site 803. Perhaps the movement of the sediment lens served to dewater the upper part of the section (where water could escape) and thus cause these apparently anomalously high densities.

The next deeper reflector (4-2, 0.100 sbsf at 83 mbsf, ca. 8.1 Ma) is marked by a density, velocity, and carbonate decrease; no grain size information is available for this interval (Figs. 40 and 41). Until grain size data are collected, it will be difficult to determine whether this event represents dissolution, winnowing, or a combination of both. Reflector 4-2 also marks the lower boundary of the upper disrupted zone of the large mass of displaced sediment (Fig. 38). A sharp increase in shear strength occurs at this depth (see "Physical Properties" section, this chapter).

Reflector 4-3 (0.121 sbsf, at 98 mbsf, ca. 9.1 Ma) marks the upper boundary of the lower disrupted zone (Fig. 38). There is a small increase in carbonate content and velocity at this level but a major increase in density, which probably accounts for the re-

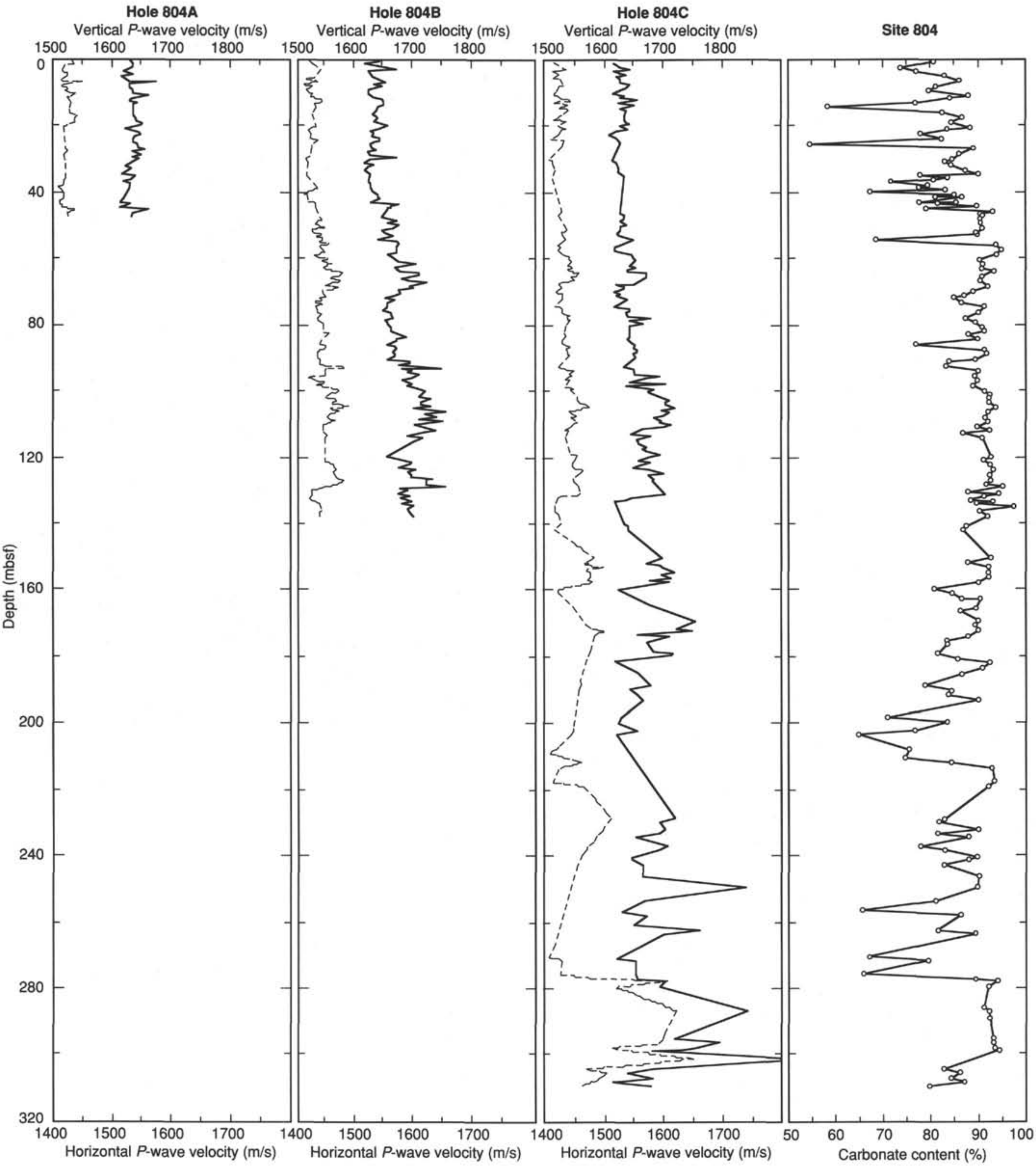

Figure 33. Vertical (dashed line) and horizontal (solid line) *P*-wave velocity for Holes 804A, 804B, and 804C and merged carbonate content vs. depth.

flector (Figs. 40 and 41). As with Reflector 4-1, there appears to be an increase in density moving into the more deformed zone.

Reflector 4-4 (0.148–0.150 sbsf at 125–129 mbsf, 9.68–9.78 Ma) is characterized by rapidly changing density, velocity, and carbonate content (low to high). Again, grain size will be a key in deciphering the paleoceanographic significance of this signal. Although Reflector 4-4 is difficult to trace within the graben (it is broken up by sediment movement), it is of the same age as a major reflector found at Site 803 and in the central equatorial Pacific (Mayer et al., 1986) and may be representative of a global oceanographic event.

Reflector 4-5 (0.170 sbsf at 145–150 mbsf, 10.3–10.6 Ma) is associated with a change from high to low carbonate and velocity. A large (1 point) density spike (decrease) is observed at

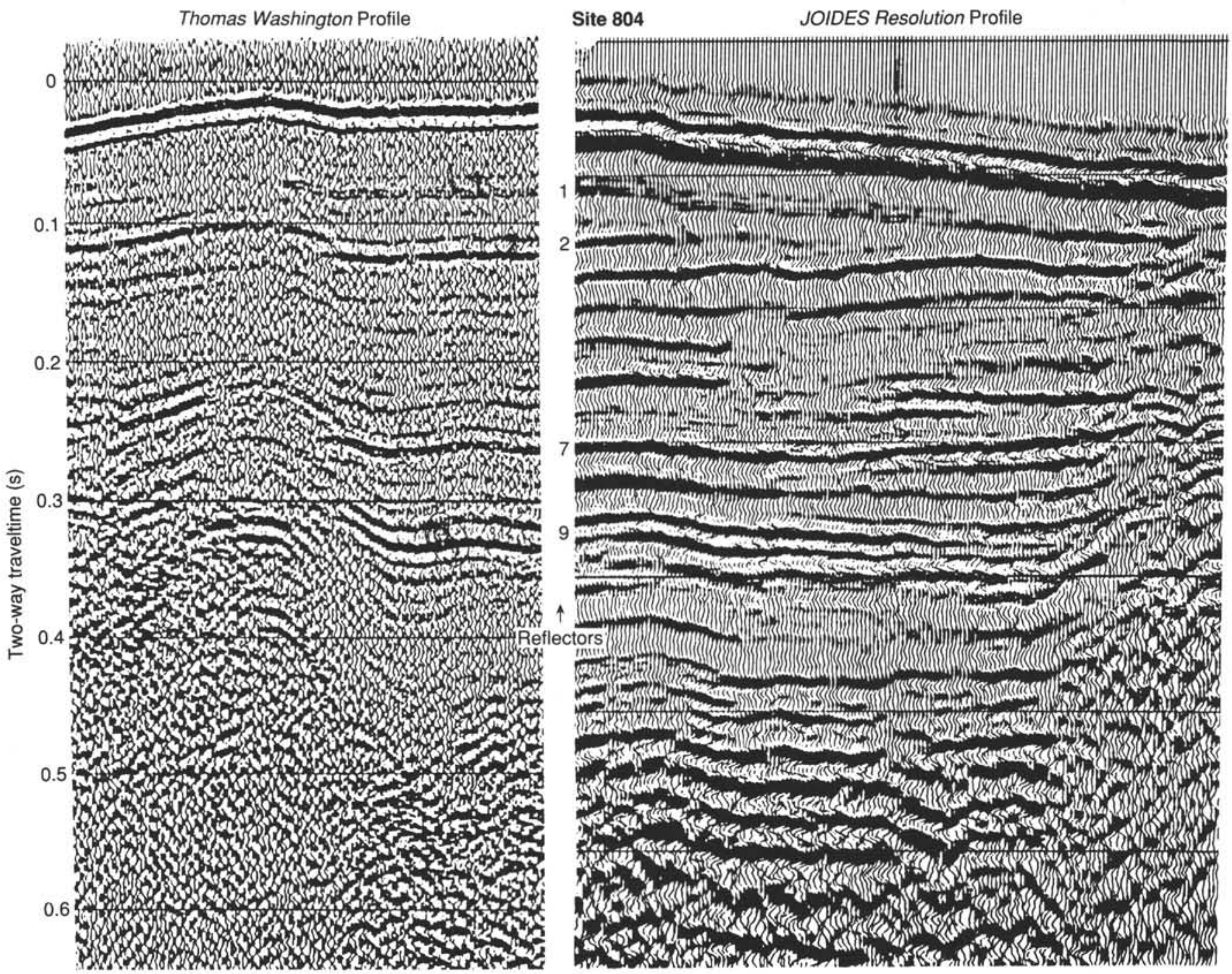

Figure 34. Seismic record collected on ROUNDABOUT Cruise 11 site survey approximately 2 km south of Site 804 (80-in.^{3} water gun, 70–250 Hz band-pass filter) and *JOIDES Resolution* profile at Site 804. For details of reflector picks, see Table 11.

about this level (Fig. 40). This excursion is not, however, supported by a change in velocity or carbonate content, which makes it suspect; further investigation will be necessary to evaluate the validity of this point. Reflector 4-5 is in the middle of the lower disrupted zone and is broken up toward the margins of the graben (Fig. 38).

A very strong reflector (4-6, 0.200 sbsf at 170–175 mbsf, 13.2–13.7 Ma) that also quickly fades out toward the margins of the graben is found within the lower disrupted zone (Figs. 34 and 39). There is a slight increase in carbonate content at this depth but no significant change in density. There is, however, a large change in velocity (Figs. 40 and 41). An increase in velocity without a large change in density is indicative of the early stages of cementation when the rigidity of the sediment is increased (and thus the velocity) without a substantial increase in the bulk density (Mayer et al., 1985). In support of this, the sedimentologists place the ooze-chalk transition several meters below the depth of this reflector (181 mbsf; see "Lithostratigraphy" section, this chapter).

Beneath Reflector 4-6 is a highly disturbed zone that is represented stratigraphically as a hiatus (15.7–20.9 Ma; see "Biostratigraphy" section, this chapter). Significantly, the carbonate content is extremely low in this zone, suggesting pervasive dissolution. This is the same hiatus found at Site 803; its global distribution is discussed by Keller and Barron (1983) and its relationship to a central Pacific-wide seismic event by Mayer et al. (1986).

Directly beneath this disturbed zone is Reflector 4-7 (0.250 sbsf, 215 mbsf, 20.2–20.5 Ma), a strong reflector traceable outside the graben and also identifiable on the *Thomas Washington* profile. This reflector appears to be the primary focus of the large, lens-shaped sediment mass. Reflector 4-7 is associated with a rapid rise in carbonate content (there is limited velocity and density data in this interval, but we would expect the carbonate increase to give rise to an increase in both velocity and density). We propose that the large lens of sediment discussed above slid on the carbonate-poor, radiolarian-rich zone above Reflector 4-7; the more porous, dissolution-weakened sediment

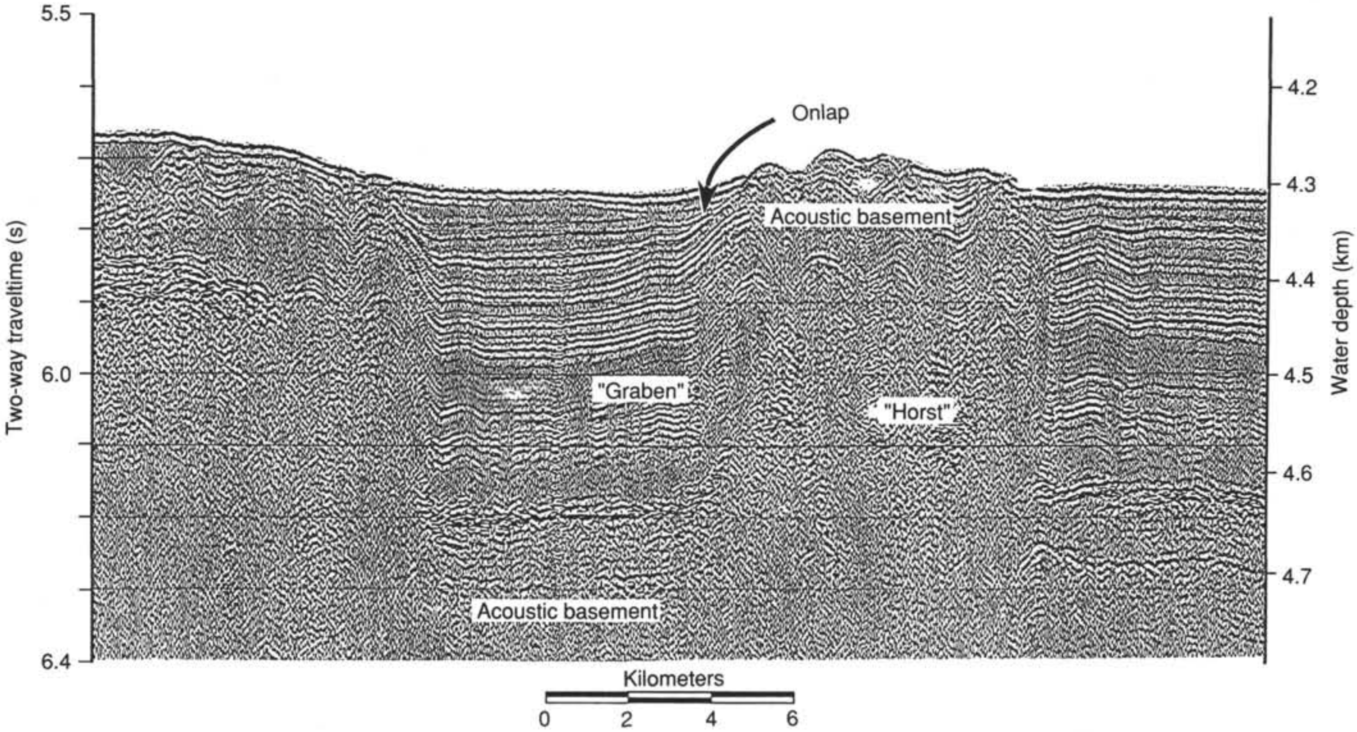

Figure 35. Seismic profile collected aboard the *Thomas Washington* showing grabenlike feature at proposed Site OJP-3.

was severely disrupted whereas the high-carbonate-content material below remained intact.

The deepest reflector within the drilled section (4-9; 0.305 sbsf at 270 mbsf, 24.6–28.36 Ma) is a strong doublet that is also identifiable on the *Thomas Washington* profile. This reflector is the result of a sharp decrease in velocity, density, and carbonate content and is coincident with a major hiatus just below the Miocene/Oligocene boundary. This same horizon is marked by a series of reverberant reflectors at the shallower Site 803.

Although drilling ended at 309 mbsf, we can use the results of Site 803 to estimate the depths and ages of the deeper reflectors. Beneath Reflector 4-9 is another transparent zone with an incoherent and crenulate appearance, possibly representing another period of sediment movement. These sediments are probably early Oligocene in age, ranging from 28 to 36 Ma. Below the transparent zone are several reverberant reflectors (0.420–0.480 sbsf) that are probably equivalent to Reflectors 3-8 through 3-10 at Site 803 and represent the large changes in carbonate/silica content between 36 and 39 Ma. The first really strong deep reflector (0.480 sbsf) is probably the first occurrence of limestone or massive chert and, if the section is similar to the one at Site 803, basement should be close below at about 0.515 sbsf or approximately 505 mbsf.

Site 804 is far from ideal for seismic stratigraphic studies in the context of Leg 130: (1) it was not surveyed with the high-resolution profiling system used for the other sites; (2) we do not have a source signature for the seismic system used; and (3) most unfortunately, its seismic record is overprinted by a series of local mass movement events. Nonetheless, there are some similarities between the seismic stratigraphy at Sites 803 and 804 that imply that, with careful study, it may be possible to extract a regional paleoceanographic picture from the seismic record even at these depths. The long outgoing pulse and the poor results from the *JOIDES Resolution* seismic system prevent us from examining the younger events that were found at Site 803 (3-1 at 2.58 Ma and 3-2 at 3.3–3.4 Ma). However, given the preliminary nature of both the seismic picks and the biostratigraphy, it is possible that Site 803 Reflector 3-a (4.3 Ma) and Site 804 Reflector 4-1 (4.1 Ma) represent the same event. The 5-Ma reflector at Site 803 (3-b) is not found in the *JOIDES Resolution* seismic record at Site 804, but it is clearly present on the synthetic seismogram and can be seen in the higher resolution *Thomas Washington* profile (Figs. 34 and 39). Reflectors 3-4 (8.0–8.1 Ma) and 4-2 (8.0–8.1 Ma) are precisely the same age, which is intriguing because at both sites they appeared to be local events. If a reflector continues to be found at this time, we will have to look carefully for a regional mechanism. The central-Pacific-wide middle/late Miocene boundary reflector (Mayer et al., 1986) is present at both sites (3-c at Site 803 and 4-4 at Site 804) as is the Miocene/Oligocene boundary reflector (3-7 at Site 803 and 4-9 at Site 804). Given the preliminary nature of our seismic analyses, the physical properties studies, and the biostratigraphy, it is still too early to do anything more than speculate on the possible regional significance of these events. If, however, they continue to appear at future sites, the arguments become more compelling.

SUMMARY AND CONCLUSIONS

Location and Objectives

Site 804 is located in the western equatorial Pacific, on the northeastern margin of the Ontong Java Plateau (latitude 1°00.3′N, longitude 161°35.6′E) in 3861 m of water, 375 km east-northeast of DSDP Sites 289/586. Our objective in drilling this site was to obtain a continuous sedimentary record to serve as the deep-water end member on a Neogene depth transect, designed to recover depth-related paleoceanographic signals. It was anticipated that we would encounter a high-resolution carbonate record in a sublysoclinal setting for studies of dissolution and biostratigraphy.

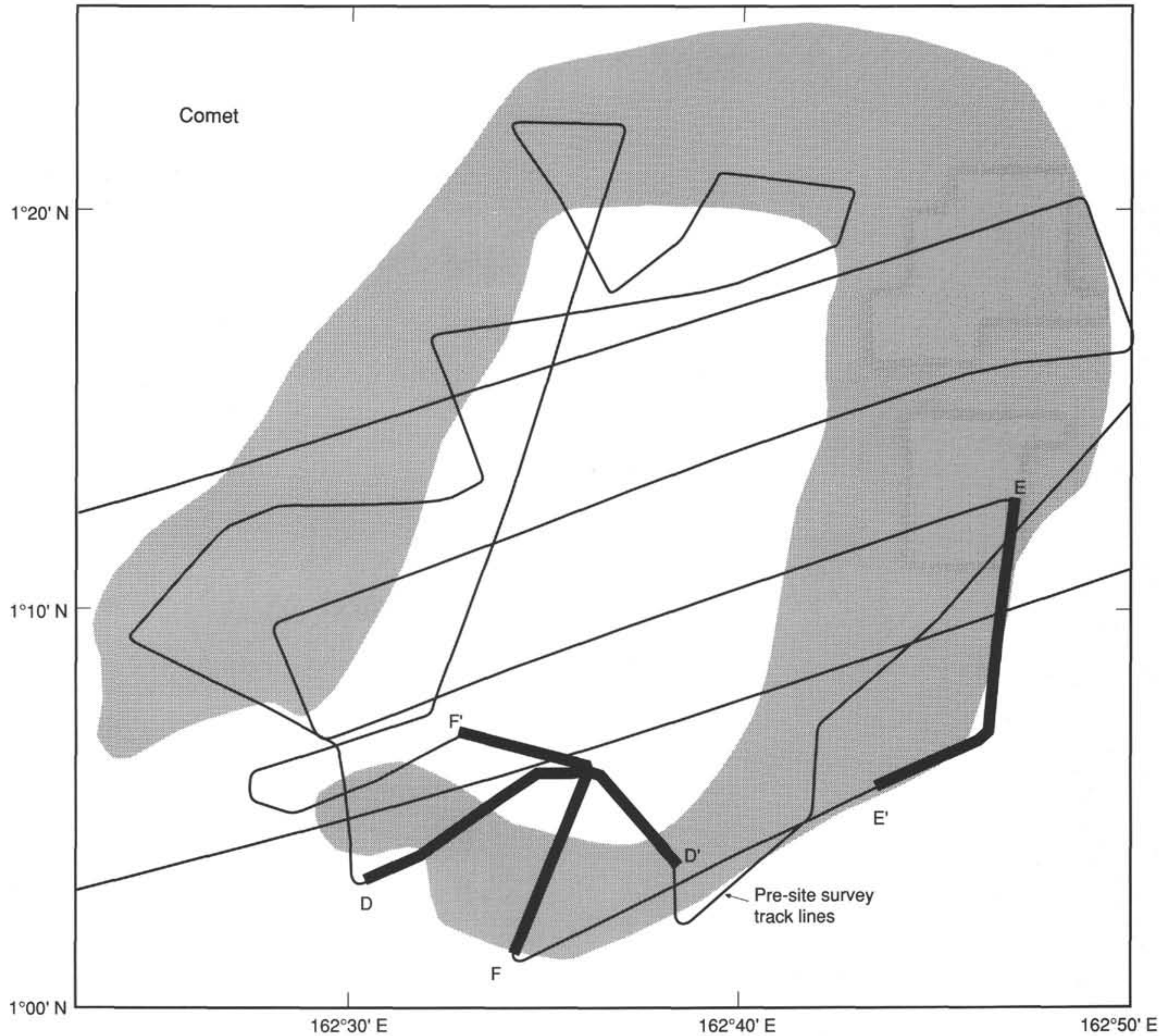

Figure 36. Map of distribution of grabenlike feature at proposed Site OJP-3. White area denotes downdropped block; gray area, upthrown block. See Mayer et al. (this volume) for details.

We positioned the site using a single-channel seismic (SCS) line acquired by the *Thomas Washington* during ROUNDABOUT Cruise 11, on the SCS crossing line of *JOIDES Resolution*. The site is located near the center of a slight depression about 4.5 km wide. The location is close to a significant offset in basement levels between the plateau and the deep ocean floor (Fig. 2). Episodic shaking from earthquakes, basement relief, and perhaps the presence of clay-rich layers at this water depth apparently create conditions favorable for large-scale slumping and debris flow on the flanks of the plateau. Removal of support at greater water depths by carbonate dissolution also may play a role in fostering mass movement (Berger and Johnson, 1976). Selection of a suitable site to drill was difficult under these conditions, and the site chosen was less than ideal for the purposes of the transect.

Coring Results

We spent 3.25 days at this site, coring 499 m of sediment and recovering 466 m. Three holes were drilled. Hole 804A, a dedicated hole, was cored with the APC to 48.7 mbsf into upper Miocene sediments, with 103.7% recovery. Hole 804B was cored with the APC to 137.7 mbsf into middle Miocene sediments, with 102.8% recovery. It was abandoned when the core barrel became stuck in the hole. Hole 804C was cored with the APC to 120.3 mbsf with a recovery of 100% on average. Below this depth, coring continued with the XCB to 312.5 mbsf, at which point it ended in lower Oligocene sediments. Average recovery for the XCB section was 80%. There was no logging.

Neogene sediments were retrieved, except for the four deepest cores in Hole 804C, which recovered early Oligocene chalk

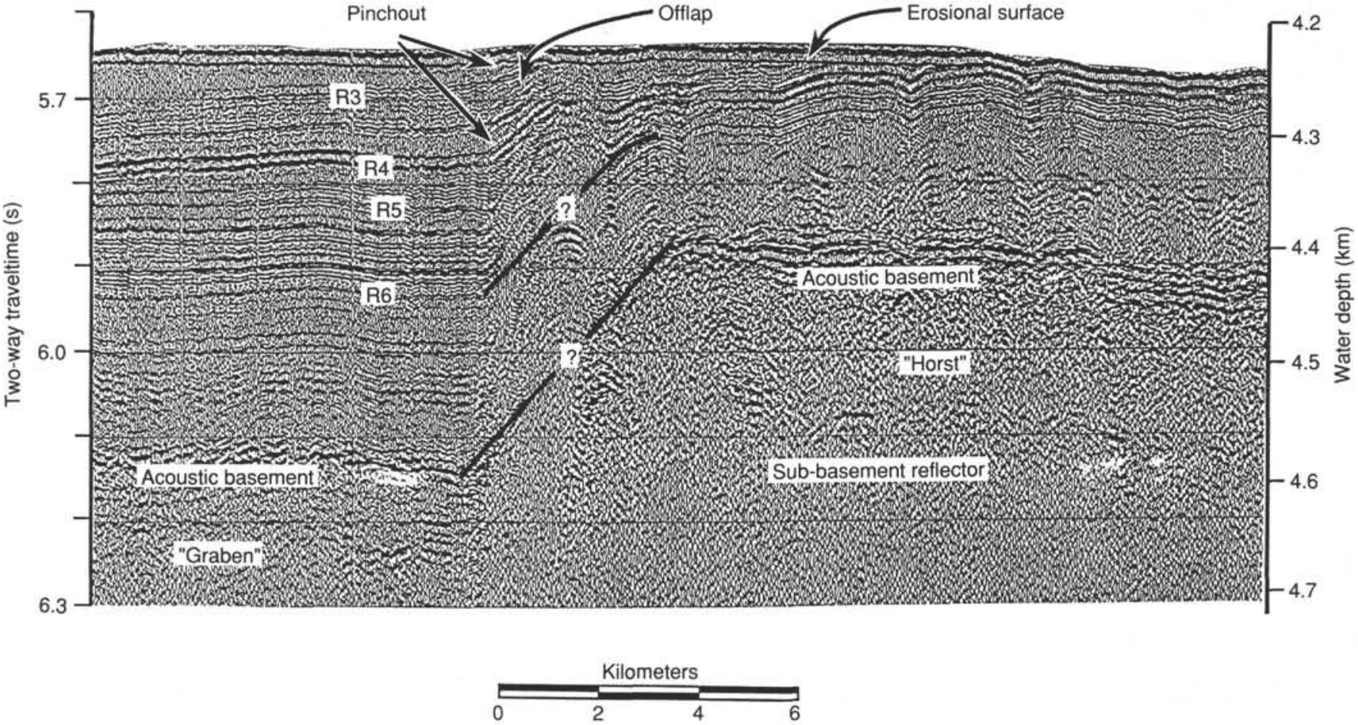

Figure 37. Detail of seismic stratigraphic relationships at margin of grabenlike feature at proposed Site OJP-3. See text for details of reflector picks.

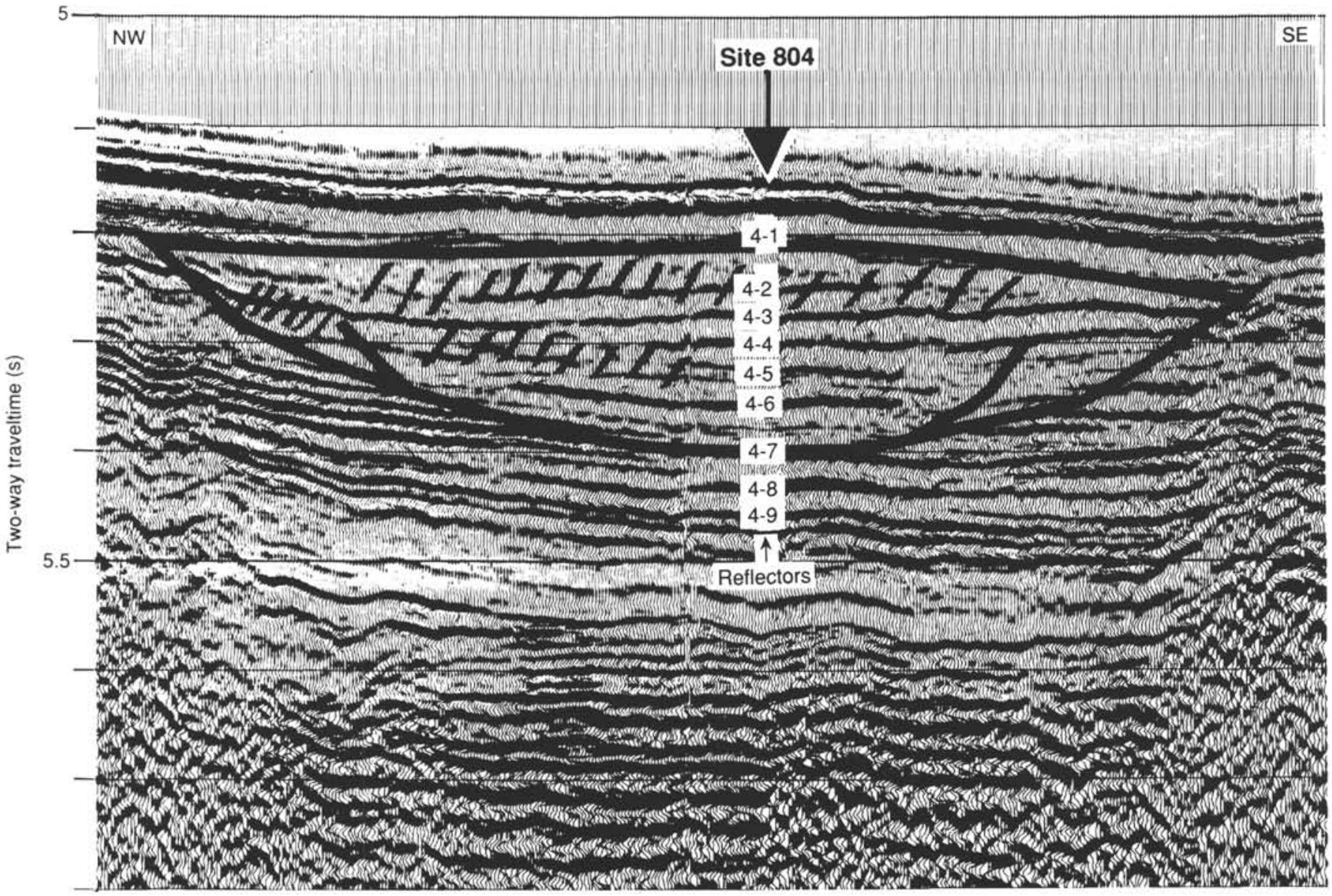

Figure 38. Intervals of disrupted sediments at Site 804 outlined in heavy lines.

Table 11. Summary of traveltimes, depths, and ages for Site 804 reflectors.

	Traveltime		Depth		
Reflector	Seismic (sbsf)	Synthetic (sbsf)	Seismic (mbsf)	Synthetic (mbsf)	Age (Ma)
4-1	0.052	0.052	42	42	4.1
4-2	0.100	0.100	83	83	8.0–8.1
4-3	0.121	0.122	98	100	8.9–9.0
4-4	0.148	0.150	124	128	9.68–9.78
4-5	0.170	0.178	145	150	10.3–10.6
4-6	0.200	0.210	173	182	13.1–13.7
4-7	0.250	0.255	215	217	20.2–20.5
4-8	0.280	?	239	?	22.8–23.0
4-9	0.305	0.310	267	270	24.6–28.4

Notes: Depths and traveltimes to seismic events are picked on both the synthetic seismogram (synthetic) and the field record (seismic). Ages are from sedimentation rate curves (see "Sedimentation Rates" section, this chapter).

(Cores 130-804C-29X to -33X). The entire column, from the earliest deposits to the seafloor, was classified as nannofossil ooze and chalk and is considered to be one lithologic unit. Major breaks occur in the upper Oligocene (hiatus at 270 mbsf, ca. 28–25 Ma) and at the lower-to-middle Miocene transition (hiatus at 197 mbsf, ca. 20–15 Ma).

There is a condensed section or hiatus in the lower Pliocene, between 5 and 4 Ma (46–43 mbsf), and possibly within the middle Miocene, between 13 and 11 Ma (near 160 mbsf). Disturbance of layers (other than from coring) was evident in the section containing the major hiatus from the early to middle Miocene (210–187 mbsf), and also between 42 and 110 mbsf (most of the upper Miocene). It was especially prominent between 70 and 80 mbsf (7–8 Ma).

Two subunits were recognized in this rather uniform section of bioturbated ooze and chalk. They are separated by the ooze/chalk transition at 181 mbsf (middle Miocene, ca. 13 Ma).

The younger section of the unit (Subunit IA, 0–181 mbsf) comprises Pleistocene to middle Miocene nannofossil ooze with foraminifers, nannofossil ooze, and nannofossil ooze with radiolarians. The oozes are light brown in the top 20–40 mbsf, grading into white ooze, with color banding (green and reddish hues) down to 100 mbsf. The banding (related to Liesegang diffusion rings) is best expressed between 44 and 59 mbsf (uppermost Miocene and lowermost Pliocene) and is well developed between 71 and 90 mbsf. Banding is disrupted and distorted in the disturbed layers mentioned, within sediments of uppermost Miocene age (ca. 7–8 Ma). Two turbidites near 93 mbsf attest to redeposition within the middle upper Miocene sequence (ca. 11 Ma).

The older portion of the unit (Subunit IB, 181–313 mbsf) consists of middle Miocene to upper lower Oligocene nannofossil chalk and nannofossil chalk with radiolarians. Colors are yellowish white, pale brown, and white. Radiolarian-bearing sediments are common in this subunit, with a strong radiolarian maximum in the lower Miocene (near 200 mbsf) just below the early/middle Miocene hiatus. Also at this depth, there are indications of ooze/chalk clasts and distorted bioturbation features, as mentioned.

Seismic Stratigraphy

Seismic profiles across the site show the effects of mass movement. These profiles exhibit incoherent crenulate reflections at several levels, as well as evidence for wedging along the basin margins (see Fig. 38). Disturbance is first clearly noticeable at 0.05 sbsf (0.05 two-way traveltime from the seafloor, around 40 mbsf), where part of the section seems to be condensed or missing. At that level, or slightly below it, there is an unconformity that is expressed as a termination of tilted deeper reflectors against the overlying section (upper unconformity; see Fig. 38). Disturbance continues down to 0.1 sbsf (around 80 mbsf) but may include the next deeper interval (to 0.12 sbsf) as well. This would correspond to the disruptions seen in the cores, especially at 70–80 mbsf (7–8 Ma), in the upper portion of the tilted block composing the upper and middle Miocene section.

Disturbance is again seen in the lower part of the block, near 0.21 sbsf (ca. 170 mbsf). At 0.22 s, there is a strong reflector that is weakly developed outside the depression; however, within the graben it is bowl shaped and concentrates energy. This reflector coincides with, or is situated immediately above, the ooze/chalk transition as located in the cores. The lower boundary of the tilted block is probably a slip plane at 0.23 sbsf (lower unconformity; see Fig. 38). In the cored sediments, there is a major hiatus at this level (197 mbsf, ca. 20–15 Ma). On either side, groups of reflectors are disrupted, presumably because of mass movement. This series of strong reflectors probably represents ooze/chalk alternations in the lower Miocene.

The Miocene/Oligocene hiatus is well expressed as a strong double reflector, with the first return at 0.30–0.31 sbsf (around 270 mbsf). Judging from the lack of strong reflectors below, a section of more than 100 m of lower Oligocene sediments might be expected here, with the (unconformable) Eocene/Oligocene boundary appearing near 0.42 sbsf. If so, another 200 or perhaps 250 m of sediment (depending on the basement pick) would be expected in this graben before reaching basement. The first strong deep reflector (at 0.48 sbsf) presumably would mark the location of Eocene limestone and chert. Outside of the basin, the apparent paucity of pre-Oligocene deposits would suggest widespread erosion early in the Cenozoic and in the Late Cretaceous, as was the case at Site 803.

There is some indication that disturbance is associated preferentially with certain layers. This gives rise to the hypothesis that such layers may be predisposed, through conditioning during deposition, to serve as slip planes later. Inasmuch as hiatus formation is contingent on paleoceanographic events, the tracing of these features by seismic profiling should yield valuable information on the nature of such events (Mayer et al., 1986).

Special Studies

Physical properties, including wet-bulk density and sound velocity, show greater variability at this site than at Site 803. Distinct minima in density occur near or within the intervals identified to have hiatuses.

Chemical gradients in interstitial waters at this site are generally similar to those at Site 803, reflecting the calcareous/siliceous nature of the sediments and the paucity of organic material. Calcium and magnesium gradients are influenced by basalt alteration reactions at depth and show the usual negative correlation ($R^2 = 0.97$). Strontium concentrations are lower than at Site 803, presumably reflecting diminished recrystallization intensity at Site 804. Dissolved silica increases with depth, indicating the continued dissolution of siliceous fossils. Near-maximum levels are reached at 100 mbsf, suggesting that below that level dissolution is reduced or balanced by precipitation.

A comparison of detailed magnetostratigraphic profiles for the Pliocene-Pleistocene sediments in the three holes allowed us to detect small changes in sedimentation rates and between-hole variations. There appears to be a small decrease in the sedimentation rate at the Pliocene/Pleistocene boundary from 11.6 to 9.8 m/m.y.

Sequence of Events

Faulting presumably started during initial cooling and sinking of the newly formed crust, early in the history of the pla-

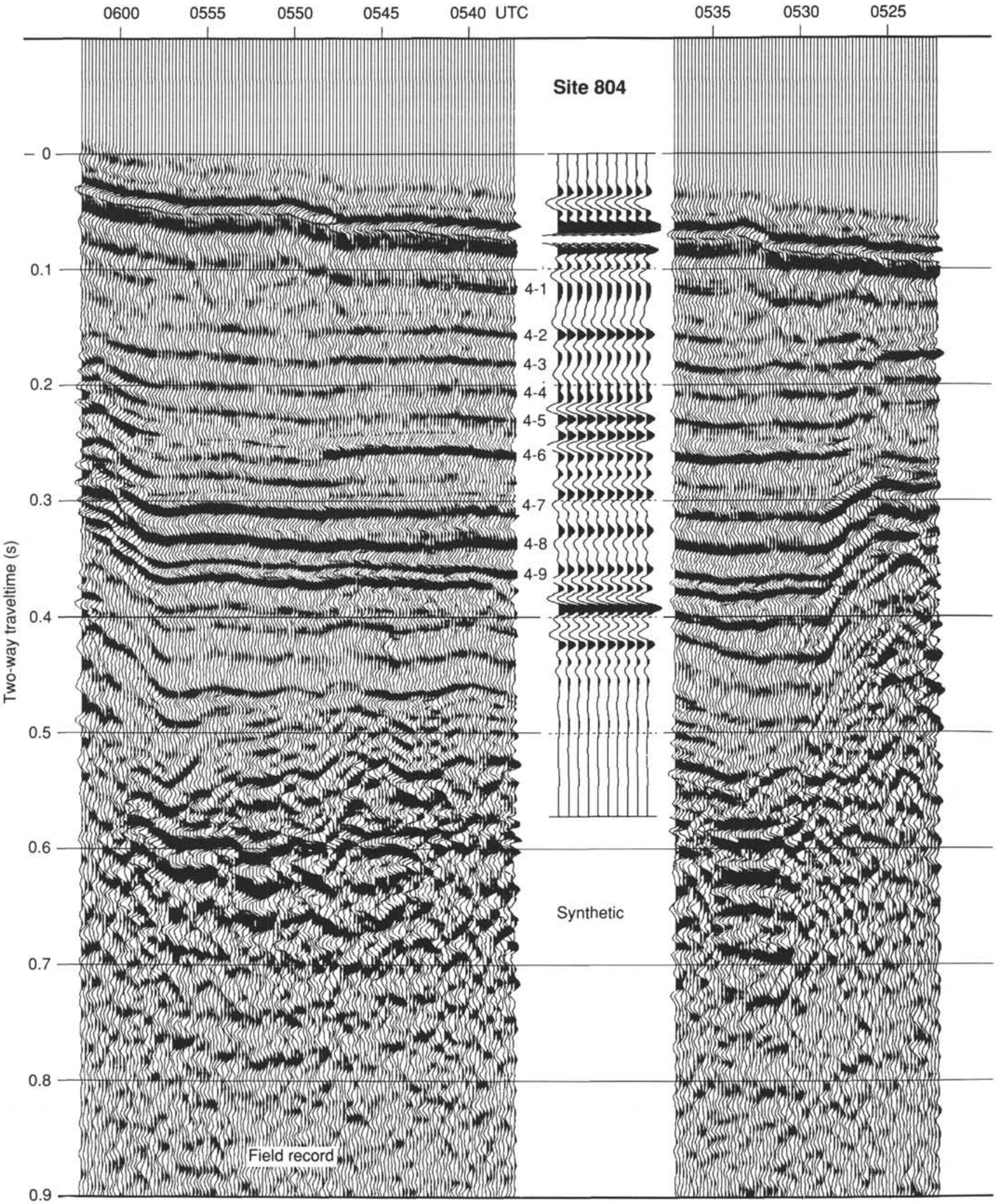

Figure 39. Comparison of synthetic seismogram and field record at Site 804. See text for discussion of Reflectors 4-1 through 4-9.

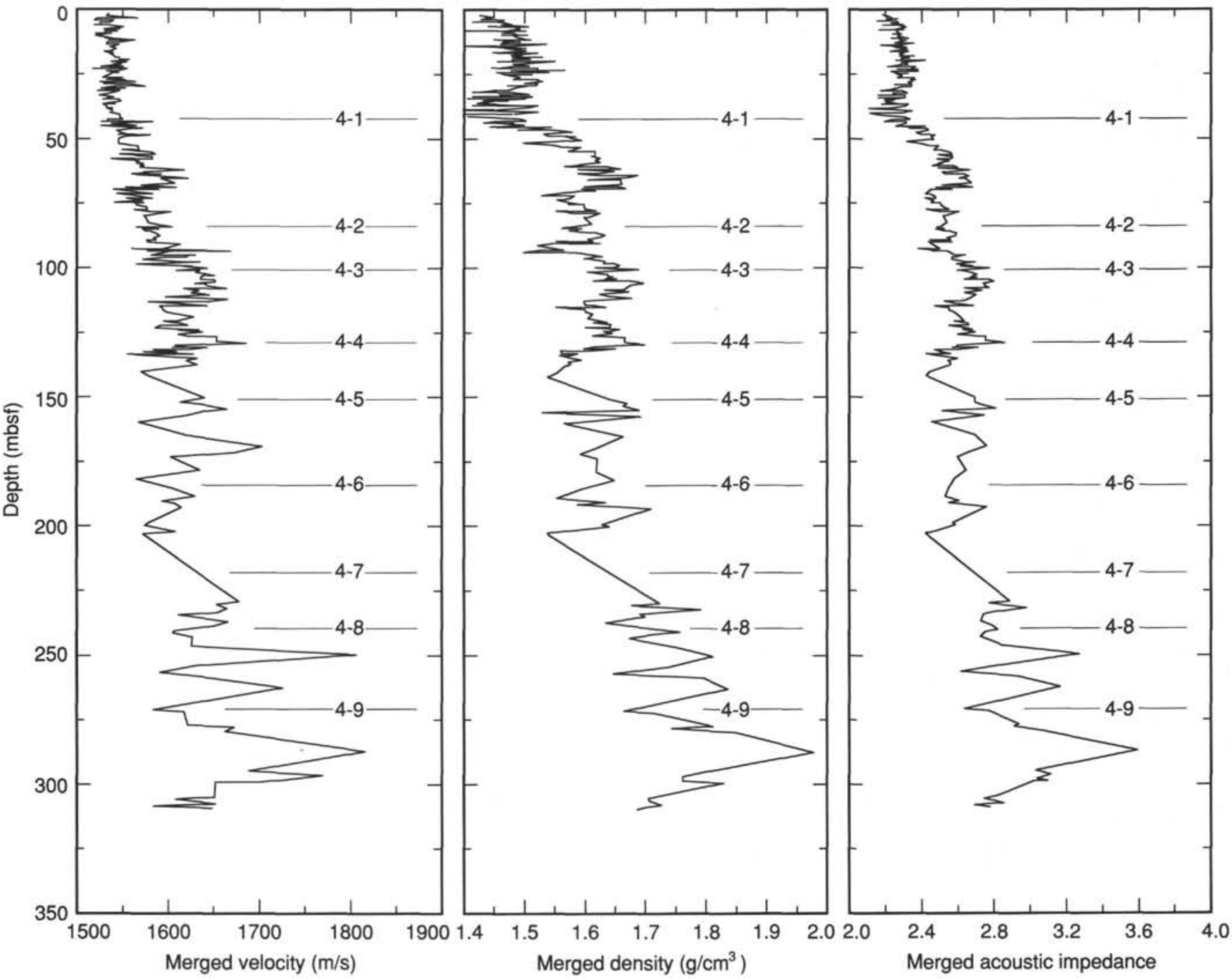

Figure 40. Merged velocity, density, and impedance records vs. depth, Site 804. Measurements are laboratory values corrected to *in situ*. Numbers refer to correlatable reflectors. See text for a discussion of reflector origins.

teau. This faulting initiated the basin within which early Cenozoic (and perhaps Late Cretaceous) sediments were preserved, as seen on the seismic profiles. Elsewhere in the area, erosion prevented deposition or removed much sediment in pre-Oligocene time. With the downward excursion of the CCD in the latest Eocene (Berger and Winterer, 1974), conditions became favorable for the accumulation of calcareous sediments, so that a continuous record could be generated, in principle, albeit at moderately low sedimentation rates (about 10 m/m.y. overall).

Sometime in the earliest Miocene, upper Oligocene sediments were removed. Low carbonate values near the Oligocene/Miocene boundary suggest that chemical erosion played a role in this process. Despite the high carbonate values in the lower Miocene (commonly >85%), dissolution apparently was important in keeping sedimentation rates low: there are zones with greatly reduced foraminifer content. Radiolarian abundances became quite high at times. In the latest early Miocene (just below the hiatus at 197 mbsf), foraminifer-poor and radiolarian-rich ooze was deposited. From that time on, silica deposition seemed to wane as silica was sequestered into the margins and into high-latitude sinks that became active because of the general cooling after 16 Ma. At this point, foraminifers also began to become more abundant, with a peak near 10 Ma and a sustained increase since the end of the Miocene.

The increase in foraminifers, and hence the possibility of fluctuations in the sand content, has important implications for the development of physical properties in the latest Cenozoic, which in turn controls acoustic stratigraphy. There is little doubt that an increase in sand supply parallels an increase in upwelling and, hence, foraminifer productivity. The question is why nannofossil supply did not keep pace. Increased winnowing and improved carbonate preservation must also be considered when trying to explain these patterns (Johnson et al., 1977).

Comparison with Sites 803 and 289

The lithology of Site 804 is the same as that at Site 803 for the total depth drilled (into the lower Oligocene) and presumably is the same back in the upper Eocene also. The carbonate content at Site 803 is somewhat higher on average. Upward from the base of the upper Miocene, both sites show roughly the same trends in foraminifer and radiolarian abundance. However, the high radiolarian abundances in the middle and lower Miocene of Site 804 do not seem to have a counterpart in Site

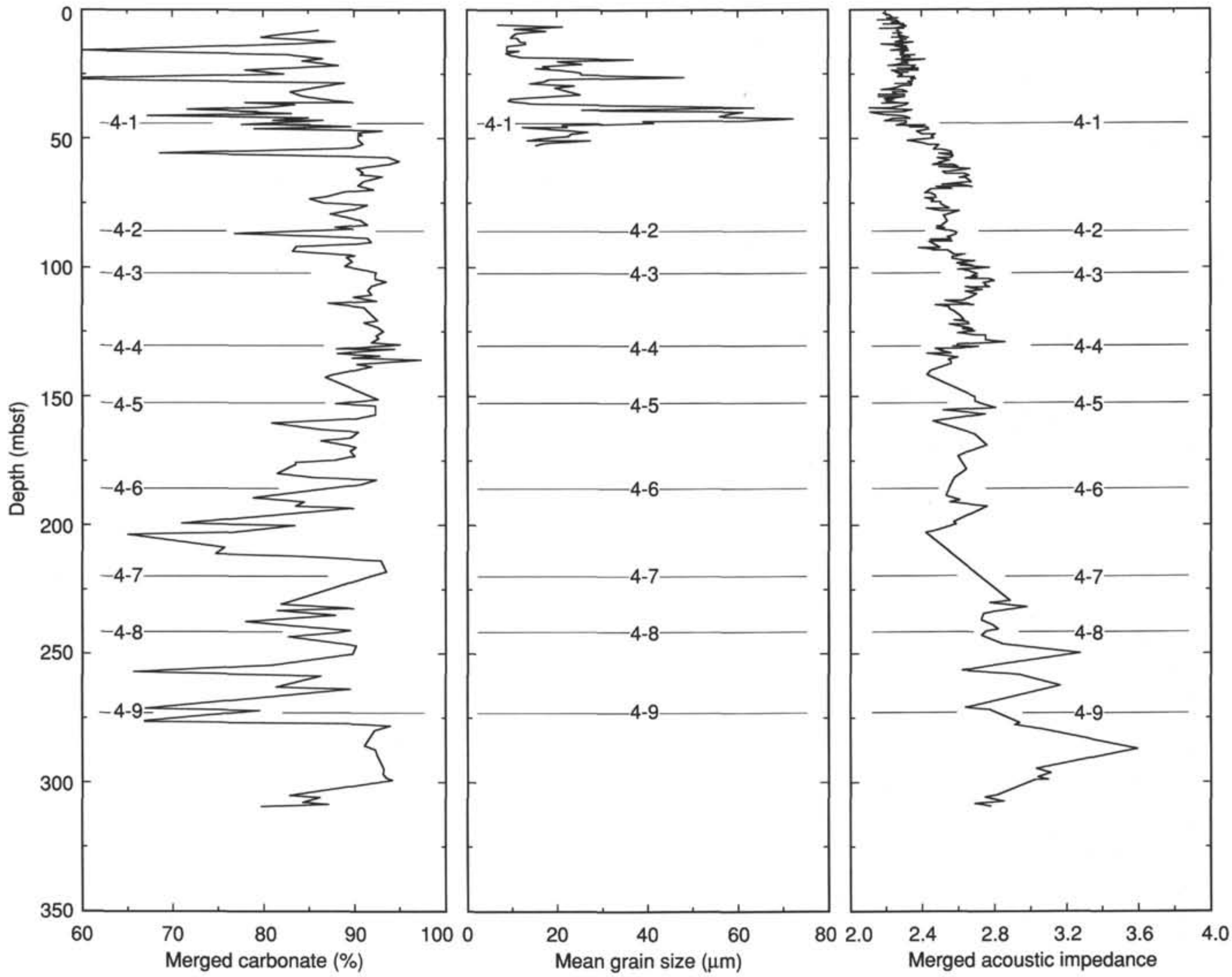

Figure 41. Carbonate content, mean grain size (from Hole 804B only), and acoustic impedance vs. depth, Site 804. Numbers refer to correlatable reflectors. See text for a discussion of reflector origins.

803. Thus, considering the distinctly lower carbonate values in Site 804 in the radiolarian-rich horizons, it appears that the difference is a result mainly of the enhanced carbonate dissolution at Site 804 in those intervals.

At DSDP Site 289, the section equivalent to the one cored at Site 804 is nannofossil foraminifer ooze and interbedded nannofossil foraminifer ooze and nannofossil foraminifer chalk. The facies (Unit I) extends down into the lower Oligocene, where it ends at a hiatus with upper Eocene limestone and chalk (Shipboard Scientific Party, 1975b). Foraminifers are much more abundant at Site 289 than at Site 804. Two processes must be considered: (1) increased winnowing at the depth of Site 289 (2200 m), and (2) the destruction of tests at the depth of Site 804 (3400 m). Radiolarian content is low throughout Unit I of Site 289. However, in the lower Miocene radiolarian concentrations are somewhat increased, just as they are at Site 804.

The ooze/chalk transition is located at 181 mbsf at Site 804. It is shallower here than at Site 803 (217 mbsf), but it has about the same age (13–14 Ma), supporting the hypothesis of Schlanger and Douglas (1974) that conditioning during the time of deposition is an important parameter in the rate of lithification. At Site 289, the transition was found near 350 mbsf in sediments that are somewhat younger (12–11 Ma). Thus, a distinctly increased overburden may accelerate the process of lithification, but not all that much.

Site 804 has a number of breaks in the stratigraphic record (near 4.5 Ma, between ca. 19–15 Ma, and between ca. 28–25 Ma), one of which is close to a hiatus in Site 803 (ca. 22–15 Ma). This hiatus is correlative with NH1 through NH2 of Keller and Barron (1987). There may be a condensed section in the uppermost lower Miocene of Site 289 that overlaps somewhat with the hiatus seen in Site 804. Rates of accumulation are about 10% lower at Site 804 than at Site 803, on the whole, in keeping with the greater depth of Site 804. In addition, about 10% of the sediment column is missing at Site 804, compared with Site 803, above the early-to-middle Miocene hiatus. Compared with those of Site 289, sedimentation rates at Site 804 are lower by a factor of 2 to 3, not counting the effect of hiatuses. This would suggest that more than one half of the carbonate at Site 804 has been removed by dissolution, on average. Thus, the high carbonate values here are not caused by the lack of dissolution, but by the lack of dilution by noncalcareous particles.

REFERENCES

Barron, J. A., 1985. Late Eocene to Holocene diatom biostratigraphy of the equatorial Pacific Ocean, Deep Sea Drilling Project Leg 85. *In*

Mayer, L., Theyer, F., Thomas, E., et al., *Init. Repts. DSDP,* 85: Washington (U.S. Govt. Printing Office), 413-456.

Barron, J. A., and Keller, G., 1982. Widespread Miocene deep-sea hiatuses: coincidence with periods of global cooling. *Geology,* 10:577-581.

Berger, W. H., 1981. Paleoceanography: the deep-sea record. *In* Emiliani, C. (Ed.), *The Sea* (Vol. 7): *The Oceanic Lithosphere:* New York (Wiley-Interscience), 1437-1519.

Berger, W. H., and Johnson, T. C., 1976. Deep-sea carbonates: dissolution and mass wasting on Ontong Java Plateau. *Science,* 192:785-787.

Berger, W. H., and Winterer, E. L., 1974. Plate stratigraphy and the fluctuating carbonate line. *In* Hsü, K. J., and Jenkyns, H. C. (Eds.), *Pelagic Sediments on Land and Under the Sea.* Spec. Publ., Int. Assoc. Sedimentol., 1:11-48.

Berggren, W. A., Kent, D. V., Flynn, J. J., and Van Couvering, J. A., 1985. Cenozoic geochronology. *Geol. Soc. Am. Bull.,* 96:1407-1418.

Elderfield, H., Gieskes, J. M., Oldfield, R. K., Hawkesworth, C. J., and Miller, R., 1982. $^{87}Sr/^{86}Sr$ and $^{18}O/^{16}O$ ratios, interstitial water chemistry and diagenesis in deep-sea carbonate sediments of the Ontong Java Plateau. *Geochim. Cosmochim. Acta,* 46:2259-2268.

Emeis, K.-C., and Kvenvolden, K. A., 1986. Shipboard organic geochemistry on *JOIDES Resolution. ODP Tech. Note,* No. 7.

Espitalié, J., Laporte, J. L., Madec, M., Marquis, F., Leplat, P., Paulet, J., and Boutfeu, A., 1977. Method rapide de caracterisation des roches mère de leur potentiel petrolier et de leur degree d'evolution. *Rev. Inst. Fr. Pet.,* 32:23-42.

Fenner, J., 1985. Late Cretaceous to Oligocene planktonic diatoms. *In* Bolli, H. M., Saunders, J. B., and Perch-Nielsen, K. (Eds.), *Plankton Stratigraphy:* Cambridge (Cambridge Univ. Press), 713-762.

Fornaciari, E., Raffi, I., Rio, D., Villa, G., Backman, J., and Olafsson, G., 1990. Quantitative distribution patterns of Oligocene and Miocene calcareous nannofossils from western equatorial Indian Ocean. *In* Duncan, R. A., Backman, J., Peterson, L. C., et al., *Proc. ODP, Sci. Results,* 115: College Station, TX (Ocean Drilling Program), 237-254.

Gieskes, J. M., 1981. Deep-sea drilling interstitial water studies: implications for chemical alteration of the oceanic crust, Layers I and II. *In* Warme, J. E., Douglas, R. G., and Winterer, E. L. (Eds.), *The Deep Sea Drilling Project: A Decade of Progress.* Soc. Econ. Paleontol. Mineral. Spec. Publ., 32:149-167.

Hamilton, E. L., 1976. Variations of density and porosity with depth in deep-sea sediments. *J. Sediment. Petrol.,* 46:280-300.

Hussong, D. M., Wipperman, L. K., and Kroenke, L. W., 1979. The crustal structure of the Ontong Java and Manahiki oceanic plateaus. *J. Geophys. Res.,* 84:6003-6010.

Johnson, T. C., Hamilton, E. L., and Berger, W. H., 1977. Physical properties of calcareous ooze: control by dissolution at depth. *Mar. Geol.,* 24:259-277.

Keller, G., and Barron, J. A., 1983. Paleoceanographic implications of Miocene deep-sea hiatuses. *Geol. Soc. Am. Bull.,* 94:590-613.

________, 1987. Paleodepth distribution of Neogene deep-sea hiatuses. *Paleoceanography,* 2:697-713.

Kroenke, L., 1972. Geology of the Ontong Java Plateau [Ph.D. dissert.]. Univ. of Hawaii, HIG .

McDuff, R. E., 1981. Major cation gradients in DSDP interstitial waters: the role of diffusive exchange between seawater and upper ocean crust. *Geochim. Cosmochim. Acta,* 45:1705-1713.

McDuff, R. E., and Gieskes, J. M., 1976. Calcium and magnesium profiles in DSDP interstitial waters: diffusion or reaction? *Earth Planet. Sci. Lett.,* 33:1-10.

Mammerickx, J., and Smith, S. M., 1985. *Bathymetry of the North Central Pacific.* Geol. Soc. Am.

Mayer, L. A., 1979. Deep sea carbonates: acoustic, physical, and stratigraphic properties. *J. Sediment. Petrol.,* 49:819-836.

________, 1980. Erosional troughs in deep-sea carbonates and their relationship to basement structure. *Mar. Geol.,* 39:59-80.

Mayer, L. A., Shipley, T. S., Theyer, F., Wilkens, R. W., and Winterer, E. L., 1985. Seismic modelling and paleoceanography at DSDP Site 574. *In* Mayer, L. A., Theyer, F., Thomas, E., et al., *Init. Repts. DSDP,* 85: Washington, (U.S. Govt. Printing Office), 947-970.

Mayer, L. A., Shipley, T. H., and Winterer, E. L., 1986. Equatorial Pacific seismic reflectors as indicators of global oceanographic events. *Science,* 233:761-764.

Nigrini, C., and Lombari, G., 1984. *A Guide to Miocene Radiolaria.* Spec. Publ., Cushman Found. Foraminiferal Res., No. 22.

Okada, H., 1990. Quaternary and Paleogene calcareous nannofossils, Leg 115. *In* Duncan, R. A., Backman, J., Peterson, L. C., et al., *Proc. ODP, Sci. Results,* 115: College Station, TX (Ocean Drilling Program), 129-174.

Sanfilippo, A., Westberg-Smith, M. J., and Riedel, W. R., 1985. Cenozoic radiolaria. *In* Bolli, H. M., Saunders, J. B., and Perch-Nielsen, K. (Eds.), *Plankton Stratigraphy:* Cambridge (Cambridge Univ. Press), 631-712.

Sato, T., Kameo, K., and Takayama, T., 1991. Coccolith biostratigraphy of the Arabian Sea and a new nannofossil zonal scheme for the Quaternary. *In* Prell, W. L., Niitsuma, N., et al., *Proc. ODP, Sci. Results,* 117: College Station, TX (Ocean Drilling Program), 37-54.

Schlanger, S. O., and Douglas, R. G., 1974. The pelagic ooze-chalk-limestone transition and its implication for marine stratigraphy. *In* Hsü, K. J., and Jenkyns, H. C. (Eds.), *Pelagic Sediments: On Land and Under the Sea.* Int. Assoc. Sedimentol. Spec. Publ., 1:117-148.

Shafik, S., 1973. Nannofossil biostratigraphy of the southwest Pacific, Deep Sea Drilling Project Leg 30. *In* Andrews, J. E., Packham, G., et al., *Init. Repts. DSDP,* 30: Washington (U.S. Govt. Printing Office), 549-598.

Shipboard Scientific Party, 1971. Site 64. *In* Winterer, E. L., Riedel, W. R., et al., *Init. Repts. DSDP,* 7: Washington (U.S. Govt. Printing Office), 473-606.

Shipboard Scientific Party, 1975a. Site 288. *In* Andrews, J. E., Packham, G., et al., *Init. Repts. DSDP,* 30: Washington (U.S. Govt. Printing Office), 175-229.

Shipboard Scientific Party, 1975b. Site 289. *In* Andrews, J. E., Packham, G., et al., *Init. Repts. DSDP,* 30: Washington (U.S. Govt. Printing Office), 231-398.

Shipboard Scientific Party, 1986a. Site 586. *In* Moberly, R., Schlanger, S. O., et al., *Init. Repts. DSDP,* 89: Washington (U.S. Govt. Printing Office), 213-281.

Shipboard Scientific Party, 1986b. Site 586: western equatorial Pacific. *In* Kennett, J. P., von der Borch, C. C., et al., *Init. Repts DSDP,* 90: Washington (U.S. Govt. Printing Office), 19-114.

Shipboard Scientific Party, 1989. Explanatory notes. *In* Prell, W. L., Niitsuma, N., et al., *Proc. ODP, Init. Repts.,* 117: College Station, TX (Ocean Drilling Program), 11-33.

Ms 130A-106

NOTE: All core description forms ("barrel sheets") and core photographs have been printed on coated paper and bound as Section 5, near the back of the book, beginning on page 559.